A CLIMATOLOGY OF ELECTRIFIED CONVECTIVE SNOWFALL EVENTS AND THEIR RADAR SIGNATURES

by

GREGORY A. WASSEL

(Under the Direction of Thomas L. Mote)

ABSTRACT

An updated climatology of electrified convective snowfall events, defined as snow occurring with lightning and thunder, is presented for 1960-2005. Results show the most common locations for electrified convective snowfall development were from Utah through the Midwest and Northeast. Also, a higher frequency of events occurred late in the cool season, specifically March and April. A diurnal maximum of events existed in the evening to early morning. Cyclonic and frontal environments were the most frequent environments associated with electrified convective snowfall; other types examined were lake effect/enhanced, orographic, and upslope. Five case studies revealed that environments with elevated convection, a low-level jet, and a low level deformation zone are conducive to electrified convective snowfall development. An environment dominated by conditional symmetric instability (CSI) was also illustrated by cross sections of the cases. Coincident radar imagery and lightning data showed a structure of heavy snowfall lines or a banding pattern.

INDEX WORDS: electrified convective snowfall, climatology, lightning, radar, thundersnow

A CLIMATOLOGY OF ELECTRIFIED CONVECTIVE SNOWFALL EVENTS AND THEIR RADAR SIGNATURES

by

GREGORY A. WASSEL

B.S., The University of Georgia, 2004

A Thesis Submitted to the Graduate Faculty of The University of Georgia in Partial Fulfillment of the Requirements for the Degree

MASTER OF SCIENCE

ATHENS, GEORGIA

2006

A CLIMATOLOGY OF ELECTRIFIED CONVECTIVE SNOWFALL EVENTS AND THEIR RADAR SIGNATURES

by

GREGORY A. WASSEL

Major Professor:	Thomas L. Mote
Committee:	Andrew J. Grundstein
	John A. Knox

Electronic Version Approved:

Maureen Grasso
Dean of the Graduate School
The University of Georgia
August 2006

ACKNOWLEDGEMENTS

I would like to take the time to acknowledge the many people who have helped me and given me support while completing this thesis and my graduate work. First and foremost, I would like to thank my fiancée Stephanie. Your love, support, and words of encouragement have helped to keep me sane and finish this thesis and my degree. This thesis is for you.

Also, I would like to acknowledge the support and love of my father and mother as they were always ready to listen when I needed someone. I am deeply grateful for the encouragement that they provided me.

To my advisor, Dr. Tom Mote, I would like to thank you for your assistance in the preparation of this thesis. With your insightful comments and guidance, this thesis has been much improved. I could not have written it without you. Also, to my committee, Drs. Andy Grundstein and John Knox, I would like to thank you both for your comments, guidance, and for lending an ear when I needed it. I am very grateful to you both.

Lastly, I would like to acknowledge the Department of Geography and Dr. Tom Mote who have supported me financially with teaching assistantships and research grants over the past two years.

Lightning data for this work was provided by Vaisala, Inc. This work was partially funded by a Sigma Xi Grant-in-Aid of research, Gregory A. Wassel, PI.

TABLE OF CONTENTS

Page

LIST OF TABLES

Page

LIST OF FIGURES

Page

CHAPTER 1
INTRODUCTION

Electrified convective snowfall events, defined as snow occurring with lightning and thunder, are often associated with heavy snowfall totals that can result in deaths, injuries, and numerous disruptions to daily activities (Trapp et al. 2001). Some of these disruptions can include the closure of transportation infrastructure, businesses, schools, and the loss of electrical and communication capabilities. In the most intense cases of electrified convective snowfalls, up to one meter of accumulation in a 24-hour period has been observed along with 8 cm of snow per hour (Trapp et al. 2001). With these large snow accumulations, felled trees, collapsed roofs, and high drifts can paralyze cities, towns, and rural areas alike.

An extreme example of an electrified convective snowfall event is the "Storm of the Century" that occurred 12-15 March 1993, shown in Fig 1.1. This event produced record snowfalls along the eastern seaboard of the United States and contained many pockets of convection. Snowfall rates were as high as 7.5 cm per hour. The weight of the snow caused many roofs to collapse. The intensity of this storm was so strong that peak wind gusts during the storm were measured at 64 ms^{-1} (Lott 1993). The lowest pressure of the storm was measured at 961 hPa near Philadelphia, PA (Lott 1993). In the wake of the storm, record low temperatures were recorded across the Southeast and Mid-Atlantic. According to the National Disaster Survey Report, 270 people were killed in this storm along with estimated damages from $3 and $6 billion. Many of the deaths and

much of the damage was a consequence of the heavy snowfalls from the convective bands as the snow caused numerous roof collapses, traffic accidents, and felled trees (Lott 1993). The storm affected 26 states and over 130 million people, which was approximately half of the population of the United States. From Alabama to Maine, more than a foot of snow fell, often in convective snow bands (Lott 1993). The effects of these intense snow bands and heavy accumulations included the closure of schools, business, roads, and the cancellation of 25 percent of the flights in the United States (Lott 1993).

A number of studies have focused on electrified convective snowfall events, which are commonly known as thundersnow events (Market et al. 2002; Curran and Pearson 1971; Colman 1990a,b; Holle et al. 1998; Holle and Cortinas 1998). The study of these events is important as they pose a threat to both life and property as highlighted by the discussion above. This thesis analyzes electrified convective snowfall events, identified as snow observed with lightning by producing a climatology of events, identifying the environment capable of producing the events, and by identifying patterns in overlays of lightning data and radar imagery.

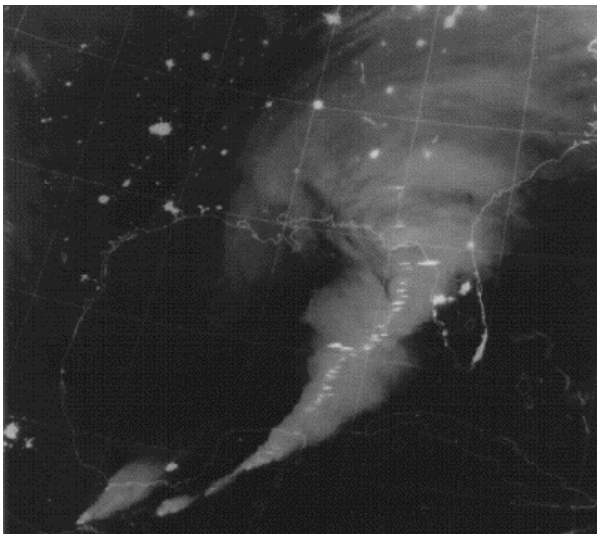

Fig 1.1: A visible nocturnal satellite image from 13 March 1993 of the "Storm of the Century" from Lott (1993).

1.1 Climatology of Electrified Convective Snowfall Events

While infrequent in nature, electrified convective snowfall events are capable of producing heavy snowfalls and thus create numerous socioeconomic disruptions (Rooney 1967). In the continental United States, only 0.07 percent of the observed snowfalls were associated with thunder, while 1.3 percent of thunder reports from October through May were reported along with snow from surface observations (Schultz 1999). While these are small percentages, the impacts, including the crippling of day-to-day activities of businesses, schools, and transportation due to the heavy snowfall accumulations, justifies further analysis of these events. Only one published study has shown a climatology of electrified convective snowfall events. Market et al. (2002) found preferred regions of these events over western Utah, the high plains of Colorado, Nebraska, and Kansas, and the southern Wisconsin area from 1961-1990 (Fig. 1.1.1). They classified electrified convective snowfall events into seven event types including: cyclone associated, orographic, cyclone associated near the coast, frontal associated, lake effect driven, upslope driven, and unclassified (Market et al. 2002). A majority of electrified convective snowfall events (100 of 191 events) were associated with a mid-latitude cyclone.

Other studies, including Curran and Pearson (1971), Colman (1990 a,b), Holle et al. (1998), and Holle and Cortinas (1998), examined the environment in which electrified convective snowfall events occur. Curran and Pearson (1971) investigated 76 events of electrified convective snowfall and showed that the environment for these events was capable of supporting elevated convection. However, this environment contained a very

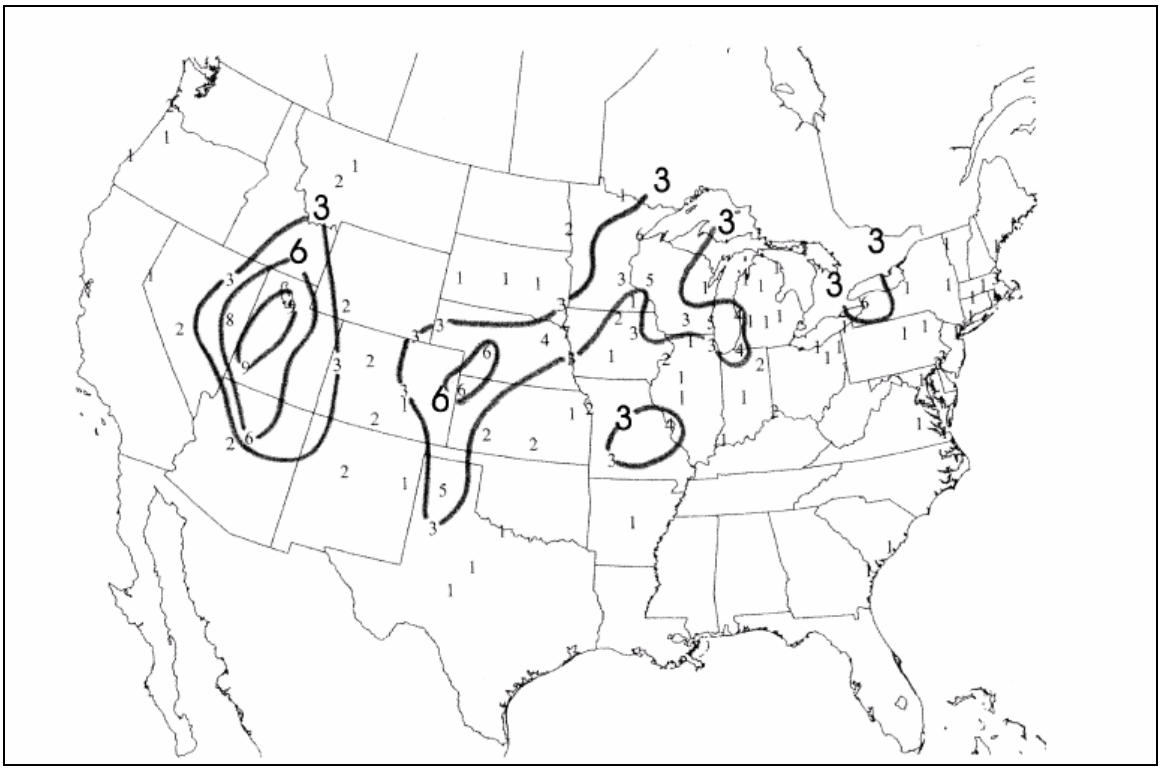

Fig. 1.1.1: The occurrence of electrified convective snowfall events from 1961-1990 as documented by Market et al. (2002)

stable boundary layer and a nearly saturated thermal profile above this layer. Parcels lifted from the boundary layer contained no convective available potential energy (CAPE), and therefore, the convection is not surface-based.

Similarly, Colman (1990a,b) investigated the environment of elevated convective events, specifically on the cold side of surface frontal zones. Colman's work was not limited to snow: rain, sleet, snow, and freezing rain were also considered in the study. Moreover, he did not limit his study to events that produced lightning. Colman (1990a), found that elevated convection occurred most frequently in eastern Kansas and was mostly confined to the areas between the Rocky and Appalachian Mountains (Fig. 1.1.2). However, when considering only October through March, two maxima of elevated convection were evident. One area was over eastern Texas, and the second was over

northern Alabama, northwestern Georgia, and southeastern Tennessee (Fig. 1.1.3). These regions may be areas which would be conducive to electrified convective snowfall events.

Holle et al. (1998) and Holle and Cortinas (1998) examined winter thunderstorms in the continental United States over a nine-year period. A total of 245 hours of thunder reports along with precipitation at a temperature less than or equal to 0˚C were found at 211 stations. Holle et al. (1998) found that these events occurred mostly over northern Utah, the northern Great Lakes region, and the central United States. Holle and Cortinas (1998) also found that freezing rain and snow reports dominated in these events from 0˚C to -5˚C, while snow was dominant at -5˚C and below.

Hunter et al. (2001) also considered lightning along with winter precipitation in the southeastern United States. Their study examined seven cases from February 1994

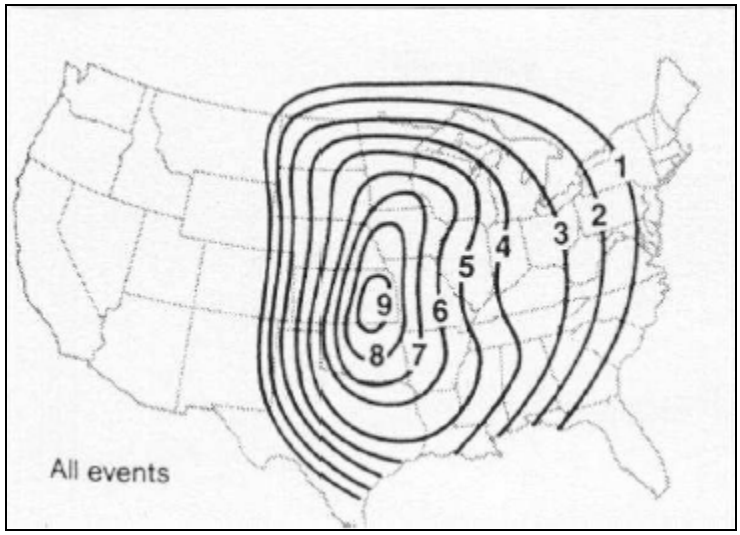

Fig 1.1.2: Locations of most frequent occurrence for elevated convection, from September 1978 to August 1982, in the United States from Colman (1990a).

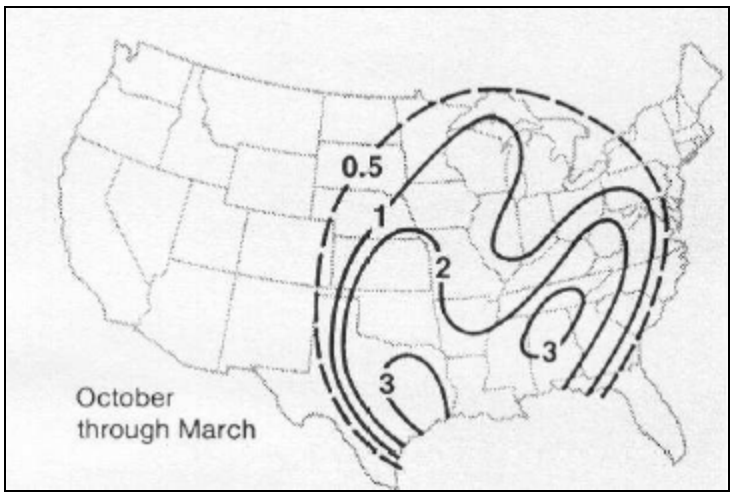

Fig 1.1.3: Locations of most frequent occurrence for elevated convection, from September 1978 to August 1982, in the United States during the cool season (October-March) from Colman (1990a).

through January 1997 using the National Lightning Detection Network (NLDN) data. In all cases, a 300 hPa trough was found in eastern Texas and the upper tropospheric wind maxima was found east of 100˚ W longitude at approximately 30˚ N latitude. Also, a split flow regime was found at 300 hPa in six of the seven cases investigated. In these cases, frontogenesis occurred as the Artic Front matured into an extra-tropical cyclone, produced the upward motion, and resulted in various forms of frozen precipitation across the Southeast.

1.2 Developmental Processes for Electrified Convective Snowfall

The processes for the development of electrified convective snowfall systems and/or mesoscale bands of frozen precipitation has been debated extensively (e.g. Bennetts and Hoskins 1979; Emanuel 1979; Emanuel 1983; Sanders and Bosart 1985,

Sanders 1986; Wolfsberg et al. 1986; Moore and Blakeley 1988; Shields et al. 1991; Moore and Lambert 1993). The presence of a non-surface-based instability in necessary for the development of these events. Table 1.2.1 illustrates various types of instabilities that may result in convective development.

Evidence has shown that the production of mesoscale precipitation bands in extra-tropical cyclones may be the result of conditional symmetric instability (CSI) and frontogenesis acting together (Nicosia and Grumm 1999). CSI is a type of moist symmetric instability and has been associated with frontogenesis (Emanuel 1985). This instability occurs in the presence of moisture aloft on slanted theta-e surfaces which is why the resulting convection is sometimes referred to as slantwise convection (Emanuel 1985).

Sherwood (2000) and Schultz et al. (2000) argued that CSI and slantwise convection are not the same feature. Slantwise convection may occur in other environments and CSI is an instability while slantwise convection must be released from an instability (Sherwood 2000; Schultz et al. (2000). A dynamical relationship between moist symmetric stability and frontogenesis was proposed by Emanuel (1985). Novak et al. (2006) described this relationship as the frontal circulation along with moist symmetric stability on the warm side of a frontal boundary develops into a strong, concentrated sloping updraft ahead of the region of maximum geostrophic frontogenetical forcing. Emanuel (1985) also stated that this relationship of CSI releasing slantwise convection results in the production of mesoscale precipitation bands. Further, it has been shown that the combination of frontogenesis and CSI leads to long-lived mesoscale

Table 1.2.1: The different types of instabilities with regard to moisture from Schultz (2006).

	Gravitational	Symmetric	Inertial
Dry (theta)	Absolute Instability	Symmetric Instability	Inertial Instability
Moist (Conditional) (theta (es))	Conditional Instability (CI)	Conditional Symmetric Instability (CSI)	N/A
Moist (Potential) (theta (e))	Potential Instability (PI)	Potential Symmetric Instability (PSI)	N/A

precipitation bands (Xu 1989). Similarly, frontogenesis and CSI were present in mesoscale snow band producing snowstorms in the northeastern United States (Sanders and Bosart 1985; Sanders 1986; Wolfsberg et al. 1986).

Moore and Blakely (1988) identified three factors in a Midwest storm of 1982 that led to bands of enhanced, electrified convective snowfall. First, a wedge of cold air was advanced in the low levels of the atmosphere and was able to support frozen precipitation. Secondly, a direct thermal circulation related to frontogenesis in the cold front region led to enhanced upward vertical motion. Finally, there was slantwise convection in the region where CSI was found. Each of these mechanisms was regarded as major factors to the development of enhanced snowfall in the storm.

Moore and Lambert (1993) investigated the role of CSI in winter storms. They emphasized that CSI is a significant source of elevated instability which produces stratiform banded precipitation in winter storms. Typically, precipitation related to CSI is

oriented parallel to thickness contours, with widths less than 100 km, and with motion in the direction of warmer air (Moore and Lambert 1993). A cross section constructed normal to the thermal wind revealed that CSI occurred where lines of pseudo-angular geostrophic momentum (M_g) were horizontal with respect to θ_e contours (Moore and Lambert 1993). The value of M_g is defined $V_g + fx$ where V_g is the along-front geostrophic wind, f is the Coriolis parameter, and x is the cross-front coordinate (Schultz and Schumacher 1999). This area was assumed to be saturated if the relative humidity was greater than 80% (Moore and Lambert 1993). These areas of CSI are also areas of large shear in the vertical, low static stability, and large anticyclonic shear. Therefore, large vertical shear is said to "flatten" M_g surfaces, low static stability pushes θ_e toward vertical, and anticyclonic shear introduces an area of weak inertial stability (Moore and Lambert 1993).

Equivalent potential vorticity (EPV) encompasses both θ_{es} and M_g and therefore is capable of diagnosing regions of CSI. A two dimensional version of EPV using the hydrostatic approximation is given by Moore and Lambert (1993) as:

$$EPV = g\left[\left(\frac{\partial M_g}{\partial p}\frac{\partial \theta_{es}}{\partial x}\right) - \left(\frac{\partial M_g}{\partial x}\frac{\partial \theta_{es}}{\partial p}\right)\right] \quad (1)$$

The first term represents the contribution of vertical wind shear and the horizontal gradient of saturated equivalent potential temperature (θ_{es}) to EPV. The second term represents the contribution of stability since absolute vorticity ($\partial M_g / \partial x$) is almost always positive in the northern hemisphere. Therefore, a negative EPV value in a stable region would indicate the presence of CSI and a presence of negative absolute vorticity on a θ_e surface. Computing EPV involves θ_{es} instead of θ_e as EPV only measures moist

process potential instability (McCann 1995). The value of θ_{es} is a function of temperature and pressure only and is defined as:

$$\theta_{es} = \theta \exp(Lq_{vs} / c_p T) \tag{2}$$

where L is the latent heat of vaporization, q_{vs} is the saturation mixing ratio, c_p is the specific heat of dry air at a constant pressure, and T is the air temperature (Schultz and Schumacher 1999). Since θ_{es} assumes saturation, it is only valid in areas with high relative humidity (McCann 1995). However, when both CSI and convective instability (CI) were present, vertical motion was created by CI and dominated the CSI (Moore and Lambert 1993). Graphically, the differences between CSI and CI can be seen in Fig. 1.2.1. Areas of CSI include the quasi-parallel relationship between M_g and θ_{es} while areas of CI are illustrated by the crossing of the contours of M_g and θ_{es}. Also, Fig. 1.2.2 illustrates (A) stable horizontal displacement of a parcel, (B) a stable vertical displacement, and (C) an unstable slantwise displacement. Finally, the illustration of parcel C demonstrates the vertical movement of the parcel after initial lifting on a slantwise plain.

Novak et al. (2004) argued that the use of M_g surfaces rather than the full wind is not a good representation of the wind as M_g surfaces do not represent curved wind flows well. However, Novak et al. (2004) have uncertainties regarding the selection of the type of "wind" and acknowledge that there is no standard wind to use. To avoid this uncertainty, other methods can be used to identify elevated convection. For example, Moore et al. (1998) presented another method for diagnosing instability involving the diagnosis of slantwise convective available potential energy (SCAPE) compared to lifting the maximum θ_e parcel to get positive CAPE. The use of SCAPE and CAPE permits a

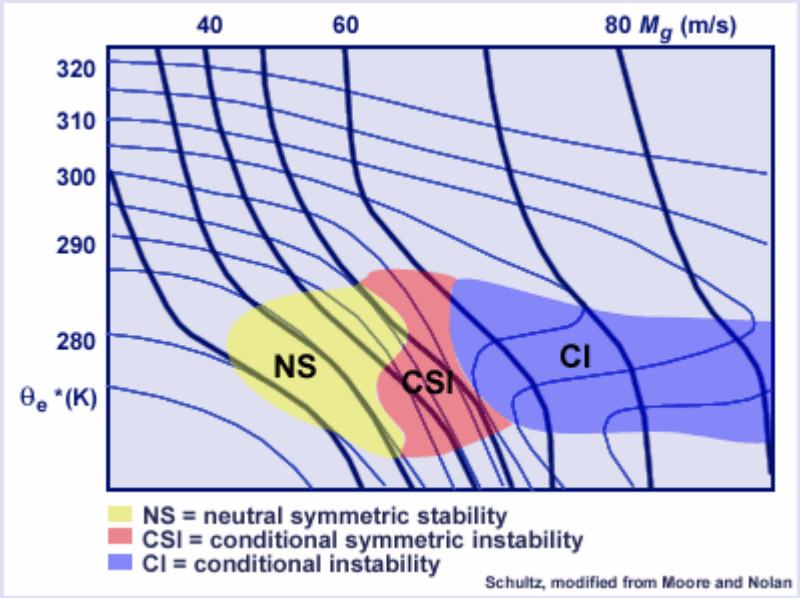

Fig. 1.2.1: A schematic cross section of M_g and θ_{es} (θ_e* in figure) illustrating the differences between regions of CSI and CI from Schultz (2006).

direct comparison of the magnitude of total available energy for both vertical and slantwise convection (Moore et al. 1998). However, Schultz et al. (2000) argued that SCAPE values tend to be small compared with modeled values, the vertical extent of SCAPE is small, and that the computation and display of SCAPE can be difficult. In this thesis, the concept of EPV is used in conjunction with cross sections of θ_{es} and M_g to assess regions of CSI.

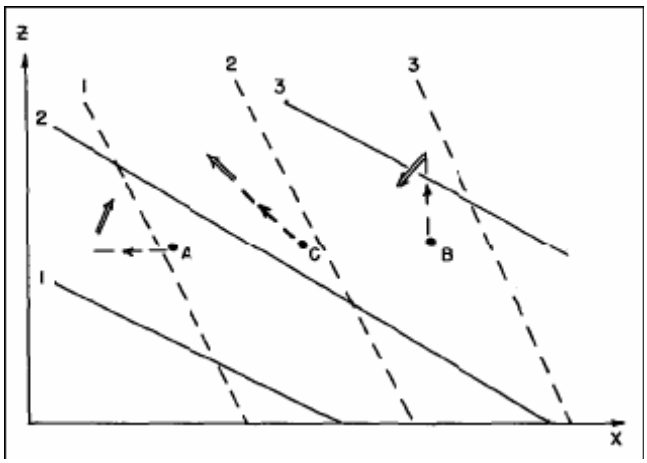

Fig. 1.2.2: A schematic illustrating (A) a stable horizontal displacement, (B) a stable vertical displacement, and (C) an unstable slantwise displacement. Solid lines represent absolute momentum of the basic flow. Dashed lines represent equivalent potential temperature. Dashed arrows show the initial displacement and the double arrows show the resulting accelerations from Sanders and Bosart (1985).

1.3 Radar Imagery of Banded Precipitation Events

Recent work by Greenstein (2006) highlighted the mesoscale structure of precipitation regions in northeast winter storms. Greenstein (2006) found five precipitation modes or types of bands existed in these storms based on the radar imagery and dependent on the ingredients of lift and instability. These five types included classic band, transient, uniform, bandlets, and fractured. However, only Schultz et al. (2004) have published findings examining an electrified convective snowfall event using radar data. Only one event (23 January 2003) was investigated in the study. Specifically, they examined snow bands (Fig. 1.2.3) created by horizontal convective rolls (Fig. 1.2.4). The bands in question were from 50 to 350 km long, approximately 10 km wide, and spaced 10 to 30 km apart. Schultz et al. (2004) found that these snow bands were associated with more intense snowfall than the rest of the storm. While the environment specific to

these bands is not investigated in this thesis, the analysis of the base reflectivity radar imagery determines a banded structure associated with a convective snowfall event.

While not a frequent event, there is a need to study electrified convective snowfall events further. Curran and Pearson (1971) serve as the starting point in the literature for the research and provides the background for the studies including Colman (1990 a,b), Holle et al. (1998), Hunter et al. (2001), and Market et al. (2002). Also, research on the development of these storms is extensive and includes the roles of CSI, frontogenesis, and isentropic upglide. However, only one published study (Schultz et al. 2004) approaches electrified convective snowfall from a perspective using radar. This study identified the appearance of convective bands on radar during January 2003. The identification of convective snowfall in radar signatures is clearly a place for further research.

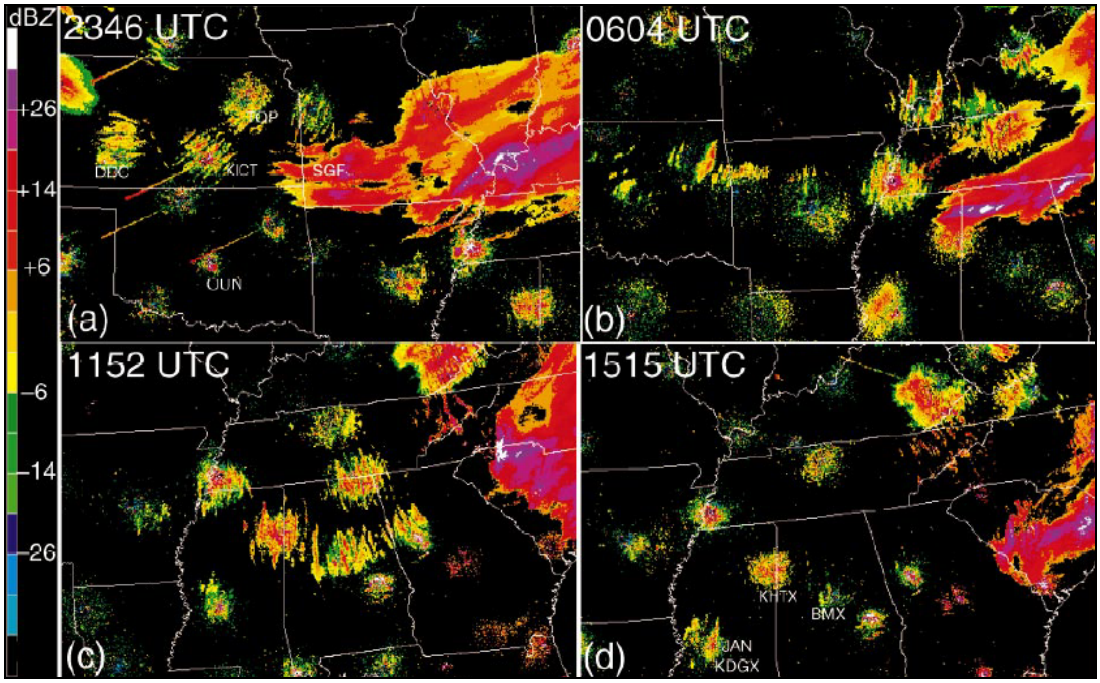

Fig 1.2.3: An example of banding in the radar imagery during a snowstorm on 23 January 2003 from Schultz et al. (2004).

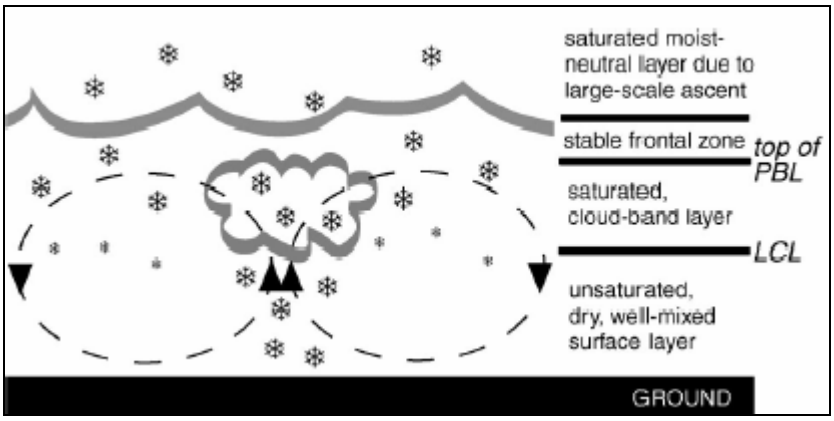

Fig 1.2.4: A schematic of a horizontal convective roll from Schultz et al. (2004).

1.4 Objectives

The main objectives of this thesis are to create an updated climatology of electrified convective snowfall events and to highlight the distinctive "signature" of electrified convective snowfall events on radar imagery in order aid their identification in a nowcasting perspective. To meet these objectives, a new climatology of electrified convective snowfall occurrence must be constructed and events must be selected for further analysis. The electrified convective snowfall events are described spatially and temporally from 1960-2005. Also, the environment capable of producing the events is investigated using five case studies. These descriptions are important to the study as they provide information about where, when, and the environment in which electrified convective snowstorms form. With this climatology completed, three specific events were chosen for further analysis with both lightning and radar data. Finally, with these data, the radar imagery was compared with areas of the events to highlight the signature on radar.

CHAPTER 2
DATA AND METHODS

This project consisted of three main parts: the creation of a climatology, the investigation of the environment producing, and the identification of the signature of electrified convective snowfall events within the radar imagery. The climatology presented in Chapter 3 highlights the spatial, temporal, and environmental characteristics of electrified convective snowfall events from 1960-2005. The construction of the climatology serves as the backbone of the project while the environment investigation describes features necessary for electrified convective snowfall event development. The three most recent cases from the environment investigation serve as the focus for further analysis using both lightning and radar data in Chapter 4 as the availability of lightning data and radar imagery limit the number of cases. Multiple datasets were necessary for the analysis in each part of the proposed project and are the focus of this chapter.

2.1 Data

Surface Aviation Observations (SAO) and Meteorological Aerodrome Report (METAR) hourly surface weather observations from 213 stations (Fig. 2.1.1) during 1960-2005 were used for the construction of the climatology of electrified convective snowfall events. These data have been quality controlled by the National Climatic Data Center (NCDC). Along with the surface station data, upper air North American Regional

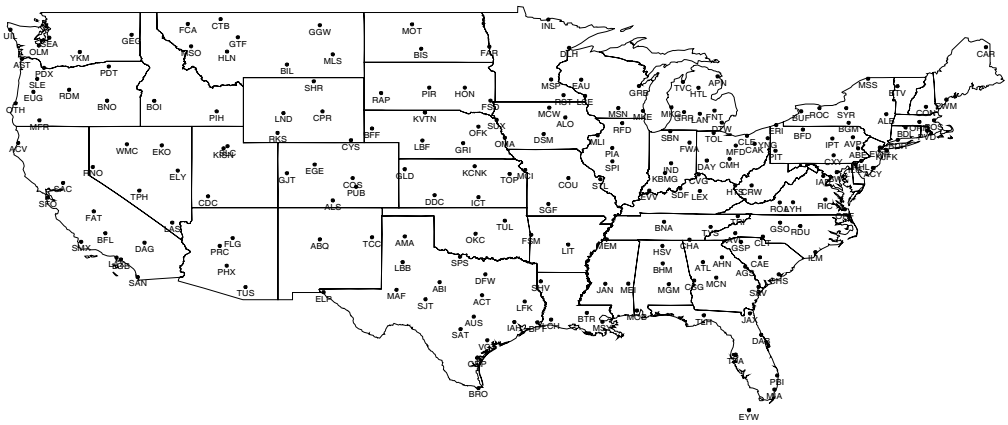

Fig. 2.1.1: The 213 surface stations where hourly weather observations were recorded and included in this study.

Reanalysis (NARR) grids (Messinger et al. 2006) along with Daily Weather Maps (National Oceanic and Atmospheric Administration 1960-2005) were employed to determine the synoptic and mesoscale environment in which electrified convective snowfall events occur. The Daily Weather Maps were used to classify each event synoptically, and the NARR data were used to describe the environment supporting the events included in the case studies. Since the Daily Weather Maps are only produced once daily, previous and post day maps were also considered for each event to determine the movement of the features. Regarding the case studies, the location of surface fronts and pressure centers along with surface isobars were identified using the surface station data. Also, 250 hPa divergence, isotachs, and heights were used to locate jet streaks and upper-level divergence. Heights and absolute vorticity at 700 hPa were analyzed to determine possible areas of upward motion near the layer supporting the elevated convection. Temperatures, heights, and winds at 850 hPa along with along with sea level pressure and 1000-500 hPa thicknesses were also used to diagnose the low-level jet and

the temperature field critical for supporting snowfall. Also, a cross section of wind, omega, potential temperature, and relative humidity were created to further analyze the low-level and upward motion within the elevated convective environment. Finally, a cross section of saturated equivalent potential temperature, absolute geostrophic momentum surfaces, and equivalent potential vorticity were created to diagnose regions of CSI. The climatology of events is discussed in Chapter 3. The environment capable of supporting electrified convective snowfall events is discussed in section 3.4.

The identification of a signature within the radar imagery was the focus of Chapter 4. To complete this work, two additional datasets were necessary. First, lightning strike data from the National Lightning Data Network (NLDN) were used to identify the locations of each electrified convective snowfall event. These data are suitable to provide the location of the lightning strikes with an accuracy of 500 m (Cummins et al. 1998). Both normal and low amperage strikes were considered, as lower amperage strikes may represent either cloud-to-cloud strikes or intra-cloud strikes, both of which are possible during an electrified thunder snow event. The additional dataset used in Chapter 4 is Level III radar data from the NCDC. The lightning data and radar imagery were overlaid and images from each event were analyzed to discover the similarities of patterns within the imagery of three electrified convective snowfall events.

2.2 Analysis

The initial objective of this project was to isolate all of the electrified convective snowfall events identified within the SAO and METAR surface station reports. A database was created using the surface reports with observations of snow of any intensity

along with thunder or lightning from the NCDC's surface data archive. All of these reports were extracted and used to define the electrified convective snowfall events. When investigating multiple reports, the first observation is considered as the event time, and reports that occur more than six hours or 1100 km apart are considered separate events. Because electrified convective snowfall events are generally considered mesoscale phenomena, an 1100 km threshold is chosen as it lies in the middle of the meso-α spatial scale (200-2000 km). The storms are considered to be in the meso-β size (20-200 km) (Orlanski 1975). The six hour criterion is used as this is twice the typical timescale for slantwise convection events as described by Emanuel (1986) (as f^{-1} is approximately 3 hours, where f is the Coriolis parameter). Also, when multiple events are considered, the geographic center is used in the spatial analysis as the location. Because electrified convective snowfall events are mesoscale phenomena that occur over a relatively short period of time, even single observations of snow of any intensity along with lightning/thunder are included as events in this study.

All events were plotted to determine the most frequent regions of electrified convective snowfall activity. The frequency of events was also examined by month and hour. The creation of these frequency plots accomplishes two tasks. First, the frequency of events by month was examined to determine the most favorable time of year for electrified convective snowfall development. Finally, diurnal effects were examined by creating hourly frequency plots of the electrified convective snowfall events.

In order to identify environments conducive to the development of electrified convective snowfalls, the events were divided into specific synoptic types: cyclone, frontal, coastal, lake effect/enhanced, orographic, upslope, and unclassifiable. This

classification of synoptic environments associated with electrified convective snowfall events is based on the classification by Market et al. (2002).

Events that consisted of a transient mid-latitude cyclone and contained two or more closed isobars at a contour interval of 4 hPa were classified as cyclone events. While cold or warm fronts may be present in the area, cyclone events are restricted to 600 km from the low pressure center (i.e. three times larger than the maximum meso- β size). The magnitude of the pressure center has no bearing on the synoptic classification.

Coastal events are similar to cyclone events, but the placement of the storm was the key criterion. Coastal low pressure centers must have been located along or just off the coast line to be classified in this group. Therefore, these events can occur on the Atlantic seaboard, the Gulf coast, and the Pacific seaboard as well. These events were also subjected to the two closed contour requirement of the cyclone events.

An event must have met three criteria to be classified as an orographic event. This classification requires the information from the station reporting the electrified convective snowfall event as well as the surrounding stations. The first criterion is that widespread precipitation must not have occurred at the time of the convective report. Secondly, neighboring stations have different reports from the station reporting the event. Reports may have been different in a number of ways including: a large difference in temperature (typically more than 7°C), a large difference in dew point (typically more than 5°C), and varying wind speeds and directions. One or both of these criteria must be met for the electrified convective snowfall event to be classified as orographic as larger phenomena may initiate the event when these criteria are not met. Lastly, the event must occur along a mountain range.

Upslope events are similar to orographic events, however upslope events have easterly rather than westerly surface winds associated with orographic events, and they occurred at or east of the Rocky Mountains. An anticyclone may have been present over the high plains or an inverted trough may stretch from north to south and form a boundary suitable for electrified convective snowfall initiation. One of these two features must be present for the event to be classified as upslope.

Lake effect or enhanced events were found within the vicinity of an unfrozen lake. Each event was indicated by strong surface flow over the unfrozen lake surface. These events can occur with or without the presence of a mid-latitude cyclone.

Finally, events not meeting the cyclone criteria most often fell into the frontal category. These events did not have a well defined cyclonic circulation or they were too far from the low pressure center to be considered cyclone events. If any event met criteria for more than one event type or no event type, then it was considered unclassifiable.

Five case studies from the 706 events were analyzed to further investigate the environment in which electrified convective snowfall events develop. These events are listed in table 2.2.1. These cases were selected from the most frequently occurring classifications: cyclonic, frontal, and orographic. With the use of the NARR data (Messenger et al. 2006), maps of 1000-500 hPa thickness and sea level pressure were created to identify the surface features and the capacity of the atmosphere to support snowfall. Geopotential heights, temperatures, and winds at 850 hPa were created to show the low-level temperature field and identify the low-level jet. Also, 700 hPa geopotential eights and absolute vorticity were plotted to diagnose possible areas of upward motion

Table 2.2.1: The five case studies analyzed to determine the environment capable of producing electrified convective snowfall events.

Date	Location	Type	Lightning/Radar Analysis
26-27 January 1996	Des Moines, IA	Cyclonic	X
24 November 2004	Peoria, IL	Cyclonic	X
3 January 1982	Dayton, OH	Frontal	
8 March 1999	Sioux Falls, SD	Frontal	X
2 December 1993	Elko, NV	Orographic	

within the layer supporting the elevated convection. Finally, 250 hPa isotachs, heights and divergence were created to diagnose the jet stream and upper level divergence. Also, cross sections of relative humidity, omega, potential temperature, and winds were produced to diagnose uplift, stability and the moisture profile. Finally, cross sections of saturated equivalent potential temperature, absolute geostrophic momentum surfaces, and equivalent potential vorticity were created and analyzed to diagnose regions of CSI. These maps and cross sections were created using GEMPAK (desJardins and Petersen, 1985).

Once this climatology was completed, three events were selected for further analysis with both the lightning data and radar imagery. Events of broad spatial and temporal extent were used to maximize available radar imagery. The selection was restricted by the availability of lightning and Level III radar imagery, and three events (26-27 January 1996, 8 March 1999, 24 November 2004) were extensive enough and long enough lived (longer than three hours) to be included.

Lightning data were used to determine the spatial extent of these three events. Lightning data pinpoint the location of the electrified convection, thus allowing an analysis in the radar imagery of both the echoes comprising the electrified convective snowfall event along with the region which boarders the event at any given time. The

event boundary is defined as the area separating the electrified and non-electrified parts of the event.

The lightning data clearly defined the spatial extent of electrified convective snowfall occurrences. With these outlines applied to the radar imagery, the images were then examined for intensity and banding patterns. Specifically, the changes around the boundaries of these events were examined in order to determine the change from the non-convective areas to the convective areas as shown by the base reflectivity. Therefore, both pattern and intensity changes across this boundary were crucial for the identification of this signature.

The datasets and methods described above are important components to this thesis and provide critical information and processes needed to meet the two primary objectives. The hourly surface station data provided information for the first objective resulting in an updated climatology of electrified convective snowfall events shown in Chapter 3. Due to the limited availability of the lightning and Level III radar data only three events were investigated for a consistent pattern or radar signature in the imagery and this is discussed in Chapter 4.

CHAPTER 3
CLIMATOLOGY OF ELECTRIFIED CONVECTIVE SNOWFALL EVENTS

A better understanding of the climatology of electrified convective snowfall events is necessary before examining the environment and radar signatures associated with these events. Ultimately, this should enable better tools for nowcasting these events and may allow people to prepare for heavy snowfalls, the crippling of the transportation infrastructure, the closure of schools, and the disruption to business.

In this chapter, a climatology of electrified convective snowfall occurrence from 1960-2005 was created so that the spatial, temporal, and environmental characteristics of electrified convective snowfall events in the continental United States may be assessed. This climatology focused on three major characteristics of electrified convective snowfall. First, the spatial distribution of overall occurrence was mapped to determine the most frequent areas of electrified convective snowfall development. Secondly, a temporal analysis demonstrated both the diurnal and seasonal preference. Finally, a synoptic classification was constructed, and five cases were selected from the most frequent classifications to illustrate details about the environment necessary for the development of these events.

3.1 Spatial Characteristics of Electrified Convective Snowfall Events

Fig. 3.1.1 shows the spatial distribution of 706 electrified convective snowfall events from 1960-2005. This figure shows events throughout the period of record (i.e., it

does not illustrate every report of electrified convective snowfall). An event is defined as an individual report of electrified convective snowfall or the initial time of a series of consecutive reports. When multiple stations reported an event, the geographic center of the events was used to illustrate the event in Fig. 3.1.1. Any reports of electrified convective snowfall more than 6 hours or 1100 km apart were considered as separate events. Using these criteria, 65 of 706 (9%) events were reported at more than one location while 624 out of 706 (88%) events were reported only once in the surface data.

Electrified convective snowfall events occurred across a large portion of the United States. A higher concentration of events is evident from eastern Nevada, through the high plains, the Midwest and into the northeastern United States. As shown in Fig. 3.1.1, this appears to be a "corridor" for electrified convective snowfall events as their occurrence decreases both north and south from this region. The western part of this corridor, including Nevada, Utah, and Arizona, is the area with the most frequent electrified convective snowfall occurrences, while the Gulf Coast and California, regions with little snowfall, are the least likely places for these events. While this analysis illustrates where the electrified convective snowfall occurrences were located over the 45-year period of record, it was necessary to investigate when these storms occurred and how the environment that produced the storms was structured in order to understand how and when electrified convective snowfall events occur. The temporal and synoptic investigations are presented throughout this chapter.

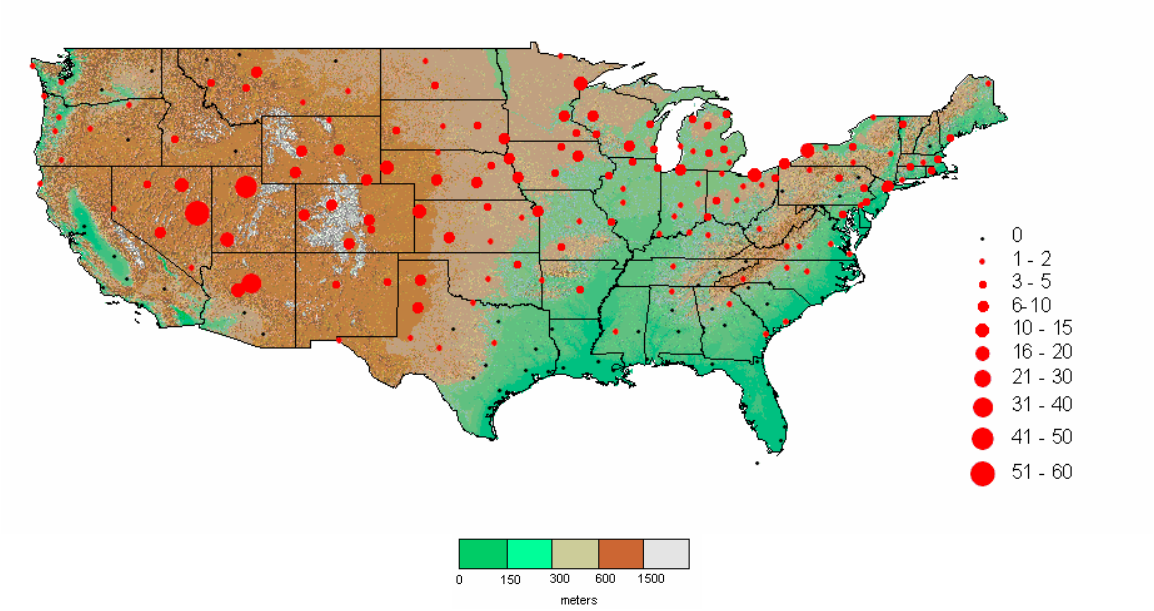

Fig. 3.1.1: The spatial distribution of 706 electrified convective snowfall events, 1960-2005. The shading represents elevation.

3.2 Temporal Characteristics of Electrified Convective Snowfall Events

A temporal analysis of electrified convective snowfall events shows the most frequent times during the cool season and the most frequent times throughout the day for development. Just as it was important to analyze where electrified convective snowfall occurred, it is important to discuss the times (both seasonally and daily) that electrified convective snowfall is likely to occur as this will aid our understanding of how and why these events develop. The season spans from September through May, as the earliest event occurred on 11 September and the latest event occurred on 12 May. As shown in Fig. 3.2.1, most electrified convective snowfall events occur late in the spring, specifically in March and April. A secondary maximum appears in November. These fall and spring maxima may be explained by the migration of the polar jet equatorward in the fall and poleward in the spring. The response of this climatological migration is an increase in the number of transient mid-latitude cyclones. The spring maximum is clearly

more prominent than the autumnal maximum and this may be described by the strengthening of storm systems and overall stronger dynamics in the spring along with the presence of cold air capable of supporting snowfall. Therefore, this suggests that cyclonic activity is a key factor in the development of electrified convective snowfall. This will be discussed in more detail later in this chapter as a part of a series of case studies.

The second aspect of the temporal analysis included a diurnal analysis of electrified convective snowfall events. When multiple reports occurred, the first report was recorded as the event time to show the initiation of the electrified convective snowfall event. Fig. 3.2.2 shows that events occurred at any time of the day, but had

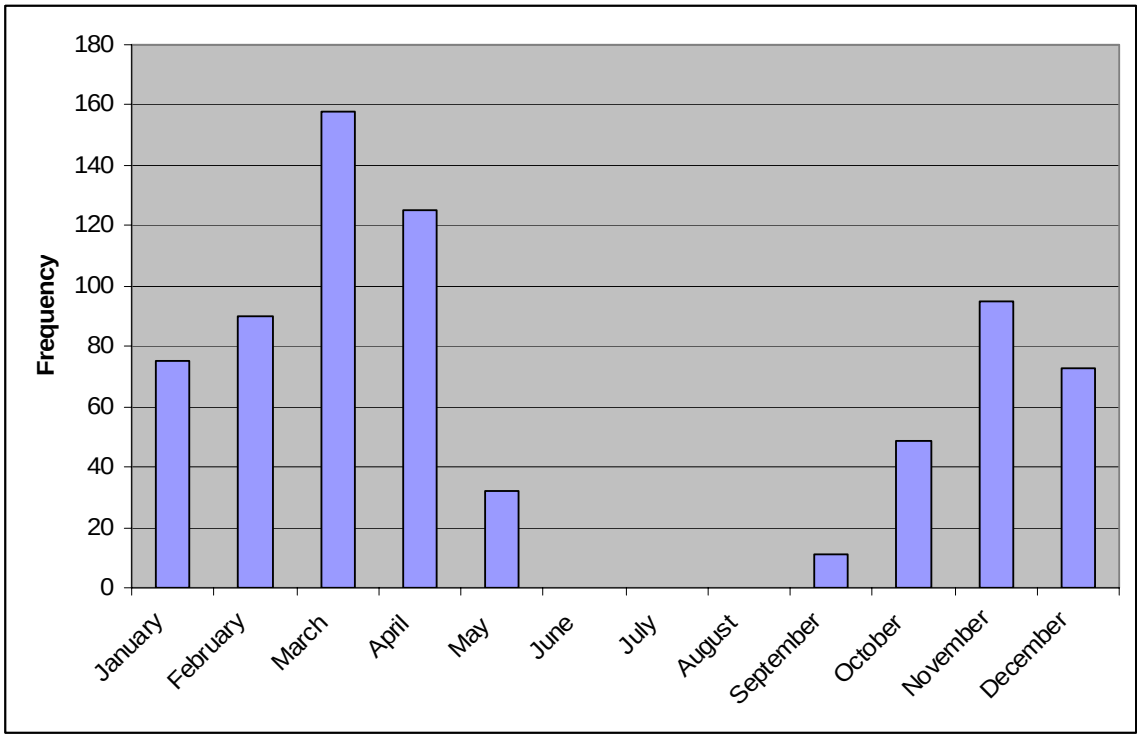

Fig 3.2.1: The monthly distribution of electrified convective snowfall events, 1960-2005.

a distinct diurnal pattern. The most common time for electrified convective snowfall was from 2100 to 0200 local time. There are two possible explanations for the pattern. First, the low-level jet is maximized during these hours (Whiteman et al. 1997) and it has been shown that the low-level jet can contribute to elevated convection, likely a key ingredient in electrified convective snowfall development (Djurić and Ladwig, 1983). Secondly, lightning is easier to detect at night as flashes can be seen over greater distances. Both of these explanations provide plausible reasons for this diurnal pattern and will be examined in subsequent sections of this chapter.

This diurnal pattern is inconsistent with the finding of no diurnal pattern by Market et al. (2002). However, this study investigated 706 electrified convective snowfall events over 45 years while Market et al. (2002) investigated 229 events from 1961-1990. This diurnal pattern of electrified convective snowfall events is important as it may provide details about mechanisms responsible for the development of these events and may reveal any biases in the detection of the events by surface observations.

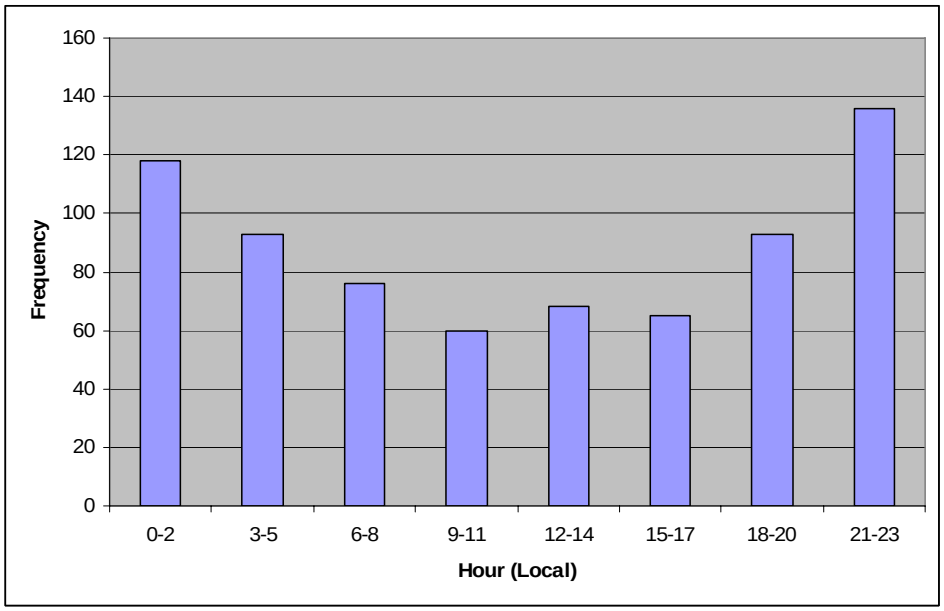

Fig 3.2.2: The hourly distribution of electrified convective snowfall events, 1960-2005.

3.3 Synoptic Characteristics of Electrified Convective Snowfall Events

All of the electrified convective snowfall events were categorized into seven synoptic types given by Market et al. (2002): coastal, mid-latitude cyclones, frontal, lake effect or enhanced, orographic, upslope, and unclassifiable. Events were classified by surface analyses using Daily Weather Maps (National Oceanic and Atmospheric Administration 1960 - 2005) and were supplemented with upper air data from the NARR. Events associated with a mid-latitude cyclone made up the largest number of events at 41% (292 of 703). Frontal events were the second most frequent type at 30% (213 of 706). The third most frequent were both coastal and orographic events at 9% each (66 of 706 were orographic and 60 of 706 were coastal events). Finally, lake effect at 6% (41 of 706 events), upslope at 4% (26 of 706), and unclassifiable events at 1% (5 of 706) were the least frequent synoptic environments. This distribution is shown in Fig. 3.3.1.

All cyclone events consisted of a transient mid-latitude cyclone containing two or more closed isobars at a contour interval of 4 hPa. An example of this is shown in Fig. 3.3.2. The electrified convective snowfall report was at Peoria, IL, at 0300 UTC on 19 March 1971 and north-westerly winds were reported; therefore, the event was located in the southwestern quadrant of the cyclonic storm with respect to the low pressure center. Most cyclonic events also exhibited frontal boundaries. However, cyclonic events were restricted to 600 km from the low pressure center to state that the event was driven by the low pressure center rather than frontal lifting.

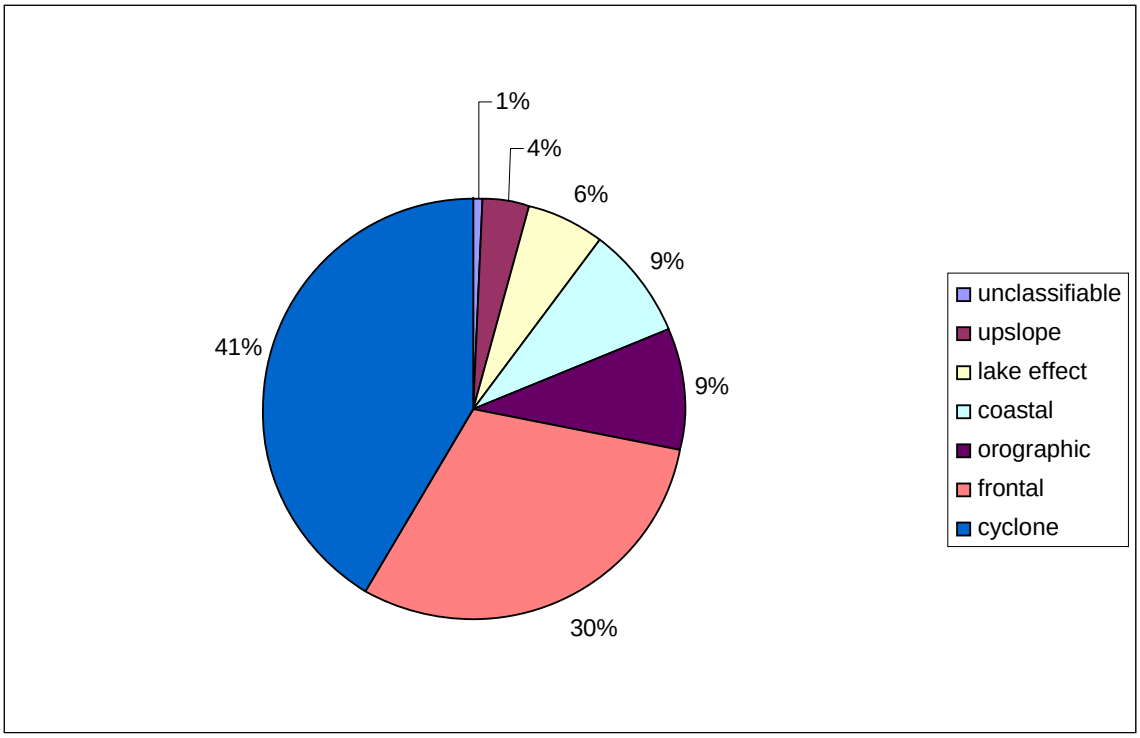

Fig. 3.3.1: The percentage of electrified convective snowfall events associated with each synoptic type.

observation. Fig. 3.3.3 shows the distribution of these events within the four quadrants of the cyclone. About two thirds of electrified convective snowfall events occurred in the northern half of the cyclone, most often in the area northwest of the low pressure center (34%). The northeast quadrant contained 33% of cyclone associated events, while 22% of the events occurred in the southwest quadrant. The southeastern quadrant contained the fewest electrified convective snowfall events at 11% likely due to the lack of frozen precipitation in the "warm sector" of the cyclone. This distribution shows that the majority of events associated with a cyclone were either downstream and north of the cyclone or within the southern half of the area upstream of the cyclone.

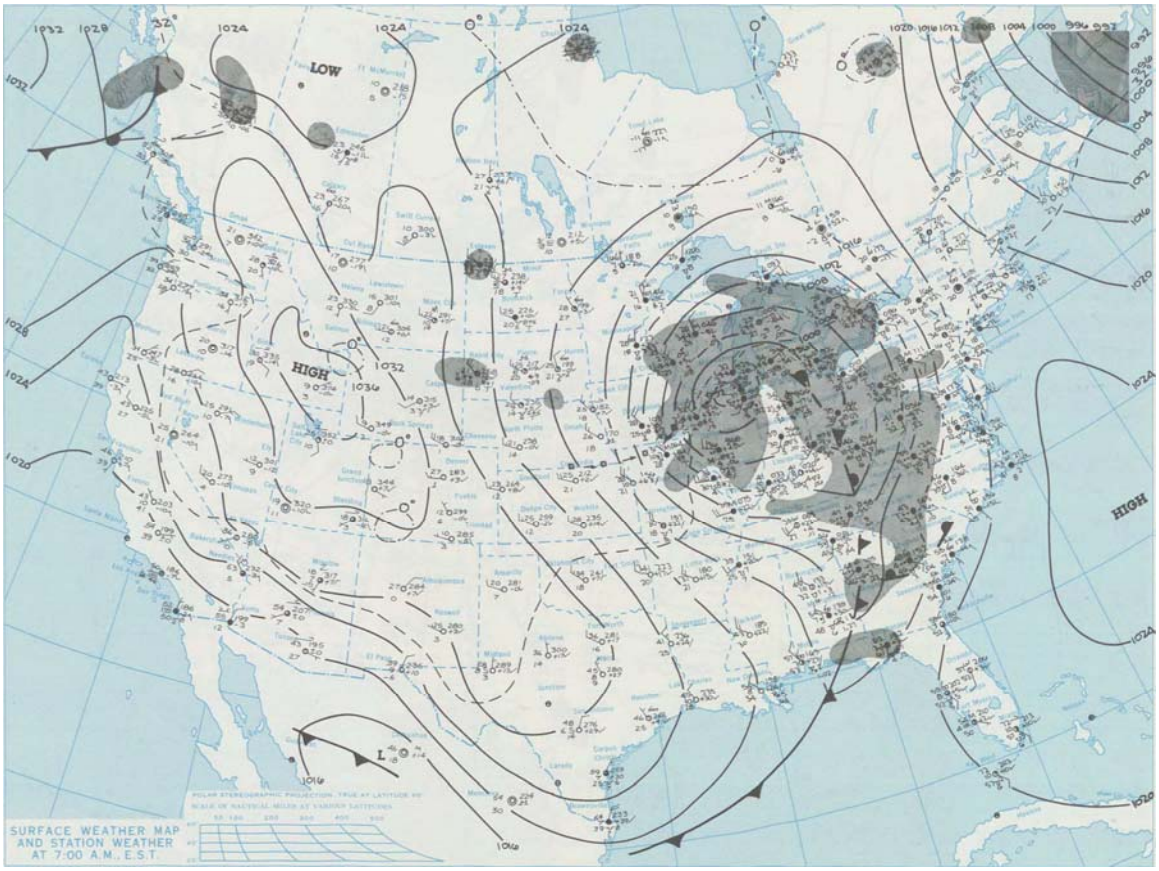

Fig. 3.3.2: A surface weather map for an example of a typical cyclonic event in the synoptic analysis. This map is dated 1200 UTC 19 March 1971. The surface analysis map is from the Daily Weather Maps Series.

Fig. 3.3.4 shows the distribution of the cyclonic events throughout the 45-year period of record. The "corridor" discussed previously was largely dominated by the cyclone events. Fig. 3.3.4 demonstrates that the majority of cyclone associated events occur from southern Nevada and northern Arizona, through Kansas and Nebraska, into the Great Lakes region. This corridor is important as it presents an area favored for the development of electrified convective snowfall. Therefore, this area can be more closely monitored during the cool season for development and can help narrow the search for heavy snowfall, elevated convection, and electrified convective snowfall events in the future.

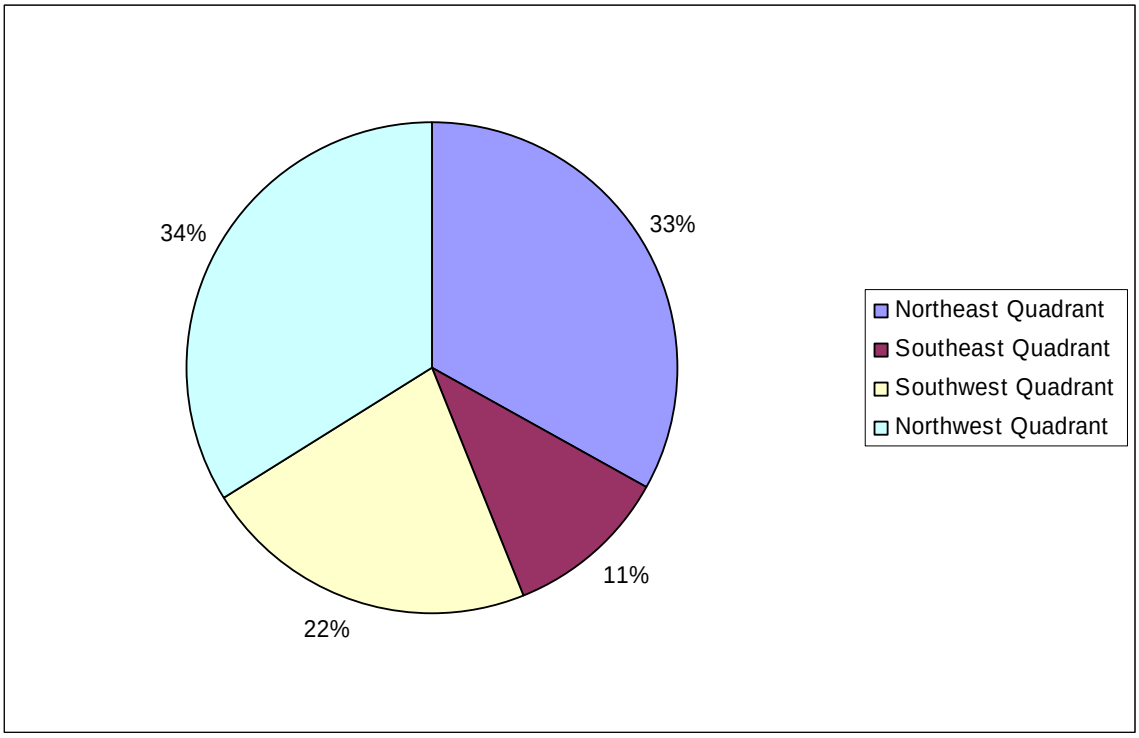

Fig. 3.3.3: The distribution of cyclone associated electrified convective snowfall events with respect to the associated low pressure center.

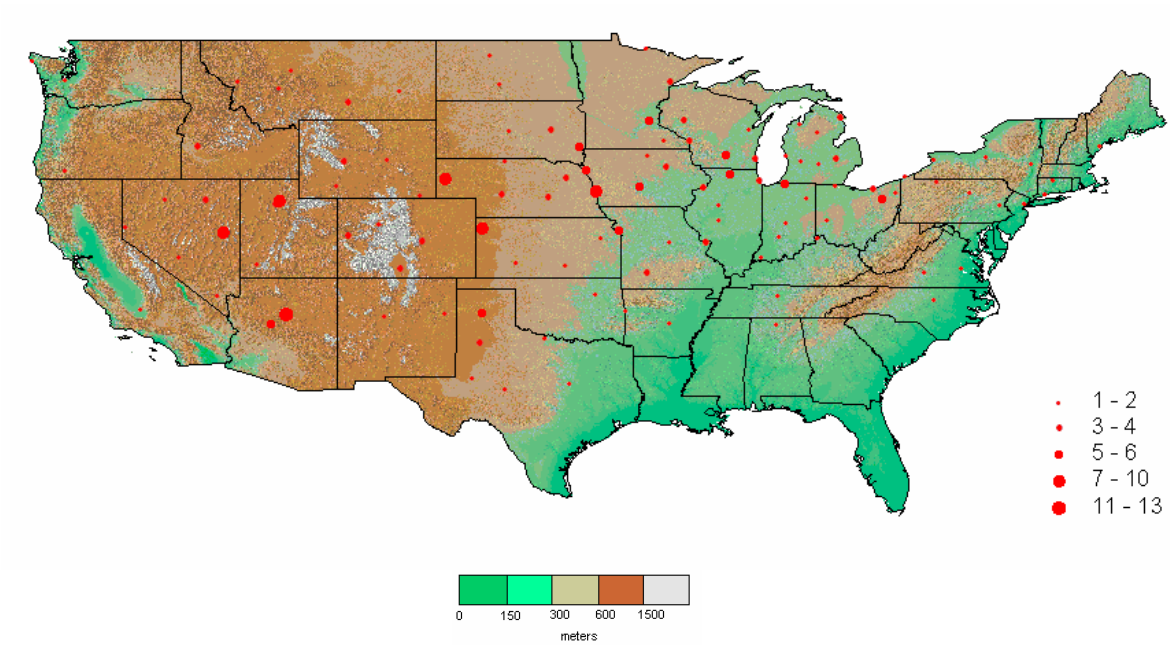

Fig. 3.3.4: The spatial distribution of cyclone associated electrified convective snowfall events, 1960-2005.

Similar to cyclone events, coastal events are described as occurring near the low pressure center of a mid-latitude cyclone. However, these storms were located along or offshore of the coasts of the Atlantic Ocean, Pacific Ocean, or the Gulf of Mexico. This classification includes, but is not limited to, both coastal "bombs" (e.g. 24 hPa drop in 24 hours) and "Nor 'Easters." A typical example of a typical surface weather map for an event classified as coastal is given in Fig. 3.3.5. The spatial distribution of coastal events can be seen in Fig. 3.3.6. Coastal events range from Georgia in the south to Maine in the north. The most common area of coastal events was concentrated in an area from Philadelphia, PA, through New York, NY, and to Boston, MA. This was likely the result

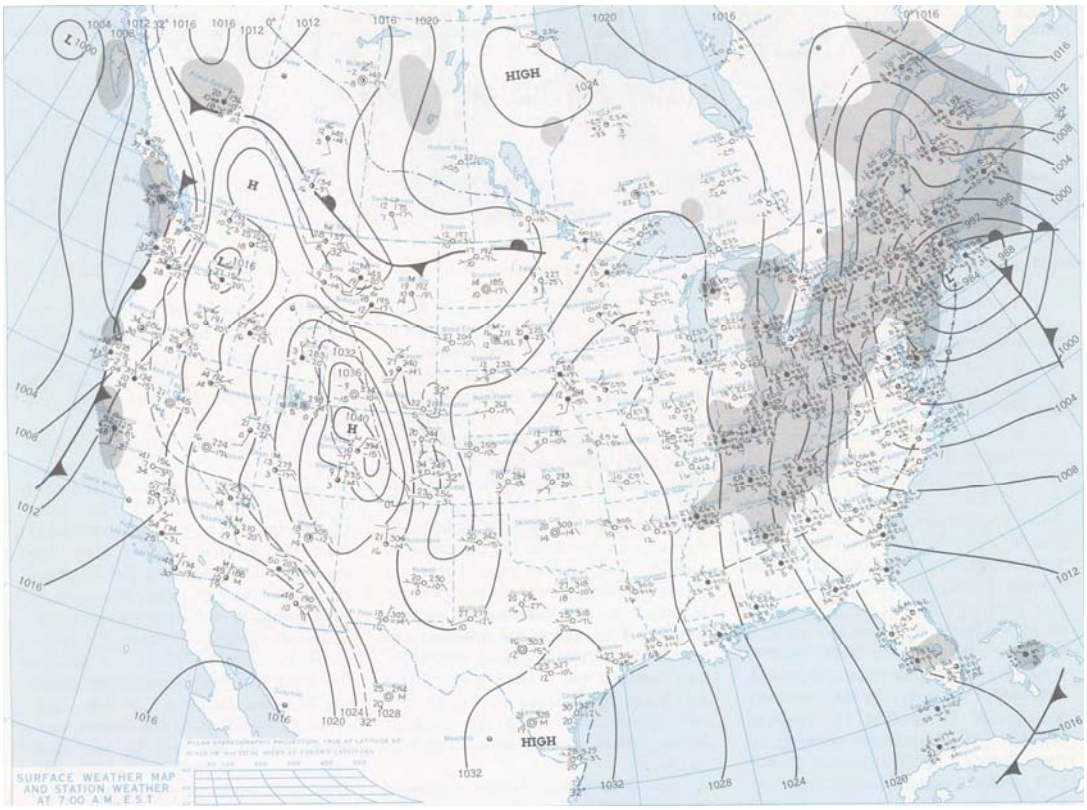

Fig. 3.3.5: A surface weather map for an example of a typical coastal event in the synoptic analysis. This map is dated 1200 UTC 29 January 1973. The surface analysis map is from the Daily Weather Maps Series.

of Nor 'Easters gaining strength as they track northward along the eastern seaboard of the United States. Coastal events can occur as far west as Kentucky and Indiana with the associated "wrap around" flow. Therefore, it is important to note that coastal events refer to the storm inducing the electrified convective snowfall and not the location of the event itself.

Orographic events required three criteria to meet this classification. The analysis of both the station reporting the electrified convective snowfall and the surrounding stations were required for this classification. First, widespread precipitation must not have occurred at neighboring stations. The second criterion for orographic events is that stations surrounding the electrified convective snowfall event will have distinctly different temperatures, dew points and wind directions (see Chapter 2 for criteria). Typically these neighboring stations reported temperatures over the freezing point, lower dew points and nearly opposing wind directions. Either of these two criteria must be met

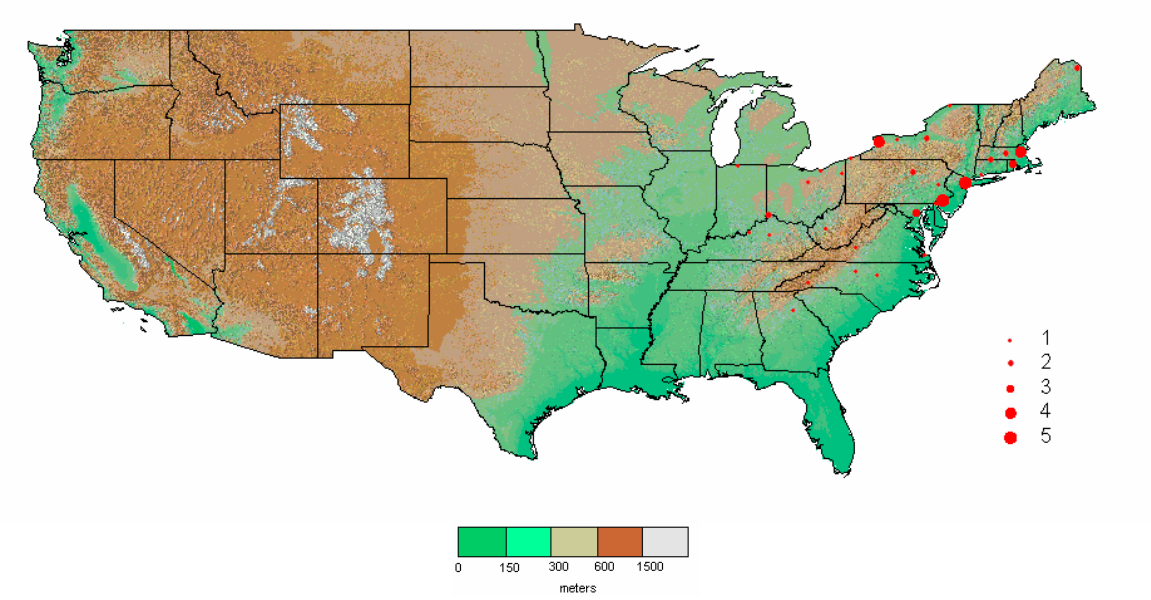

Fig. 3.3.6: The spatial distribution of coastal electrified convective snowfall events, 1960-2005.

for the event to be classified as orographic. Lastly, the event must occur in the area of a mountain range.

Fig. 3.3.7 shows a surface weather map for an orographic electrified convective snowfall occurred that at Ely, NV, at 1300 UTC on 12 November 1980. A high pressure center was located to the over the Wyoming and South Dakota indicating the absence of cyclonic or frontal lifting. Widespread precipitation was not occurring throughout the area, and westerly flow was present in the area. All orographic convective snowfall events occurred from the Rocky Mountains and west with none in the Appalachian Mountains (Fig. 3.3.8). The most common location for orographic events was

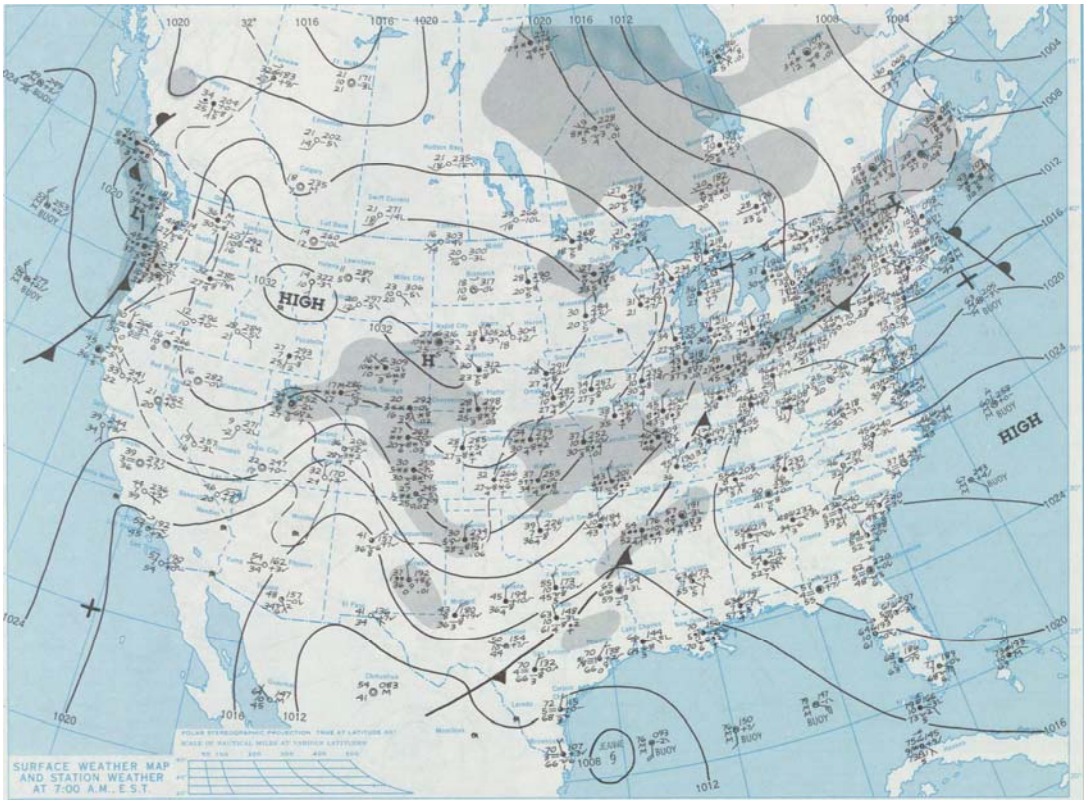

Fig. 3.3.7: A surface weather map for an example of a typical orographic event in the synoptic analysis. This map is dated 1200 UTC 12 November 1980. The surface analysis map is from the Daily Weather Maps Series.

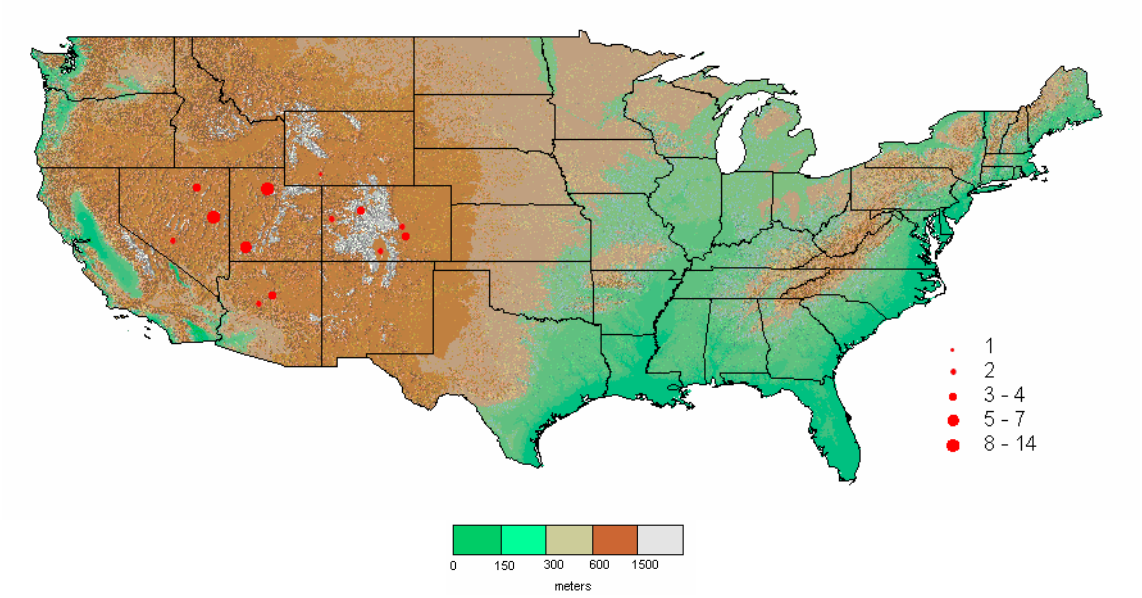

Fig 3.3.8: The spatial distribution of orographic electrified convective snowfall events, 1960-2005.

Salt Lake City, UT, and Ely, NV. Orographic events occurred only in five states: Arizona, Colorado, Nevada, Utah, and Wyoming and were the most common synoptic type in this region.

Lake effect or enhanced were found in two areas: throughout the Great Lakes region and the Great Salt Lake. All of these events were indicated by strong surface flow over unfrozen lake surfaces. Typically, these events occurred within the cooler air behind a mid-latitude cyclone (lake effect); however, events outside the criteria (further than 600 km from the low pressure center) for cyclone and frontal events were considered lake enhanced events when appropriate.

Fig. 3.3.9 shows a lake enhanced electrified convective snowfall event at Buffalo, NY, on 25 November 1991. In this case, the low pressure center was too far removed from the event to consider the report as a cyclone event. However, due to the pressure gradient introduced by the cyclone and a high pressure center located near Grand Forks,

ND, significant lake enhanced snowfall occurred across much of the Great Lakes region. During this event, a northwesterly wind was present to initiate the enhanced snowfall.

As shown in Fig. 3.3.10, the most frequent places for lake effect/enhanced electrified convective snowfall included Buffalo, NY, Erie, PA, and Cleveland, OH. These three cities experienced more lake effect/enhanced electrified convective snowfall events than the Great Salt Lake. This higher frequency can be attributed to the larger number of lake enhanced events that occurred over the Great Lakes compared to the Great Salt Lake, the larger size of the Great Lakes, and the greater number of stations surrounding the Great Lakes.

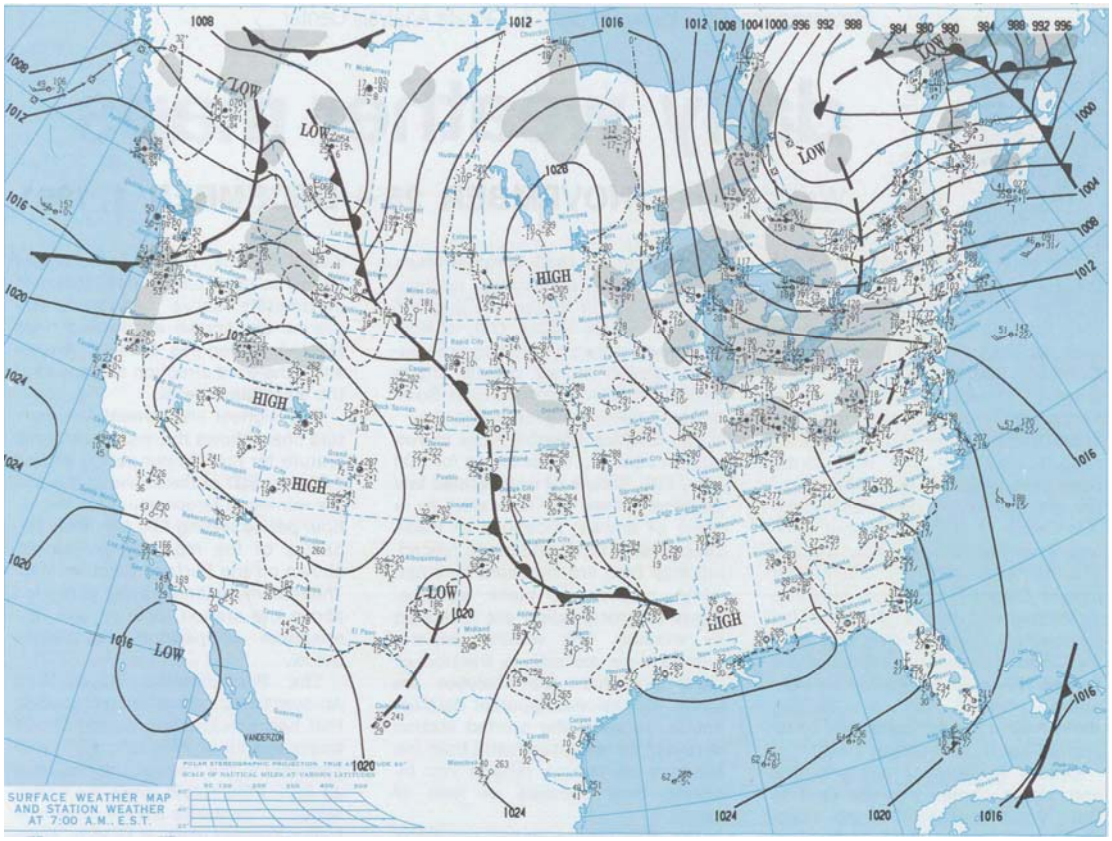

Fig. 3.3.9: A surface weather map for an example of a typical lake effect/enhanced event in the synoptic analysis. This map is dated 1200 UTC 25 November 1991. The surface analysis map is from the Daily Weather Maps Series.

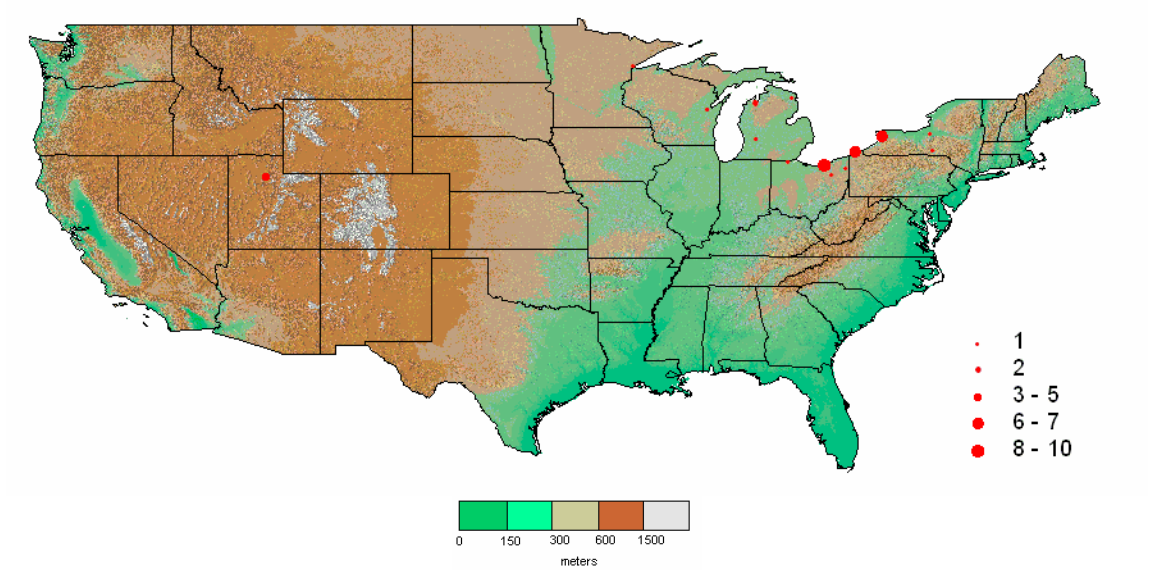

Fig. 3.3.10: The spatial distribution of lake effect/enhanced electrified convective snowfall events, 1960-2005.

A synoptic environment dominated by frontal lifting is also capable of supporting electrified convective snowfall events. These events did not have a well defined cyclonic circulation, or they were too far removed from the low pressure center to be considered cyclone events. Typically, the electrified convective snowfall report was poleward of a warm front. While not a criterion, these events were typically associated with weaker storms than the events classified as cyclone events. Fig. 3.3.11 shows a frontal event that occurred poleward of a quasi-stationary frontal boundary.

In general, frontal events occurred along the same "corridor" as identified in the cyclonic classification. This pattern can be attributed to the similarities of frontal events to cyclone events and that frontal events occur along the front, but typically they are too far removed from the low pressure center to be classified as a cyclone event. Therefore, frontal events further reinforce this "corridor" of electrified convective snowfall events, particularly in the western United States as shown by Fig. 3.3.12.

The final and least frequent synoptic environment for electrified convective snowfall events is dominated by upslope winds along the eastern slopes of the Rocky Mountains and the High Plains. All of these events occurred from Montana and North Dakota in the north to Colorado and Kansas in the south. Each event showed an easterly surface wind due to the presence of an anticyclone in the north-central United States (e.g. North Dakota or Minnesota) coupled with a weak cyclonic circulation near or west of the Rocky Mountains. Another possible mechanism was the presence of an inverted trough

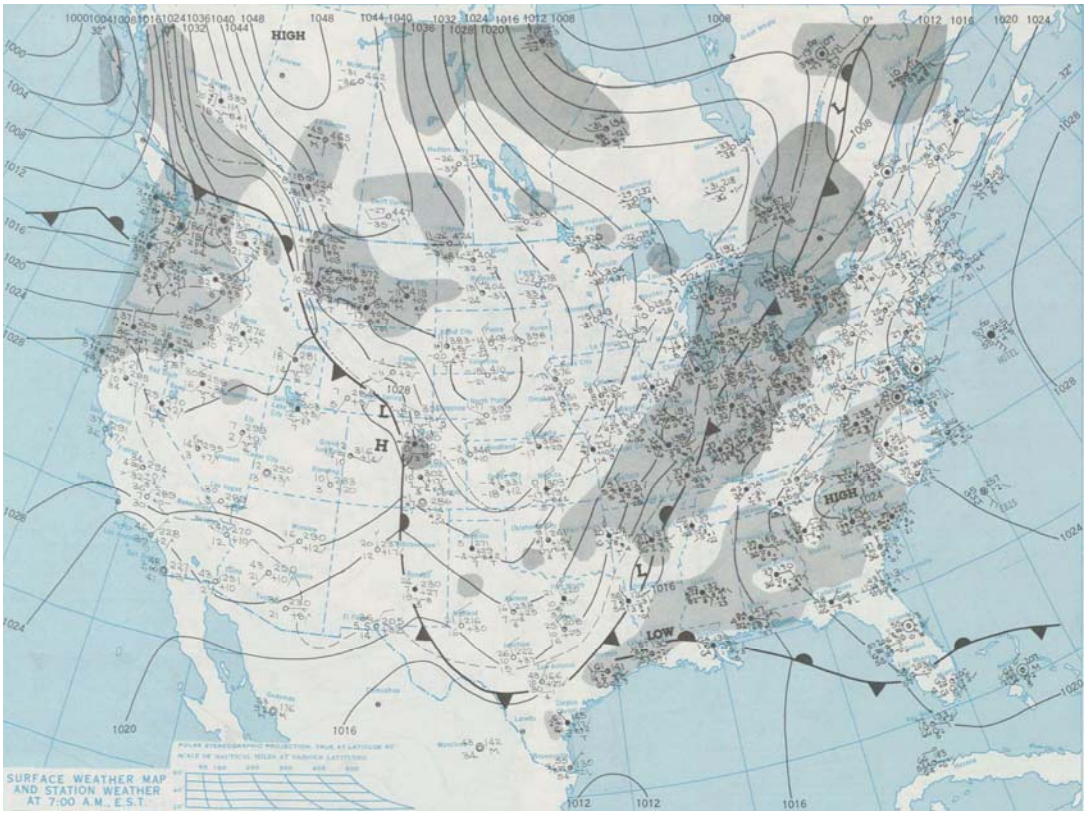

Fig. 3.3.11: A surface weather map for an example of a typical frontal event in the synoptic analysis. This map is dated 1200 UTC 7 January 1976. The surface analysis map is from the Daily Weather Maps Series.

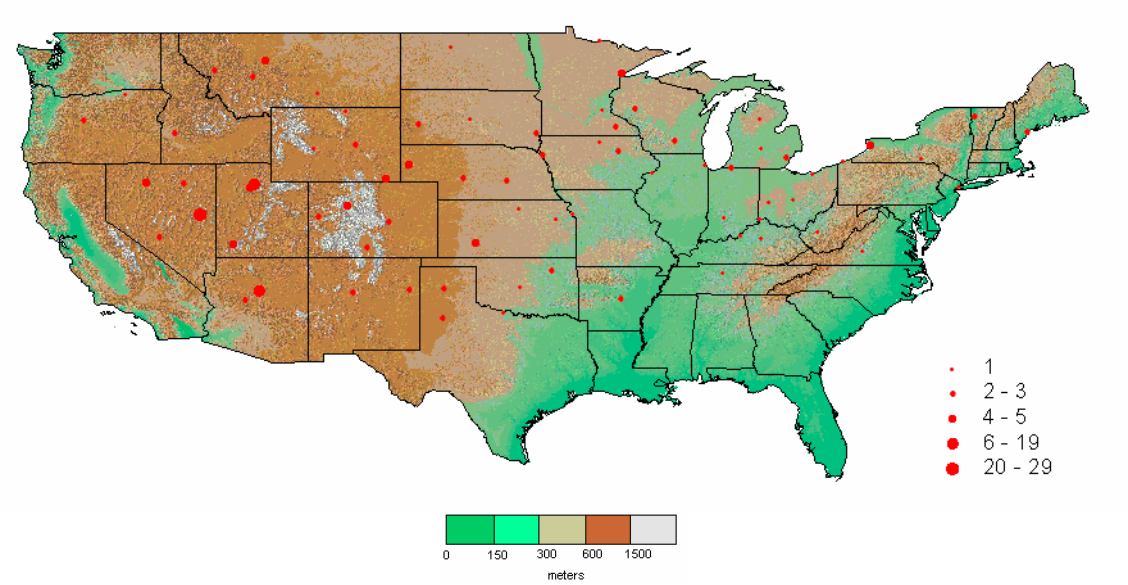

Fig 3.3.12: The spatial distribution of frontal electrified convective snowfall events, 1960-2005.

along the eastern slopes of the Rocky Mountains, southward into the panhandle of Texas. Fig. 3.3.13 shows this inverted trough in this event at 0600 UTC in Cheyenne, WY, on 20 April 1984 along with an easterly surface wind and a cyclonic circulation near the Front Range of the Rocky Mountains.

All upslope events occurred west of the Mississippi River typically along or east of the Rocky Mountains. Along with orographic events, the upslope classification of electrified convective snowfall events was spatially constricted to only seven states including Montana, North Dakota, Wyoming, South Dakota, Colorado, Nebraska, and Kansas. From Fig. 3.3.14 it is clear that Wyoming was the most frequent area for upslope induced electrified convective snowfall events, as 10 of 21 events occurred in this state. Finally, the seven which met the criteria for multiple synoptic categories or met none of these criteria were then grouped together accordingly in the unclassifiable category and no spatial pattern was recognized.

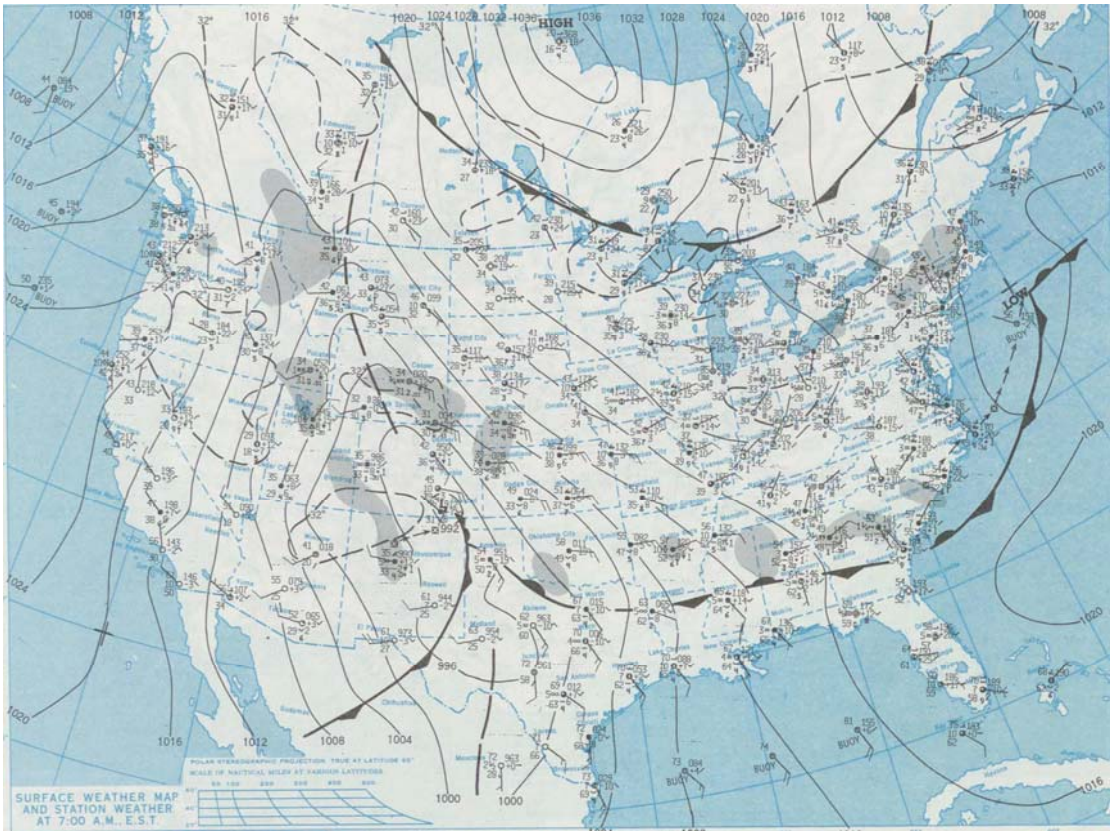

Fig. 3.3.13: A surface weather map for an example of a typical upslope event in the synoptic analysis. This map is dated 1200 UTC 20 April 1984. The surface analysis map is from the Daily Weather Maps Series.

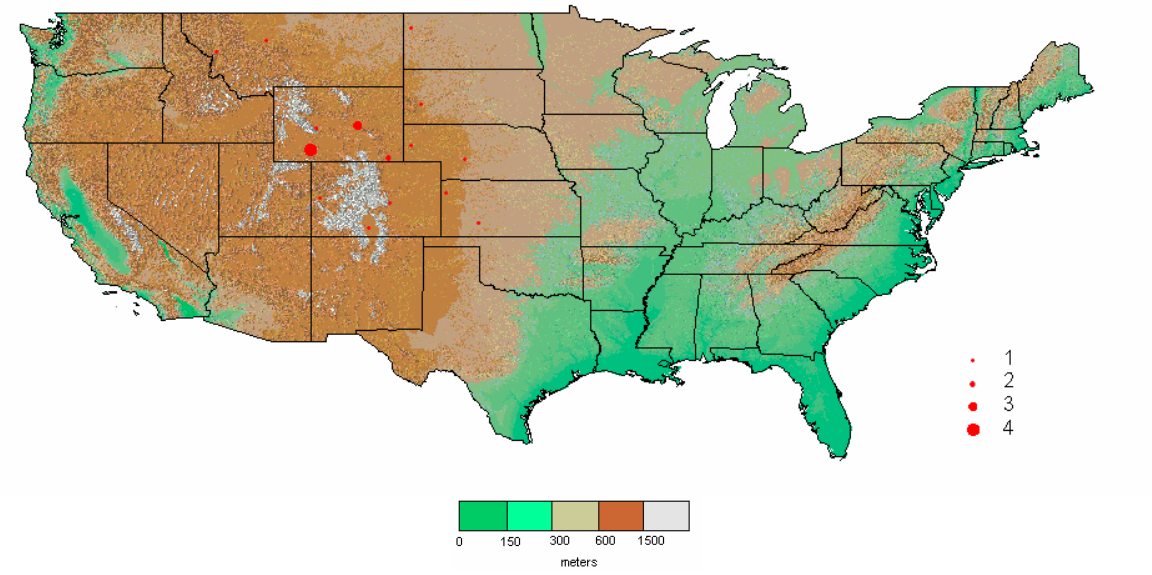

Fig 3.3.14: The spatial distribution of upslope electrified convective snowfall events, 1960-2005.

3.4 Case Studies

To illustrate the environment in which electrified convective snowfall events occurred and therefore understand how and why they develop, five events including two cyclone events (26-27 January 1996 and 24 November 2004), two frontal events (3 January 1982 and 8 March 1999), and one orographic event (2 December 1983) were analyzed. These events were selected because each occurred over a period longer than two hours, and therefore, more data is available for analysis. Also, these electrified convective snowfall events are representative of the three most prevalent synoptic classifications: cyclonic, frontal, and orographic.

a. 26-27 January 1996 Cyclonic Event

A cross section of wind barbs, potential temperature, omega, and relative humidity from New Orleans, LA, to International Falls, MN, created from the NARR data illustrates the vertical environment during the 26-27 January 1996 cyclonic electrified convective snowfall event at Des Moines, IA (DSM) (Fig. 3.4.1). The first report of the event occurred at 1800 UTC on 26 January 1996 and the last at 0000 UTC on 26 January 1996 all at DSM. A moist tongue was present through and north of the event location; coupled with omega values of approximately -10 μbs^{-1} at 700 hPa, this indicates the presence of isentropic upglide. An unstable environment is identified by the tightly packed isentropes from 925 hPa to 700 hPa, indicating elevated convection. Also, southerly to south-easterly winds in a veering profile dominated the surface to 700 hPa, and coupled with the increasing values of potential temperature from south to north, warm air advection in this area may have induced upward motion in proximity to DSM.

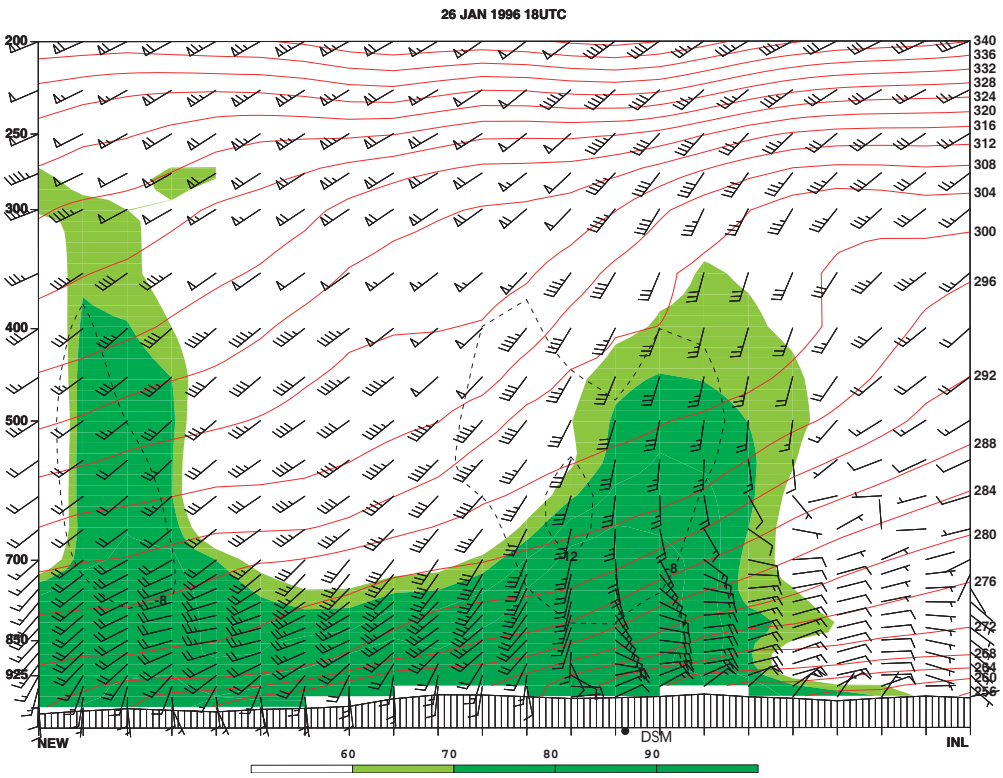

Fig. 3.4.1: A cross section of wind barbs (ms^{-1}), potential temperature (K, in red), omega (μbs^{-1}, dashed black) and relative humidity (percent, shaded) from New Orleans, LA, to International Falls, MN, at 1800UTC 26 January 1996.

A skew-t thermodynamic diagram created from the NARR data at DSM, 1800 UTC 26 January 1996 illustrates that the atmosphere was sufficiently moist for equivalent potential vorticity (EPV) diagnosis from the surface up to 500 hPa as relative humidity values exceeded 60% (Fig. 3.4.2). Examining this same layer in the Fig. 3.4.3 reveals that negative values of EPV existed between 600 and 500 hPa. This indicates that either CSI or CI was present in the layer. However, the contours of saturated equivalent potential temperature (Θ_{es}) run quasi-parallel with contours of absolute geostrophic momentum (M_g). As discussed in Chapter 1, this relationship between EPV and M_g indicates that CSI was present within the layer. Therefore, the presence of CSI likely drove the elevated convection and thus the event in this layer between 600 and 500 hPa.

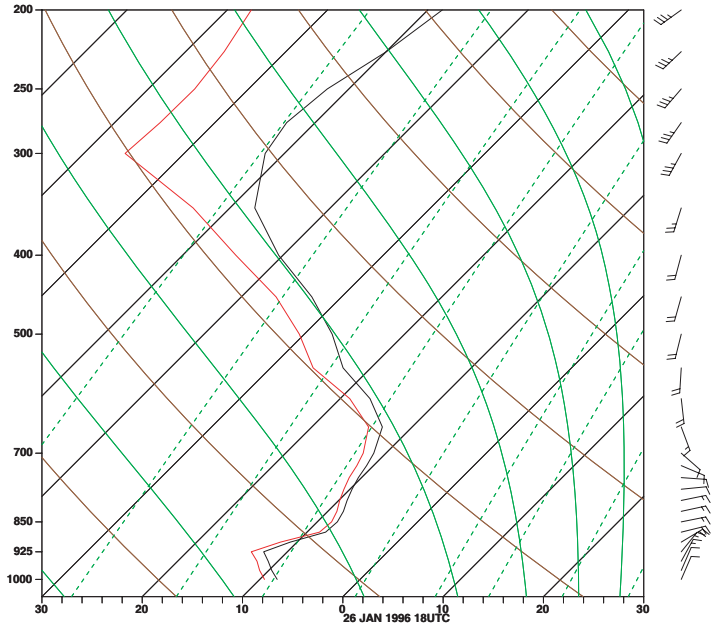

Fig. 3.4.2: A skew-t thermodynamic diagram from Des Moines, IA, at 1800 UTC 26 January 1996. The solid green lines are moist adiabats, brown are dry adiabats, dashed green lines are saturation mixing ratio, the black trace is temperature and the red trace is dew point temperature.

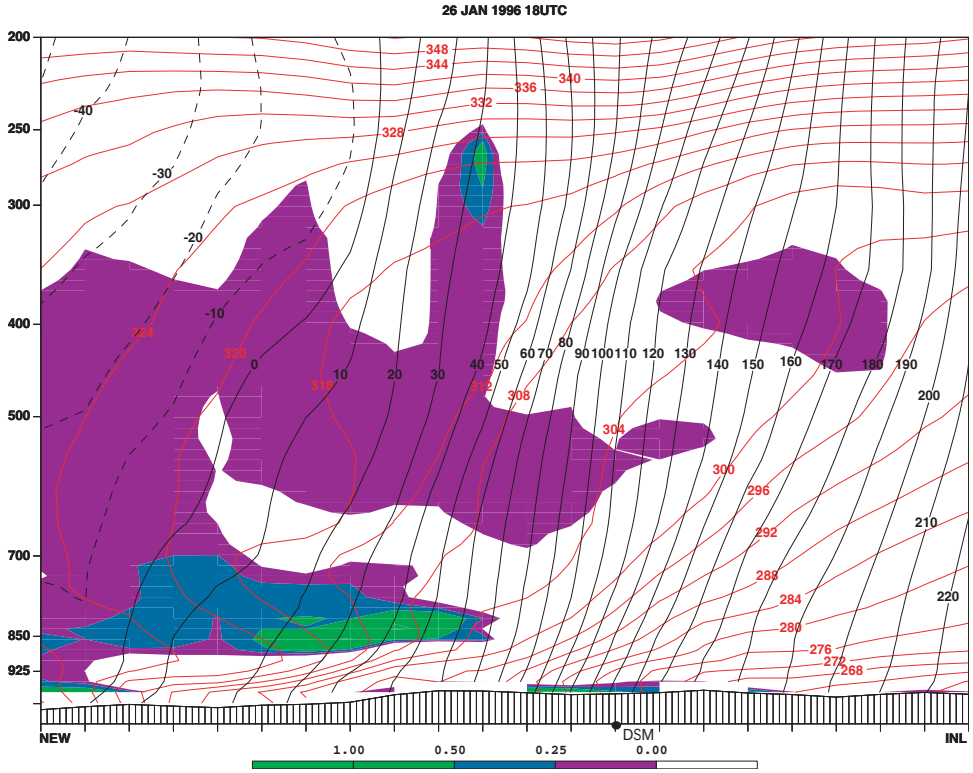

Fig. 3.4.3: A cross section of saturated equivalent potential temperature (K, red), absolute geostrophic momentum (ms^{-1}, black) and equivalent potential vorticity (PVU (10^{-6} m^2 K s^{-1} kg^{-1}), shaded) from New Orleans, LA, to International Falls, MN, at 1800 UTC 26 January 1996.

The cyclone associated with the storm was centered over western Iowa and northern Illinois and cooler air behind the cyclone is indicated by the lower thicknesses (Fig. 3.4.4). The 5400 gpm line was located south and east of Des Moines and the temperature sounding was less than 0°C. This suggests, the atmosphere was cold enough to sustain snowfall in the area. At 850 hPa, the low pressure center was located just to the east of Des Moines and the temperature field indicates temperatures were at or below -10°C (Fig. 3.4.5). A 700 hPa absolute vorticity maximum was located over the Des Moines area and indicates an area of possible upward motion (Fig. 3.4.6). Finally, a jet stream analysis reveals that Des Moines and the surrounding areas were located north of the jet stream and therefore within the cooler Artic air mass. Therefore, the jet stream dynamics do not appear to play a key role (Fig. 3.4.7).

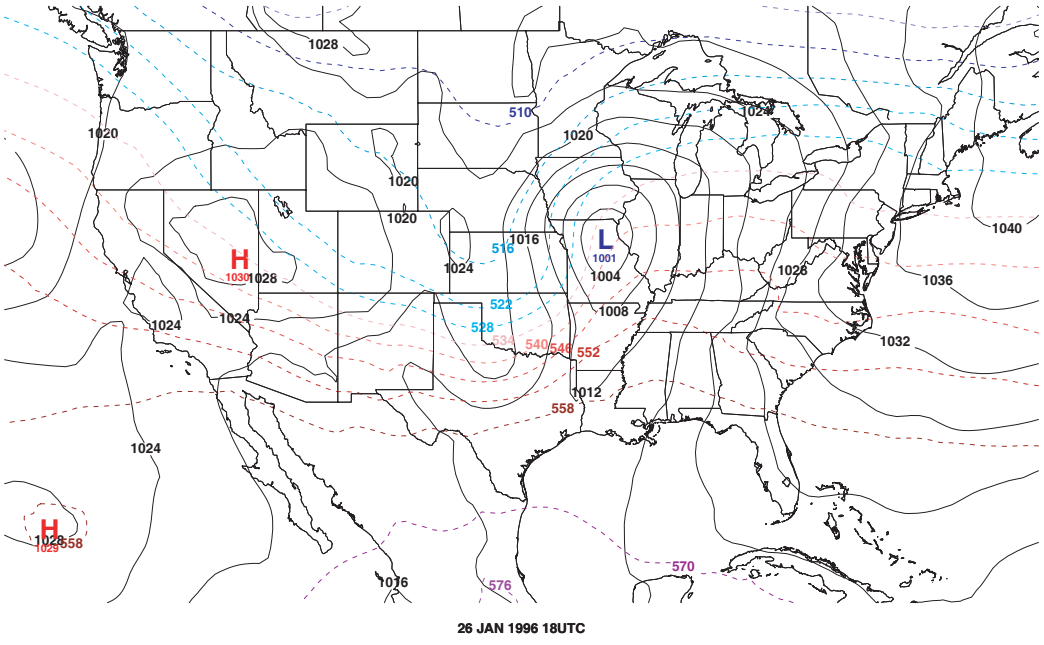

Fig. 3.4.4: Sea level pressure (hPa, black contours) and 1000-500 hPa thickness (gpm, dashed contours) at 1800 UTC 26 January 1996.

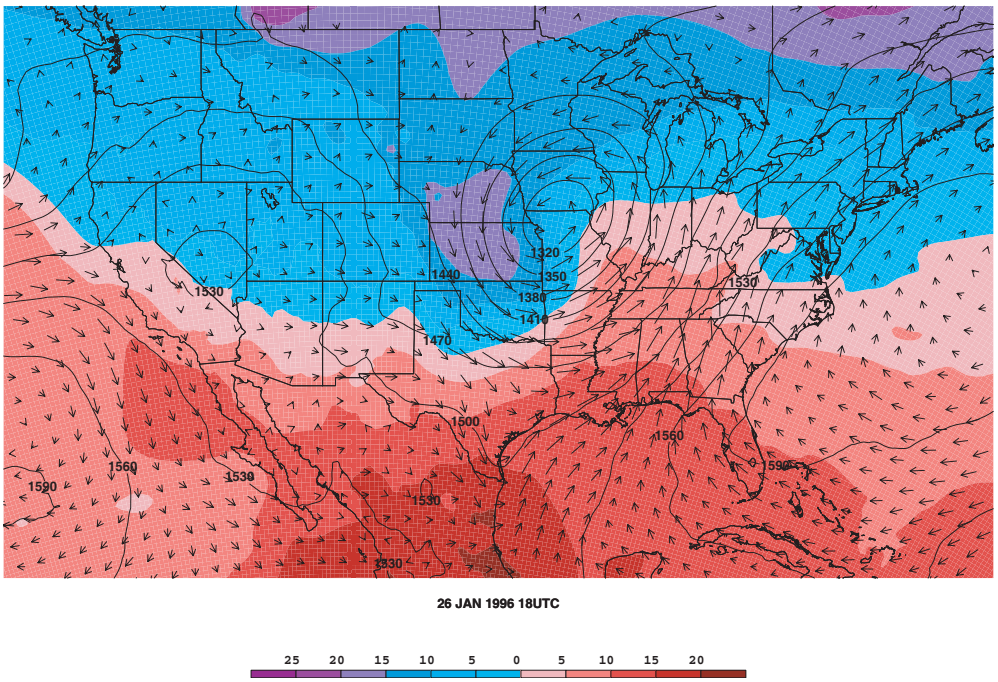

Fig. 3.4.5: 850 hPa temperature (°C, shaded color), geopotential height (gpm, black contours) and wind vectors (ms^{-1}, black arrows) at 1800 UTC 26 January 1996.

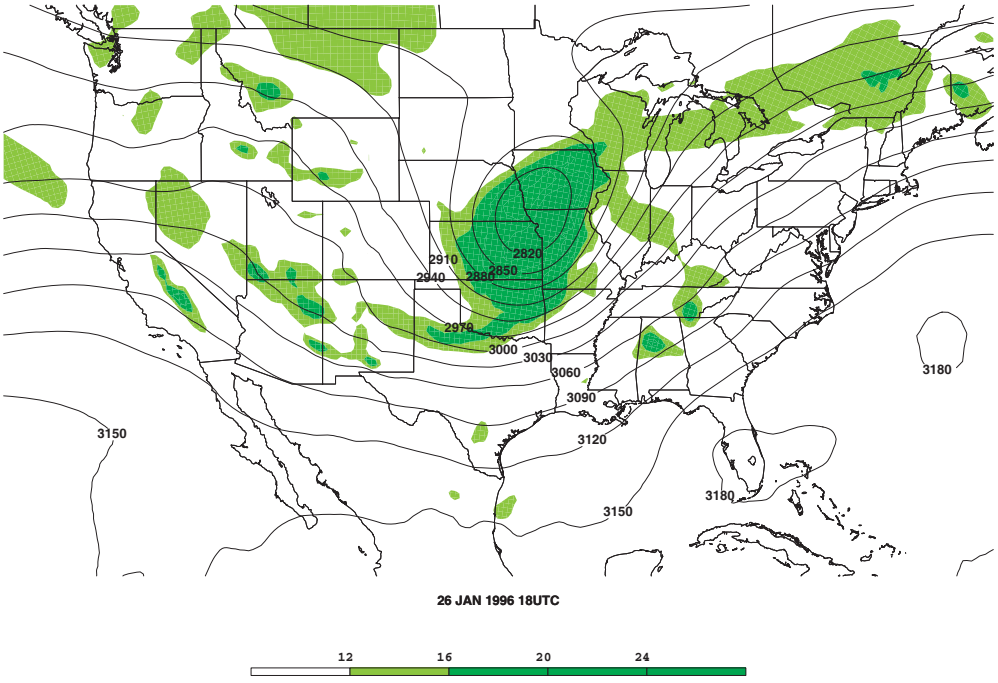

Fig. 3.4.6: 700 hPa absolute vorticity (s^{-1}, shaded color) and geopotential height (gpm, black contours) at 1800 UTC 26 January 1996.

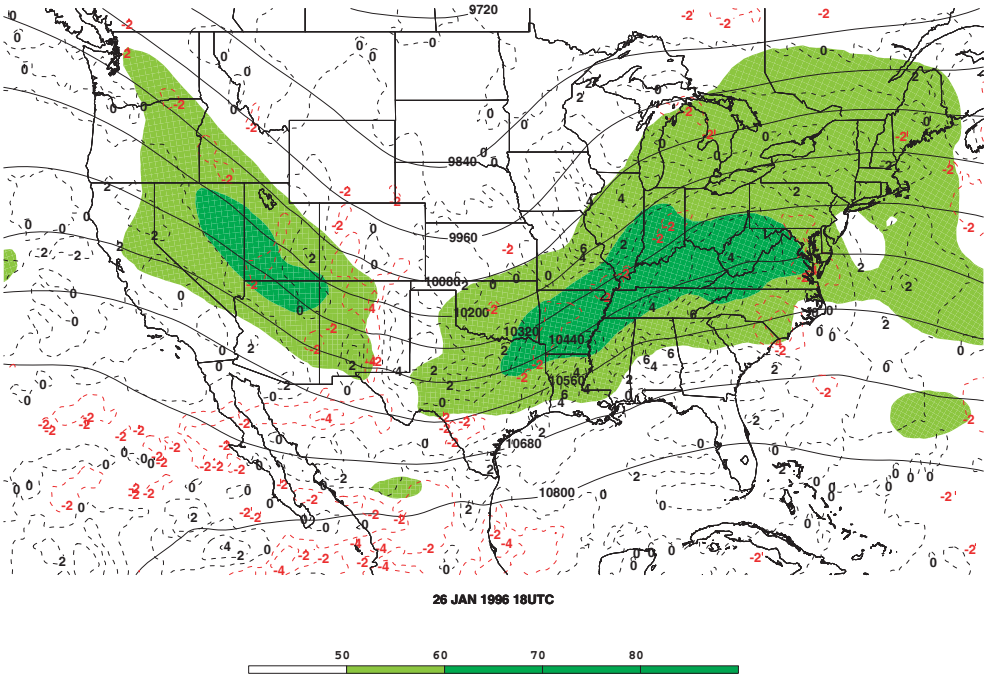

Fig. 3.4.7: 250 hPa isotachs (ms^{-1}, shaded color), divergence (10^{-5} s^{-1}, red and black dashed contours), and geopotential height (gpm, black contours) at 1800 UTC 26 January 1996.

b. 24 November 2004 Cyclonic Event

On 24 November 2004 a cyclonic electrified convective snowfall event occurred at Peoria, IL, (PIA) and a cross section of the atmosphere illustrates the state of the atmosphere during the event. Reports of thunder snow associated with this event occurred at PIA from 0600 UTC to 1800 UTC. Ample moisture coupled with north north-easterly surface winds indicate that the event occurred on the western side of the cyclone (Fig. 3.4.8). Also indicated by the cross section is warm air advection by the increase in potential temperature from north to south and the strong veering profile. Also, omega values of -4 μbs^{-1} were located in the area. Therefore, the synoptic scale ascent associated with this event was weaker than the other cases. However, the packed isentropes between 925 hPa and 750 hPa indicate a less stable environment.

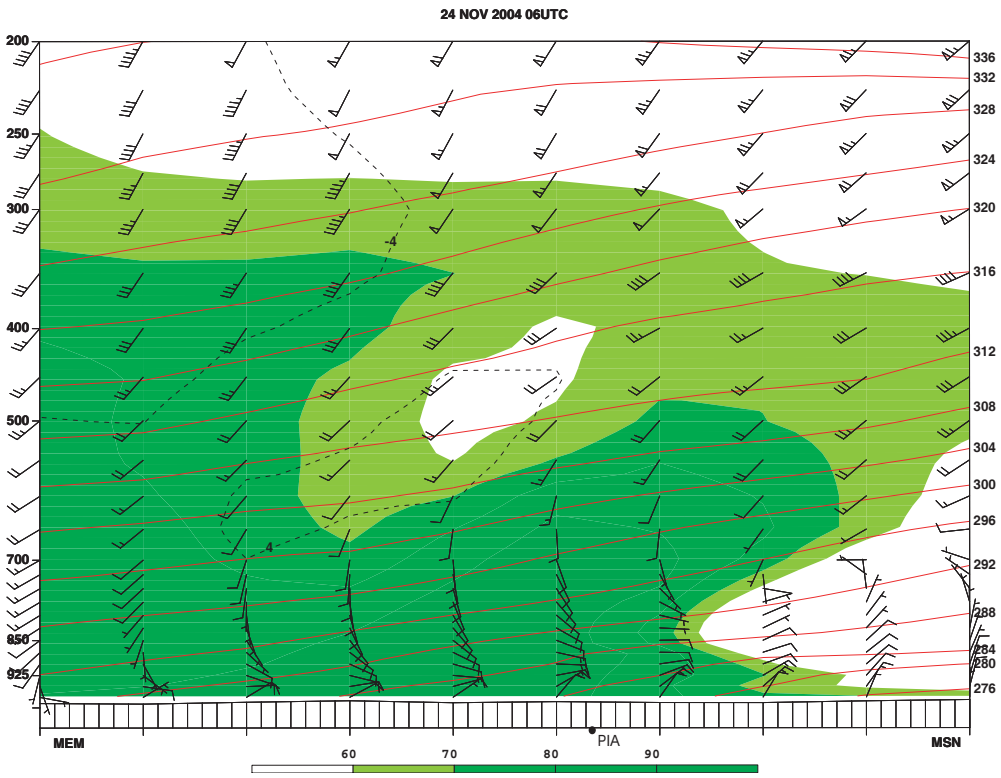

Fig. 3.4.8: A cross section of wind barbs (ms^{-1}), potential temperature (K, in red), omega (μbs^{-1}, dashed black) and relative humidity (percent, shaded) from Memphis, TN, to Madison, WI, at 0600 UTC 24 November 2004.

The skew-t thermodynamic diagram created from the NARR data from Peoria, IL, at 0600 UTC 24 November 2004 indicates a sufficiently moist layer from 750 to 650 hPa (Fig. 3.4.9). An analysis of this same layer in Fig. 3.4.10 illustrates negative values of EPV. These negative values indicate the likely presence of CSI or CI in the layer. The presence of CSI in this layer is evidenced by the quasi-parallel relationship between the contours of M_g and Θ_{es} as illustrated in the vertical cross section (Fig. 3.4.10). Therefore, CSI is the instability within the layer from 750 to 650 hPa that was the dominating feature associated with the electrified convective snowfall event.

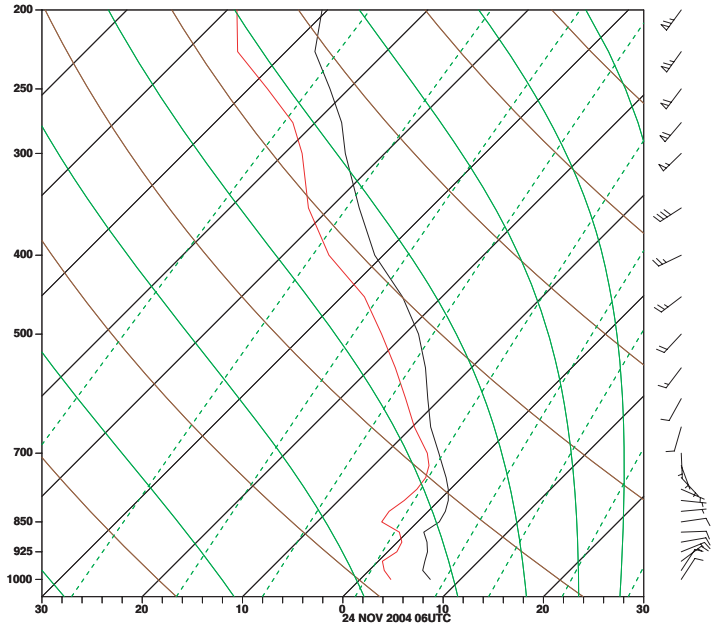

Fig. 3.4.9: A skew-t thermodynamic diagram from Peoria, IL, at 0600 UTC 24 November 2004. The solid green lines are moist adiabats, brown are dry adiabats, dashed green lines are saturation mixing ratio, the black trace is temperature and the red trace is dew point temperature.

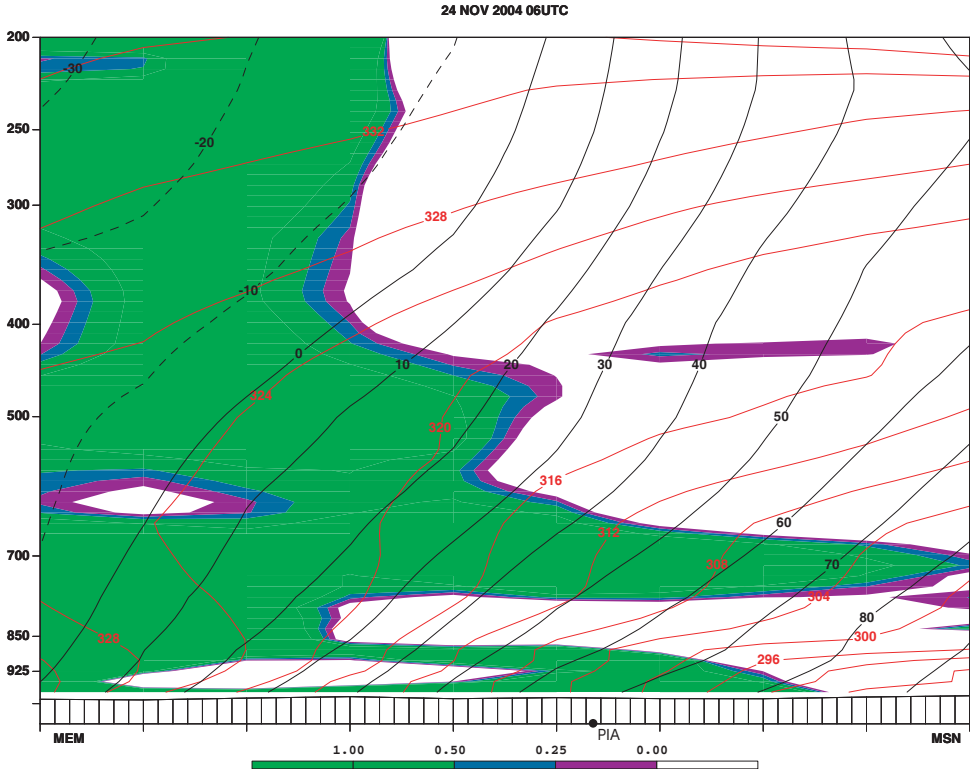

Fig. 3.4.10: A cross section of saturated equivalent potential temperature (K, red), absolute geostrophic momentum (ms^{-1}, black) and equivalent potential vorticity (PVU (10^{-6} m^2 K s^{-1} kg^{-1}), shaded) from Memphis, TN, to Madison, WI, at 0600 UTC 24 November 2004.

An analysis of the sea-level pressure field indicates that the surface cyclone was located to the south of the electrified convective snowfall event (Fig. 3.4.11). Also, at 850 hPa, a cold pool of air was pulled southward behind the storm system providing a low-level environment capable of producing snowfall (Fig. 3.4.12). A zone of deformation is indicated in the lower levels from central Missouri to western Ohio at the nose of the low-level jet (Fig. 3.4.12). At 700 hPa, slight positive vorticity advection was occurring near and south of the event location and therefore may be leading to slight upward motion along with the possible development of a low-level jet in the area (Fig. 3.4.13). The jet stream analysis indicates that Peoria was near the right entrance region of one jet streak and the left exit of another. Thus, this is a coupled jet and a probable area of upward motion. Also, upper air divergence was present (Fig. 3.4.14).

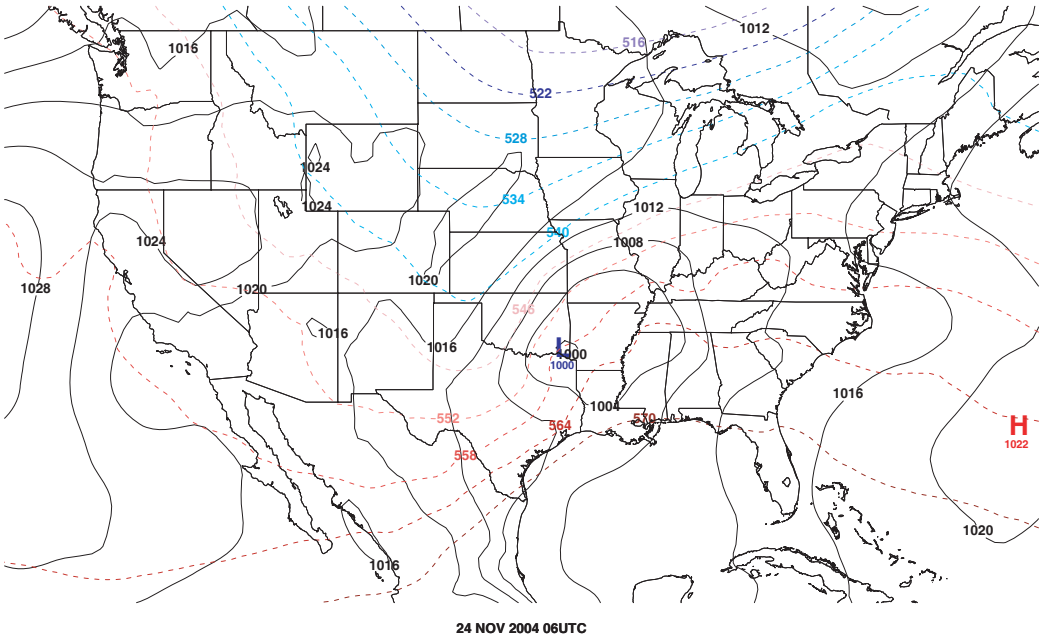

Fig. 3.4.11: Sea level pressure (hPa, black contours) and 1000-500 hPa thickness (gpm, dashed contours) at 0600 UTC 24 November 2004.

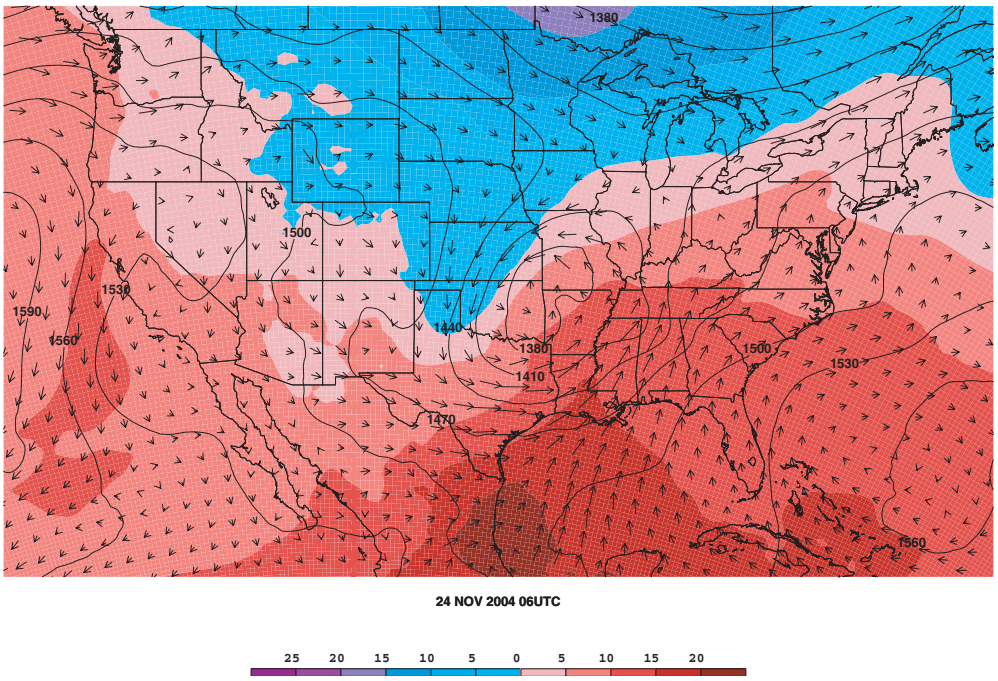

Fig. 3.4.12: 850 hPa temperature (°C, shaded color), geopotential height (gpm, black contours) and wind vectors (ms^{-1}, black arrows) at 0600 UTC 24 November 2004.

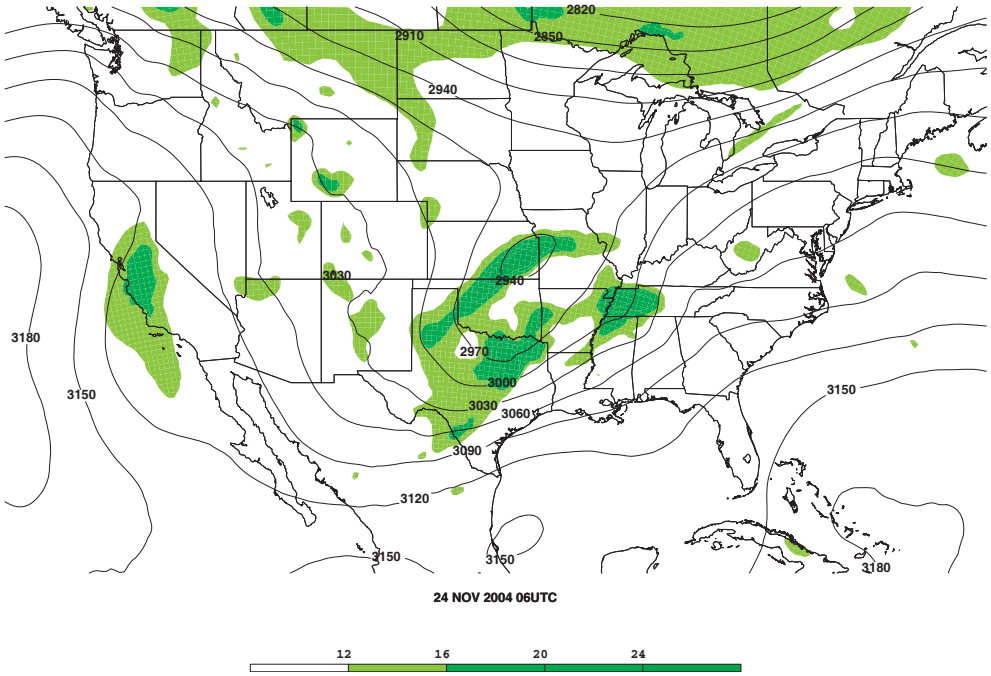

Fig. 3.4.13: 700 hPa absolute vorticity (s^{-1}, shaded color) and geopotential height (gpm, black contours) at 0600 UTC 24 November 2004.

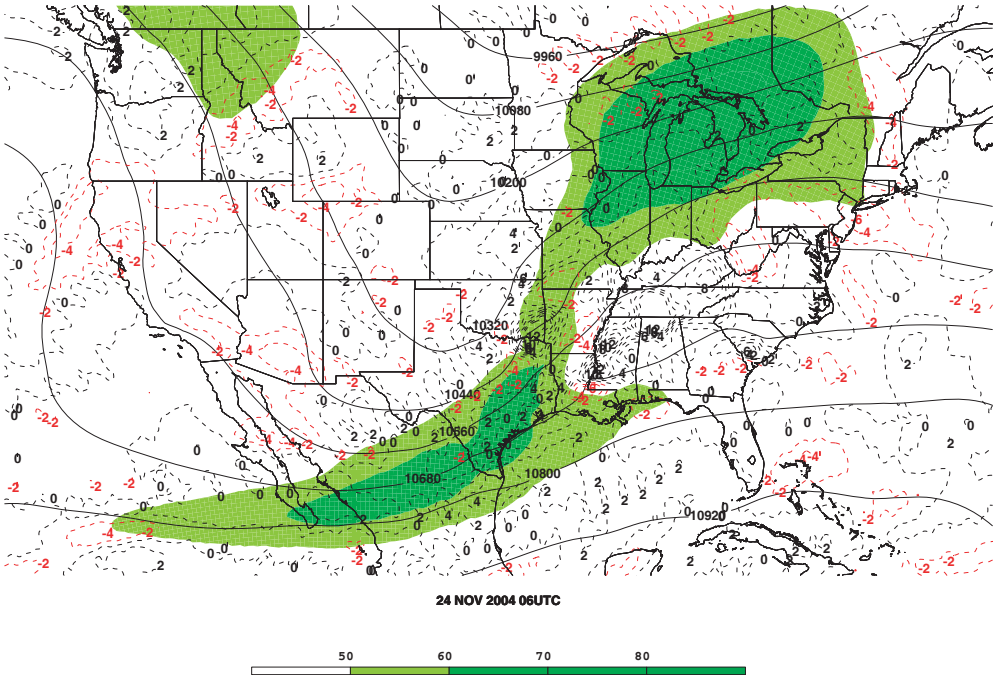

Fig. 3.4.14: 250 hPa isotachs (ms^{-1}, shaded color), divergence (10^{-5} s^{-1}, red and black dashed contours), and geopotential height (gpm, black contours) at 0600 UTC 24 November 2004.

c. 3 January 1982 Frontal Event

The frontal electrified convective snowfall event of 3 January 1982 at Dayton, OH, (DAY) was dominated by southerly winds from the surface to 700 mb indicating that the event occurred behind a warm frontal boundary and thundersnow was first reported at 0000 UTC and last reported at 0300 UTC with all reports at DAY (Fig. 3.4.15). In this case, a strong veering wind profile was present, indicating that warm air advection was present as indicated by the NARR data. Also, values of -8 μbs^{-1} were present from 700 to 500 hPa indicating an elevated area of upward motion and convection. The elevated convection combined with the moist layer indicated between 850 and 600 hPa are critical ingredients to the development of this electrified convective snowfall event. Finally, the cross section indicates a relatively horizontal potential temperature field was present, indicating that no isentropic upglide was present.

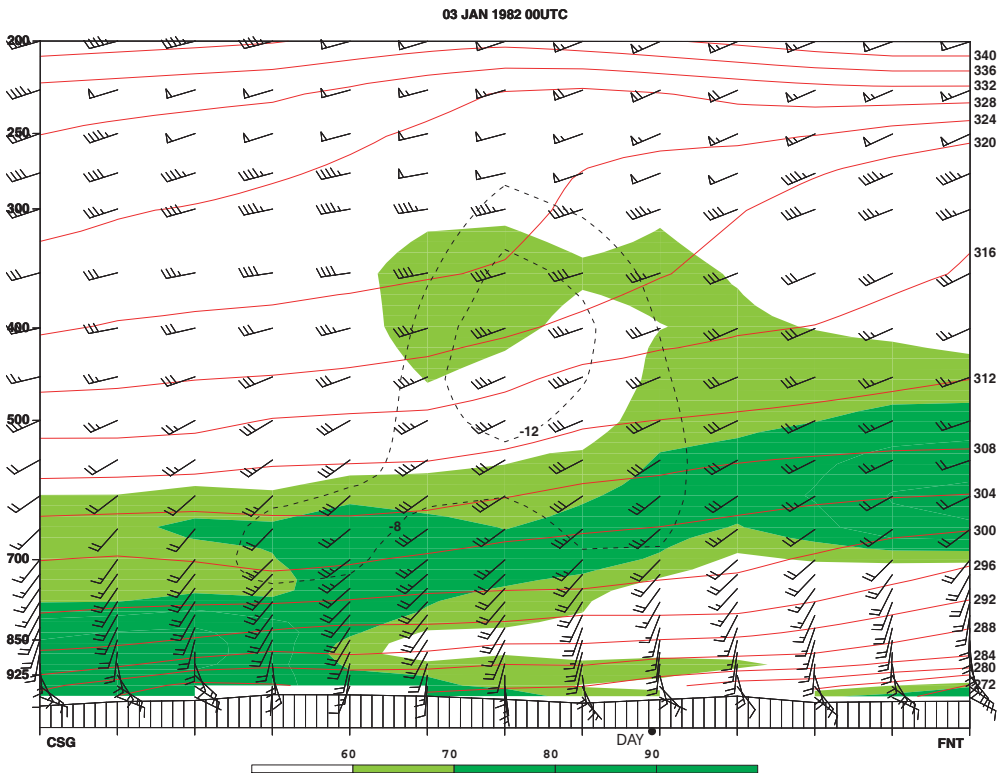

Fig. 3.4.15: A cross section of wind barbs (ms^{-1}), potential temperature (K, in red), omega (μbs^{-1}, dashed black) and relative humidity (percent, shaded) from Columbus, GA, to Flint, MI, at 0000 UTC 3 January 1982.

The skew-t thermodynamic diagram of Dayton, OH at 0000 UTC 3 January 1982 illustrates two moist areas at 925 hPa and the second at approximately 700 hPa (Fig. 3.4.16). These moist areas are also illustrated in Fig. 3.4.15. The second cross section illustrates the presence of negative EPV around 700 hPa (Fig. 3.4.17). The presence of EPV indicates the presence of CSI or CI. An examination of the M_g and Θ_{es} contours reveals a quasi-parallel relationship. This relationship between M_g and Θ_{es} indicates that CSI was present in this layer. Therefore, the elevated convection associated with the electrified convective snowfall event was driven by the presence of CSI at and around 700 hPa.

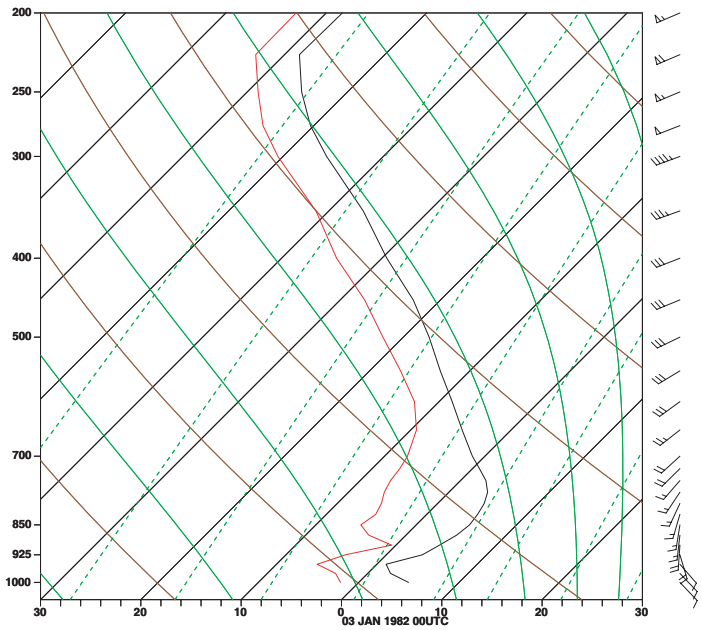

Fig. 3.4.16: A skew-t thermodynamic diagram from Dayton, OH, at 0000 UTC 3 January 1982. The solid green lines are moist adiabats, brown are dry adiabats, dashed green lines are saturation mixing ratio, the black trace is temperature and the red trace is dew point temperature.

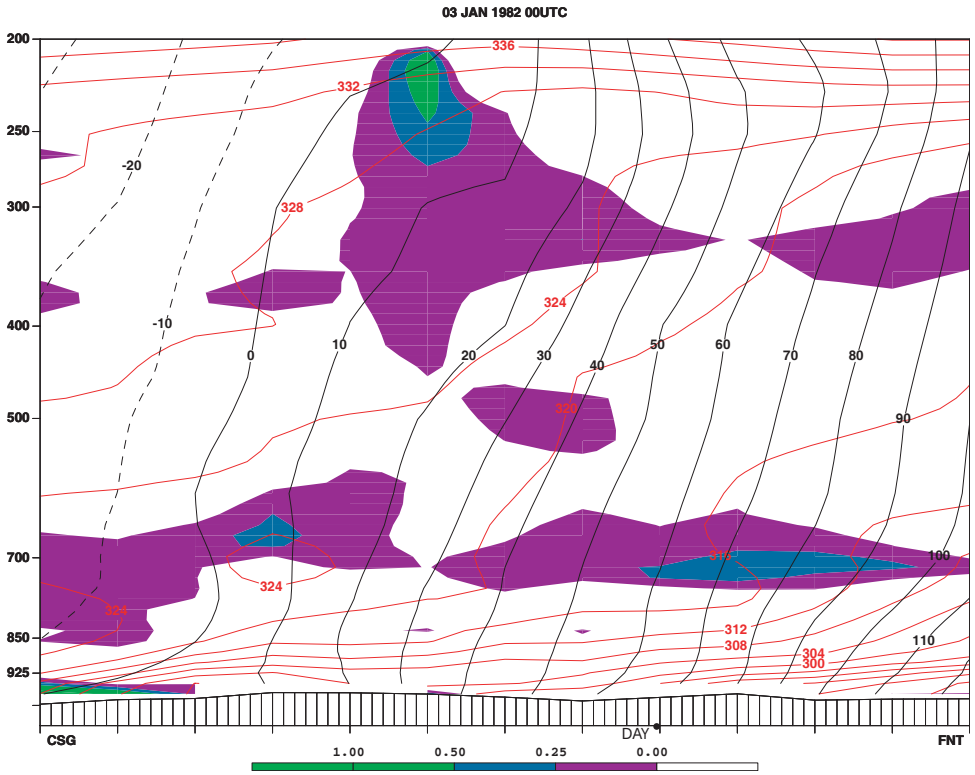

Fig. 3.4.17: A cross section of saturated equivalent potential temperature (K, red), absolute geostrophic momentum (ms^{-1}, black) and equivalent potential vorticity (PVU (10^{-6} m^2 K s^{-1} kg^{-1}), shaded) from Columbus, GA, to Flint, MI, at 0000 UTC 3 January 1982.

At the surface, DAY was located between the large area of lower pressure to the west and a large high pressure center to the northeast (Fig. 3.4.18). Warm air advection at 850 hPa was indicated along with strong southerly flow associated with the low-level jet, supporting upward motion (Fig. 3.4.19). Also, temperatures at 850 hPa were near the threshold for snowfall. Small areas of positive absolute vorticity advection were near the event location and the area was dominated by southwesterly winds at 700 hPa (Fig. 3.4.20). Finally, little to no upper air divergence is indicated by Fig. 3.4.21.

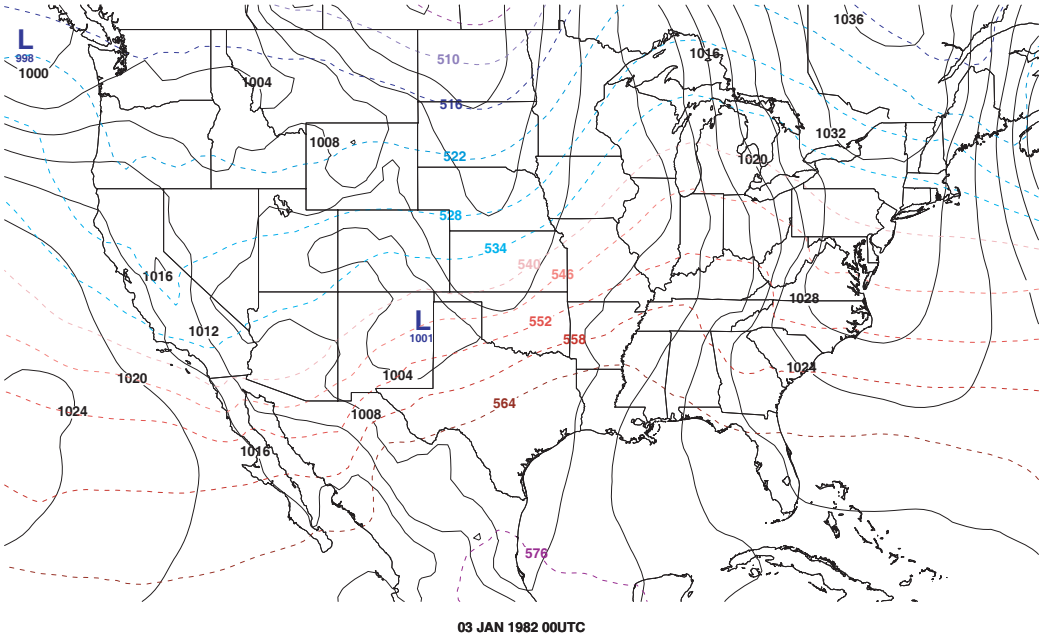

Fig. 3.4.18: Sea level pressure (hPa, black contours) and 1000-500 hPa thickness (gpm, dashed contours) at 0000 UTC 3 January 1982.

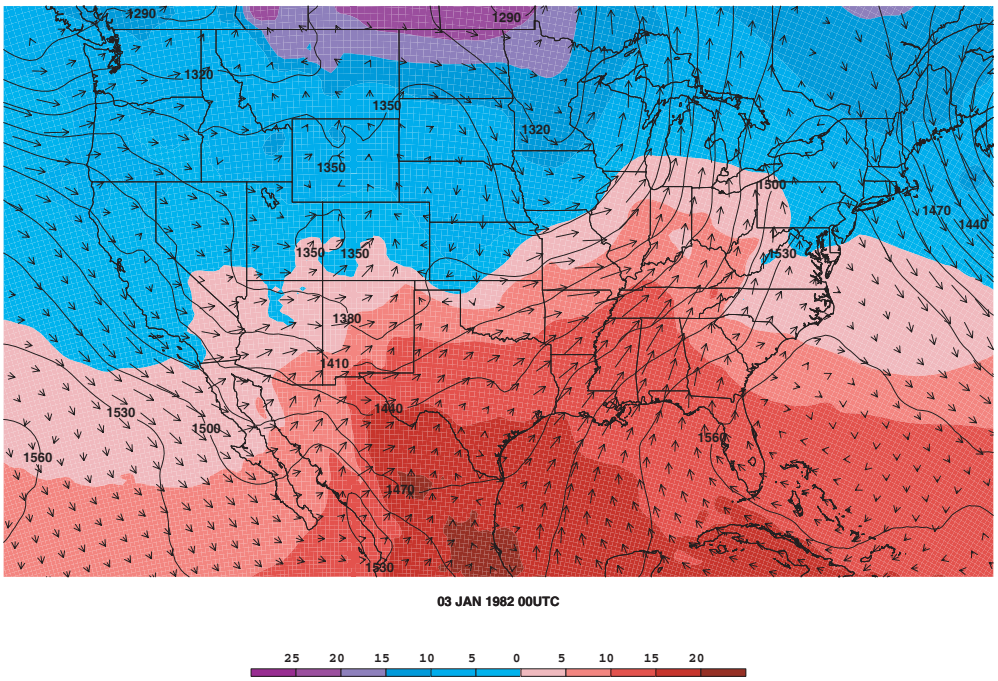

Fig. 3.4.19: 850 hPa temperature (°C, shaded color), geopotential height (gpm, black contours) and wind vectors (ms^{-1}, black arrows) at 0000 UTC 3 January 1982.

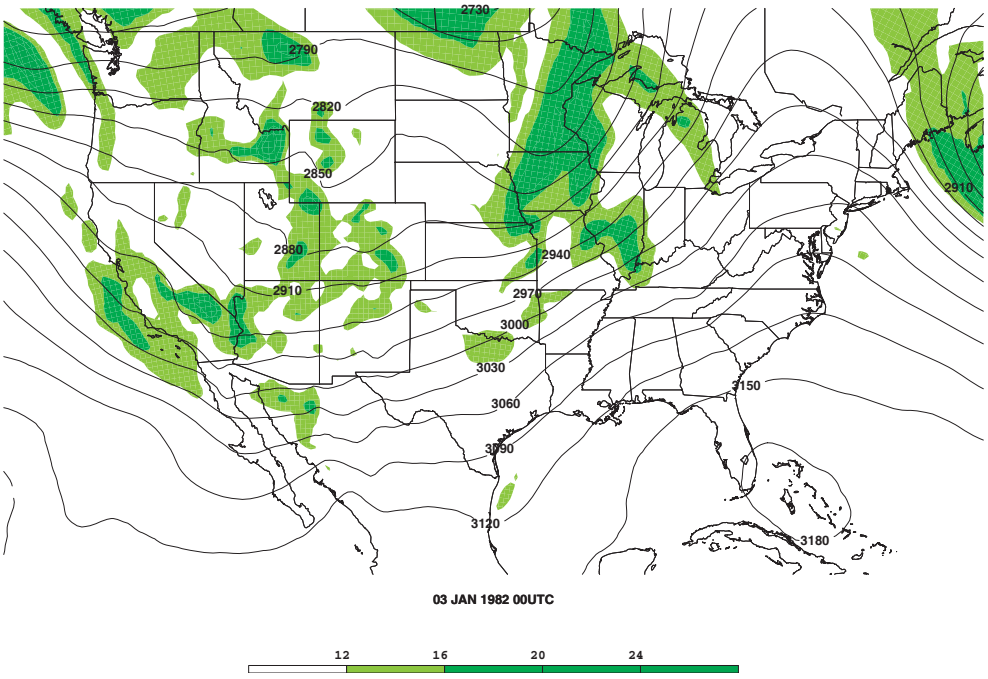

Fig. 3.4.20: 700 hPa absolute vorticity (s^{-1}, shaded color) and geopotential height (gpm, black contours) at 0000 UTC 3 January 1982.

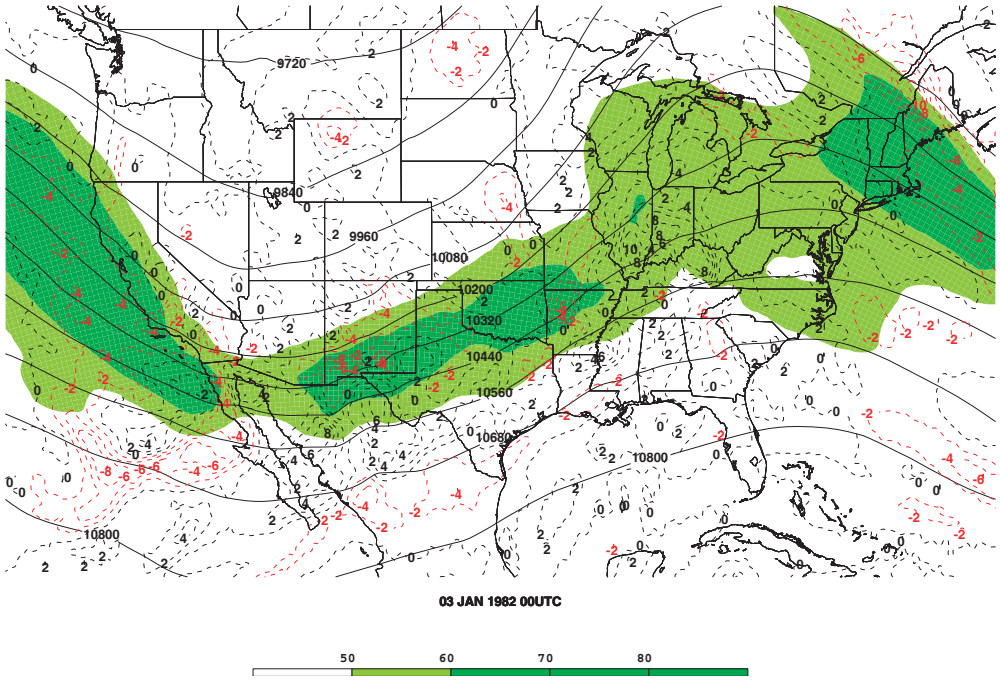

Fig. 3.4.21: 250 hPa isotachs (ms^{-1}, shaded color), divergence (10^{-5} s^{-1}, red and black dashed contours), and geopotential height (gpm, black contours) at 0000 UTC 3 January 1982.

d. 8 March 1999 Frontal Event

Fig. 3.4.22 indicates that an ample amount of moisture was present throughout much of the troposphere during the 8 March 1999 frontal electrified convective snowfall event at Sioux Falls, SD, (FSD). This event was first reported at FSD at 0600 UTC and last reported at 0900 UTC. In this cross section from Dallas-Ft. Worth, TX, (DFW) to Grand Forks, ND, (GFK), an area of -8 μbs^{-1} omega was located just to the south of the event location. Also, the upward slope of the potential temperature contours along with a veering wind profile indicates the presence of isentropic upglide and warm air advection throughout the region. The gradient of the isentropes suggests the presence of elevated convection.

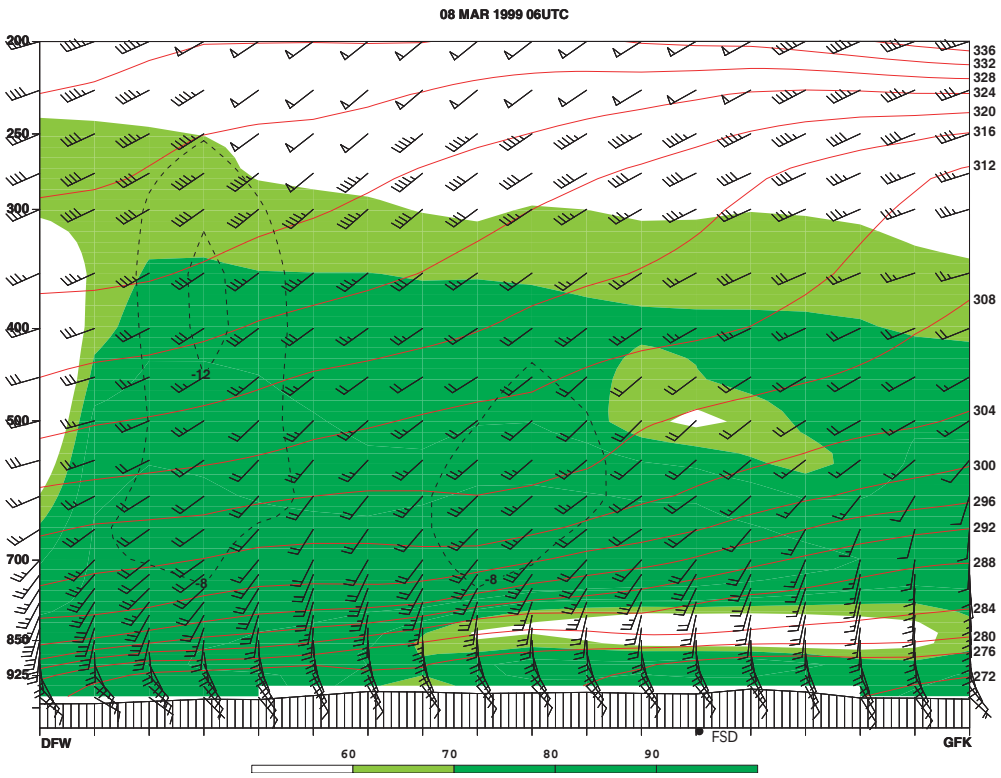

Fig. 3.4.22: A cross section of wind barbs (ms^{-1}), potential temperature (K, in red), omega (μbs^{-1}, dashed black) and relative humidity (percent, shaded) from Dallas, TX, to Grand Forks, ND, at 0600 UTC 8 March 1999.

An analysis of the skew-t thermodynamic diagram produced from the NARR data at FSD, 0600 UTC 8 March 1999 illustrates a moist area present in the profile from 700 to 500 hPa (Fig. 3.4.23). When analyzing this same layer in the cross section of EPV, negative values are present; therefore, CSI or CI was present in the layer (Fig. 3.4.24). By analyzing the contours of M_g and Θ_{es}, a quasi-parallel relationship is illustrated. By this relationship of M_g and Θ_{es}, the presence of CSI in this layer was identified as the driving force behind the elevated convection associated with this electrified convective snowfall event.

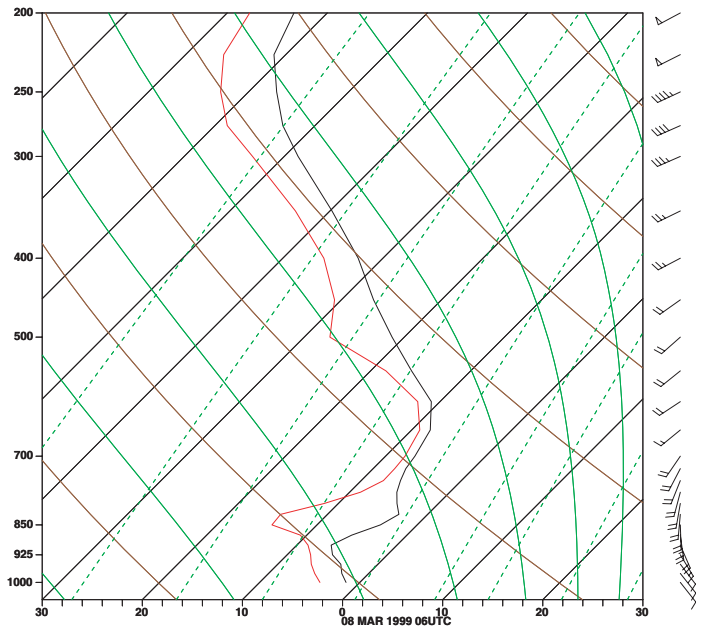

Fig. 3.4.23: A skew-t thermodynamic diagram from Sioux Falls, SD, at 0600 UTC 8 March 1999. The solid green lines are moist adiabats, brown are dry adiabats, dashed green lines are saturation mixing ratio, the black trace is temperature and the red trace is dew point temperature.

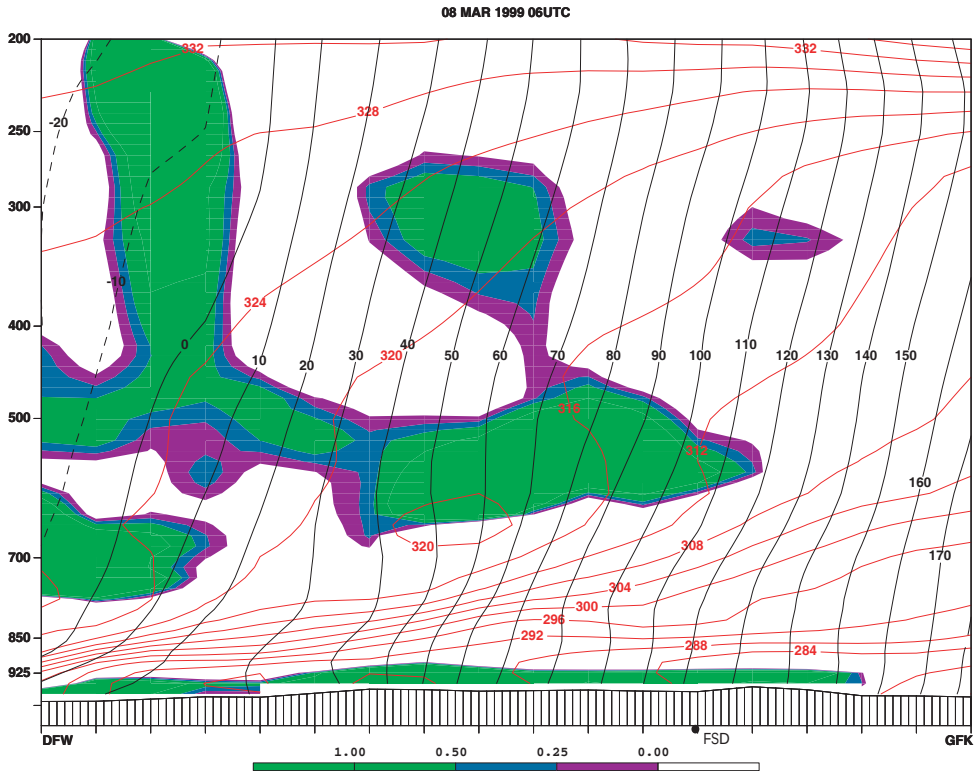

Fig. 3.4.24: A cross section of saturated equivalent potential temperature (K, red), absolute geostrophic momentum (ms^{-1}, black) and equivalent potential vorticity (PVU (10^{-6} m^2 K s^{-1} kg^{-1}), shaded) from Dallas, TX, to Grand Forks, ND, at 0600 UTC 8 March 1999.

A surface analysis revealed that a center of low pressure was located south and west of the electrified convective snowfall event at FSD (Fig. 3.4.25). This provides further evidence that the event occurred along a warm frontal boundary. At 850 hPa, strong south, south-easterly winds dominated the region and the temperature field illustrates that the atmosphere was cold enough to support snowfall (Fig. 3.4.26). A slight area of negative vorticity advection is evident in Fig. 3.4.27; however this did not appear to hinder the development of this event. The analysis of the jet stream reveals that very little upper level divergence was present and the event was located in a ridge formed by the jet stream as expected since this event occurred downstream of the surface cyclone (Fig. 3.4.28).

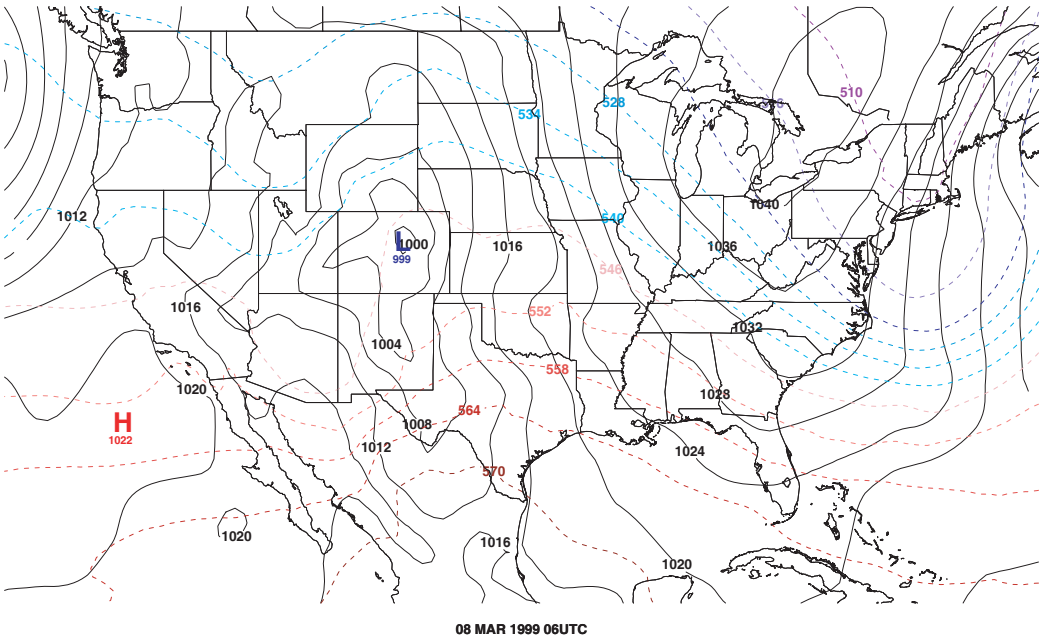

Fig. 3.4.25: Sea level pressure (hPa, black contours) and 1000-500 hPa thickness (gpm, dashed contours) at 0600 UTC 8 March 1999.

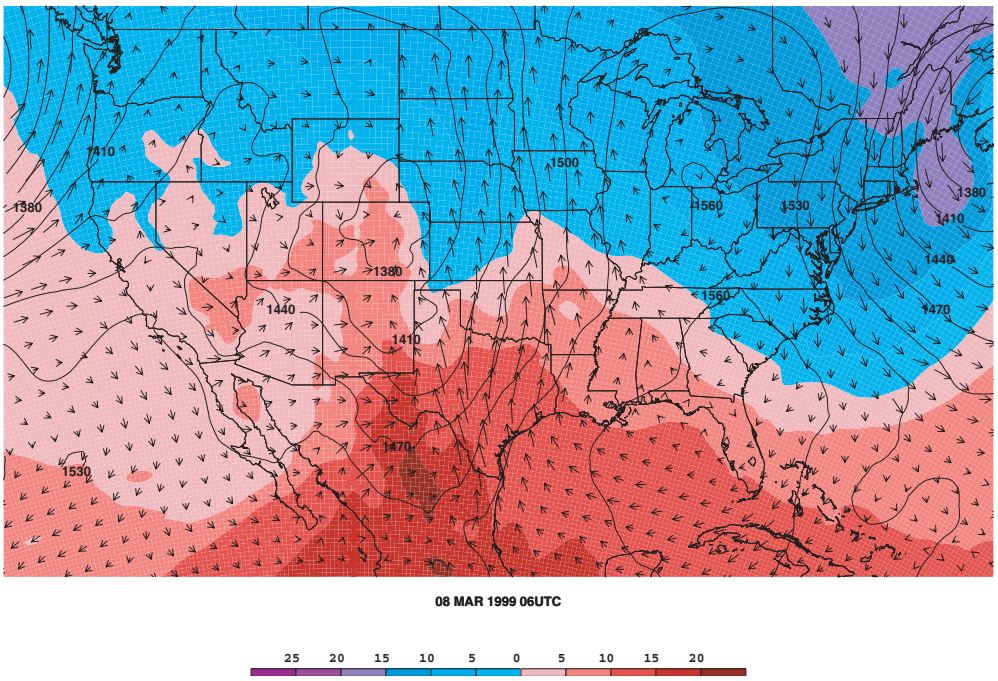

Fig. 3.4.26: 850 hPa temperature (°C, shaded color), geopotential height (gpm, black contours) and wind vectors (ms^{-1}, black arrows) at 0600 UTC 8 March 1999.

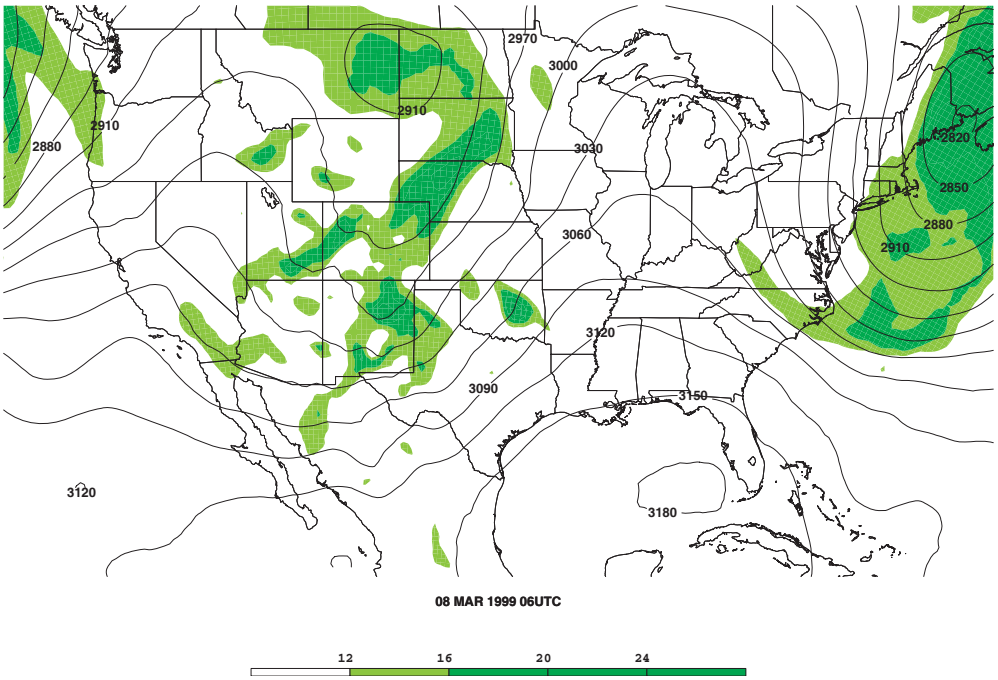

Fig. 3.4.27: 700 hPa absolute vorticity (s^{-1}, shaded color) and geopotential height (gpm, black contours) at 0600 UTC 8 March 1999.

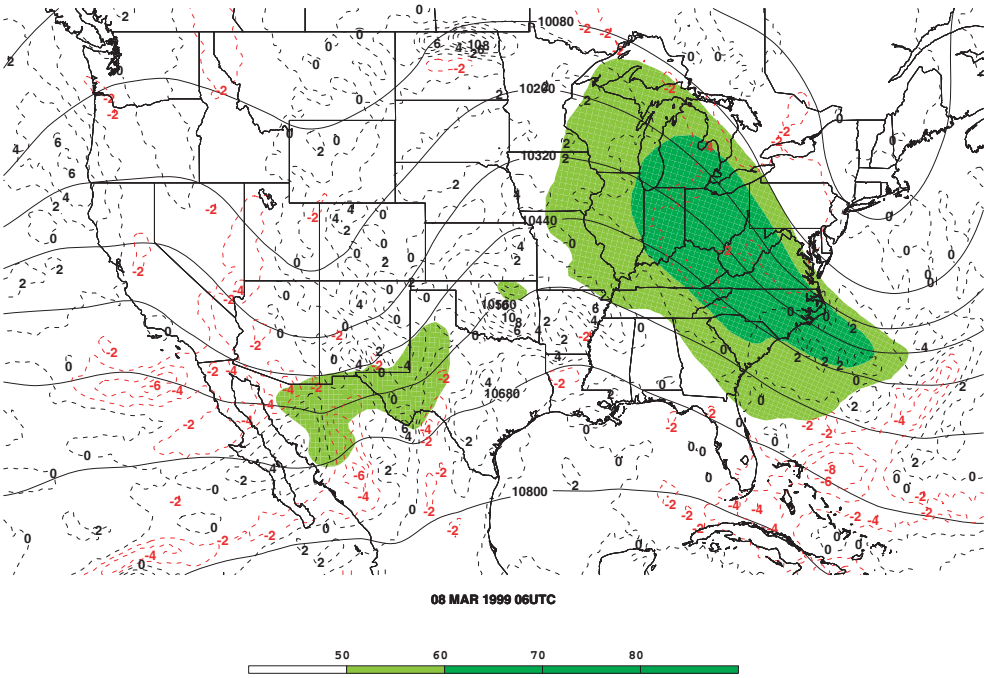

Fig. 3.4.28: 250 hPa isotachs (ms^{-1}, shaded color), divergence (10^{-5} s^{-1}, red and black dashed contours), and geopotential height (gpm, black contours) at 0600 UTC 8 March 1999.

e. 2 December 1983 Orographic Event

A cross section from Las Vegas, NV, (LAS) to Spokane, WA, (GEG) reveals abundant moisture from the surface to approximately 300 hPa was present at Elko, NV (EKO) (Fig. 3.4.29). This event was reported only at 0600 UTC at EKO. Also, the event was located between an area of downward motion to the south and upward motion to the north. A veering pattern indicated the presence of warm air advection. Finally, from 850 hPa to the tropopause, the area was dominated by westerly winds. Therefore, little evidence of elevated convection or other driving factors was present. This is expected as orographic convective snowfall events are localized phenomena.

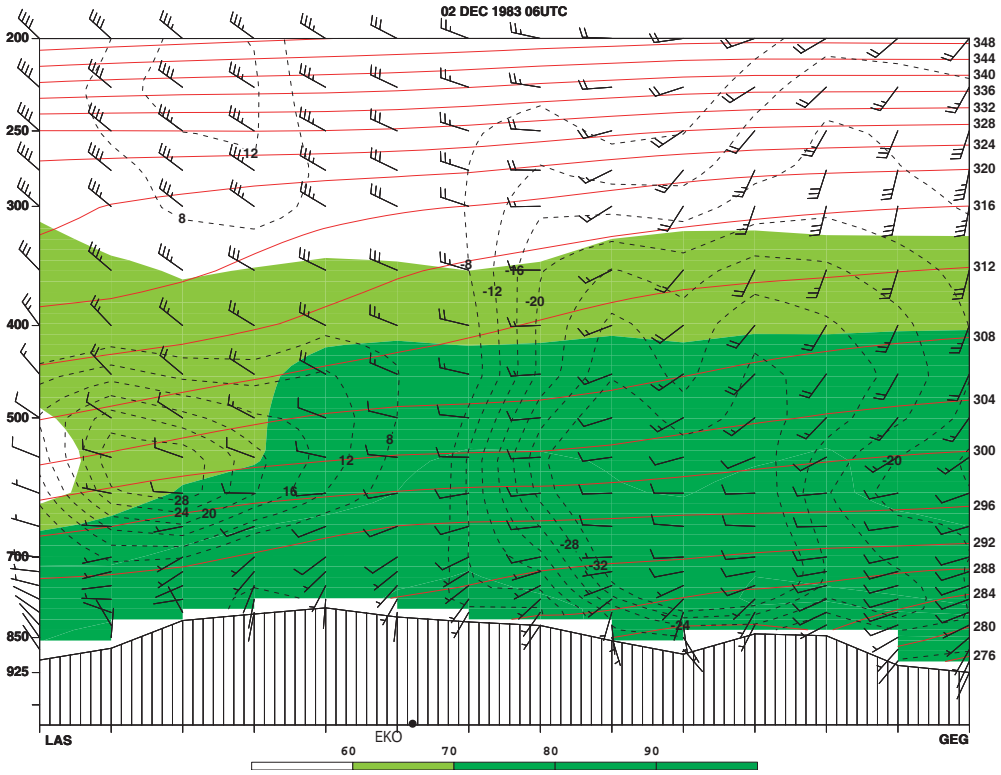

Fig. 3.4.29: A cross section of wind barbs (ms^{-1}), potential temperature (K, in red), omega (μbs^{-1}, dashed black) and relative humidity (percent, shaded) from Las Vegas, NV, to Spokane, WA, at 0600 UTC 2 December 1983.

The skew-t thermodynamic diagram at EKO illustrates a moist layer from the surface to 700 hPa (Fig. 3.4.30). A cross section indicates the presence of CSI or CI in this layer by demonstrating negative values of EPV throughout this same layer (Fig. 3.4.31). The examination of M_g and Θ_{es} contours in the cross section illustrates a fold of the θ_{es} contours in the area where EPV was indicated. Therefore, CI was present in this layer and was the driving force of the elevated convection associated with this electrified convective snowfall event.

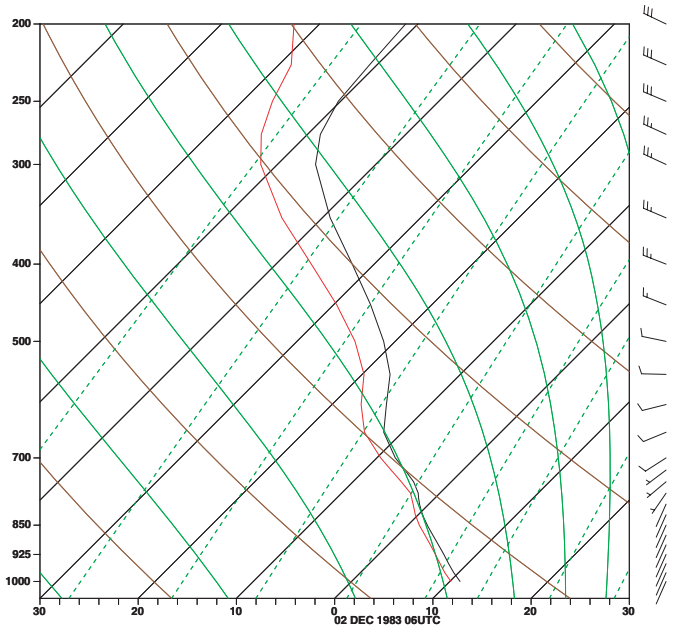

Fig. 3.4.30: A skew-t thermodynamic diagram from Elko, NV, at 0600 UTC 2 December 1983. The solid green lines are moist adiabats, brown are dry adiabats, dashed green lines are saturation mixing ratio, the black trace is temperature and the red trace is dew point temperature.

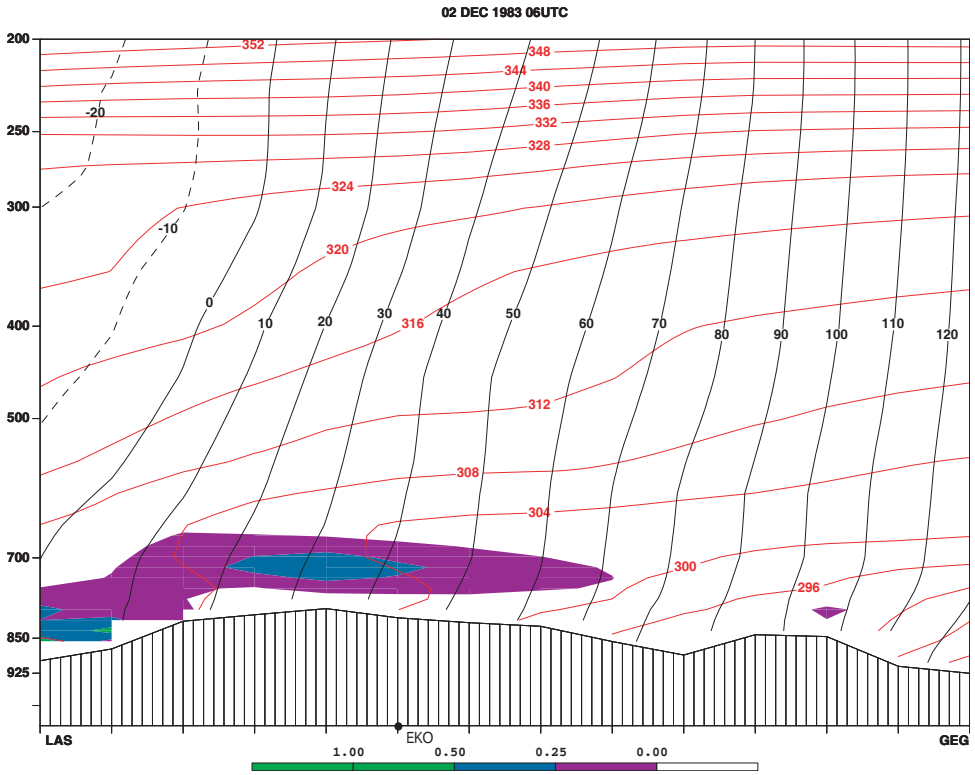

Fig. 3.4.31: A cross section of saturated equivalent potential temperature (K, red), absolute geostrophic momentum (ms^{-1}, black) and equivalent potential vorticity (PVU (10^{-6} m^2 K s^{-1} kg^{-1}), shaded) from Las Vegas, NV, to Spokane, WA, at 0600 UTC 2 December 1983.

The analysis of the sea-level pressure field reveals little about the lifting associated with the event (Fig. 3.4.32). No large pressure centers were located in the vicinity of the electrified convective snowfall event. This pattern holds similar at 850, 750, and up to 250 hPa as no dominant large scale features were present (Fig. 3.4.33 – Fig. 3.4.35). Again this lack of a dominant feature is expected as the main driving force for an orographic electrified convective snowfall event is a localized westerly wind lifted up by the mountain range. The CI indicated was present and the angle of the uplift was caused by the mountains.

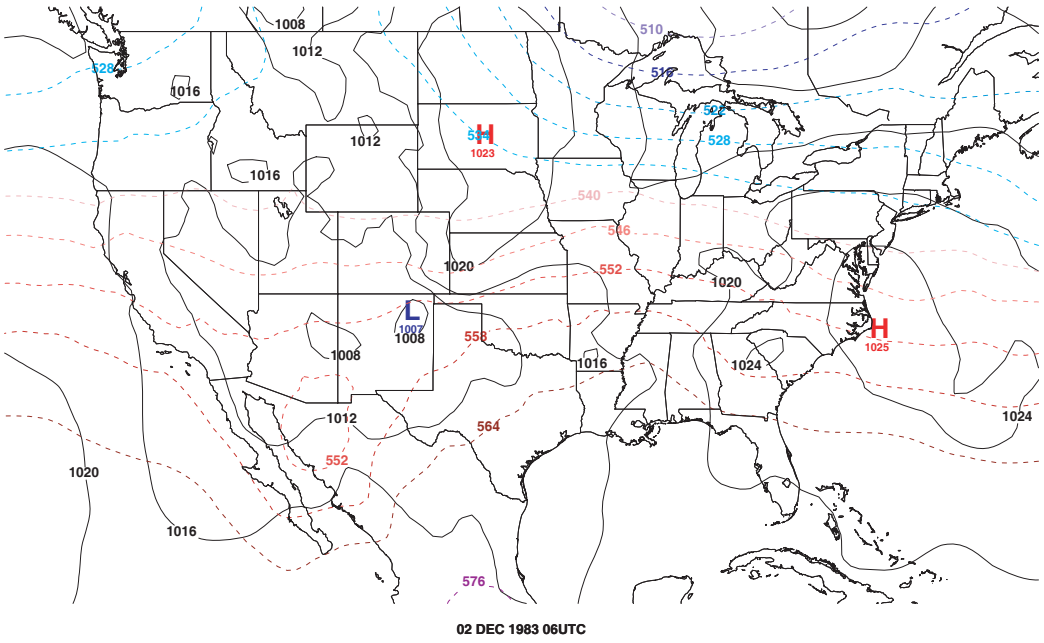

Fig. 3.4.32: Sea level pressure (hPa, black contours) and 1000-500 hPa thickness (gpm, dashed contours) at 0600 UTC 2 December 1983.

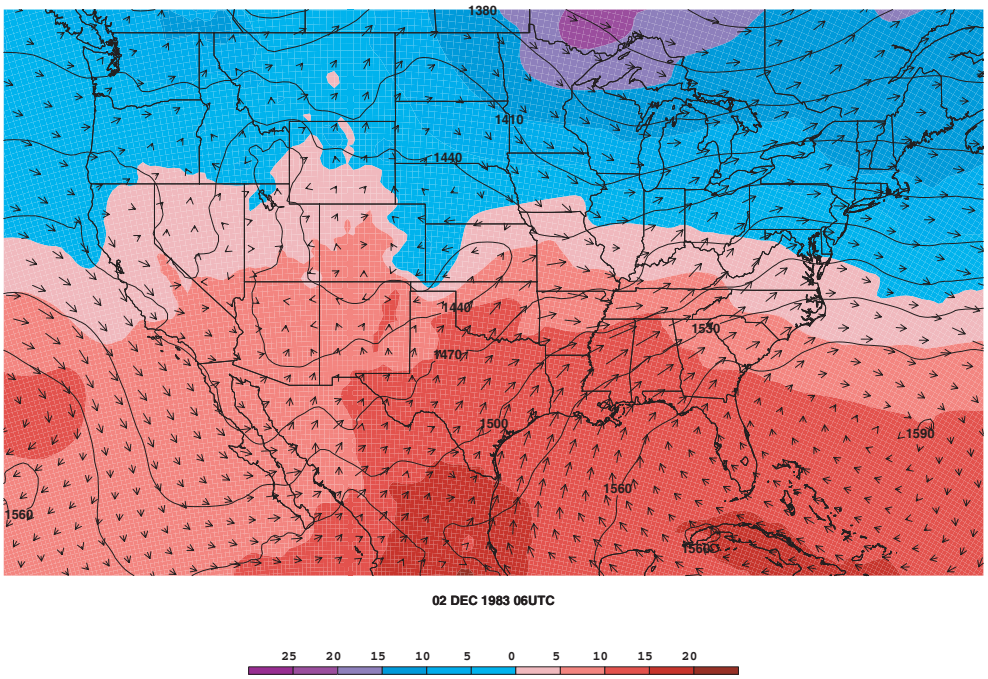

Fig. 3.4.33: 850 hPa temperature (°C, shaded color), geopotential height (gpm, black contour) and wind vectors (ms^{-1}, black arrows) at 0600 UTC 2 December 1983.

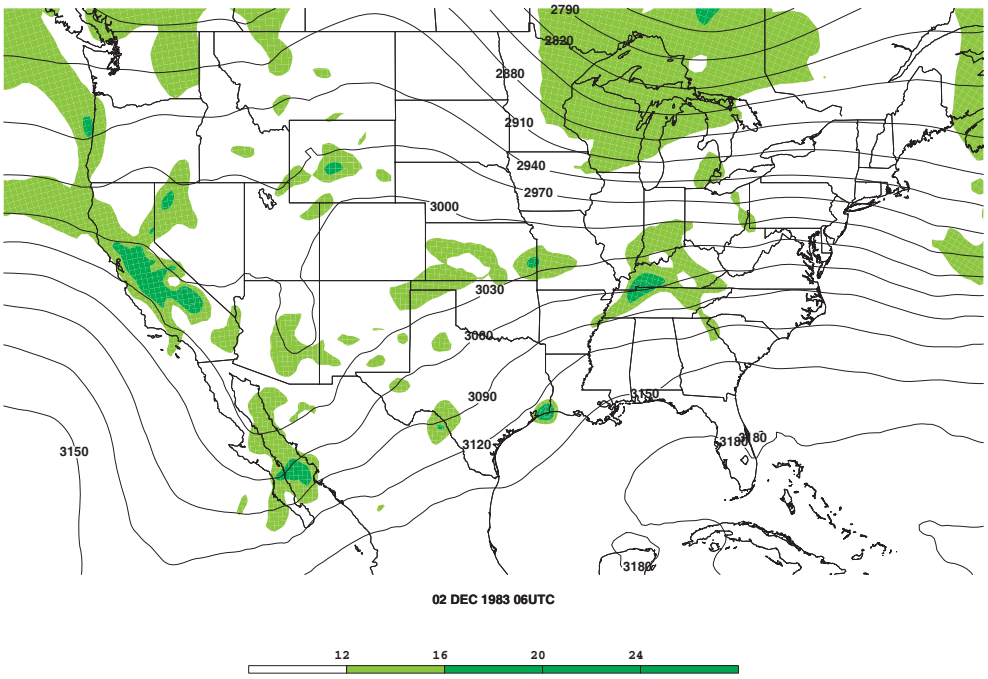

Fig. 3.4.34: 700 hPa absolute vorticity (s^{-1}, shaded color) and geopotential height (gpm, black contours) at 0600 UTC 2 December 1983.

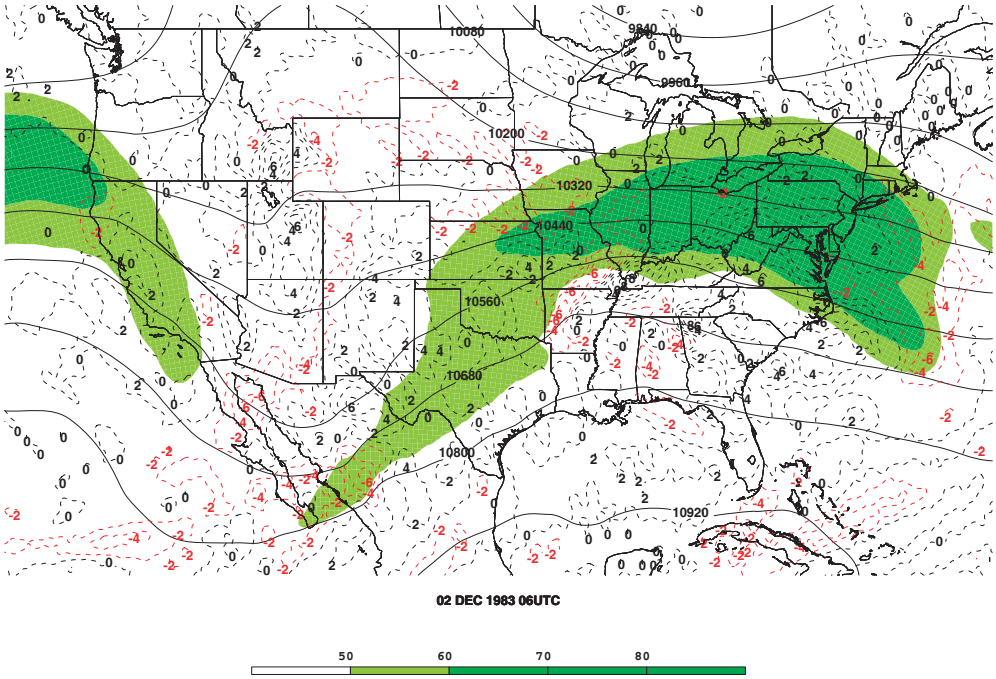

Fig. 3.4.35: 250 hPa isotachs (ms^{-1}, shaded color), divergence (10^{-5} s^{-1}, red and black dashed contours), and geopotential height (gpm, black contours) at 0600 UTC 2 December 1983.

f. Conclusions from Case Studies

The analysis of these five cases (2 cyclonic, 2 frontal, 1 orographic) has illustrated common environmental characteristics of electrified convective snowfall events. For each case, cross sections of potential temperature, wind barbs, relative humidity, and omega were created to diagnose the specific layer of the atmosphere capable of supporting the elevated convection that drives electrified convective snowfall events. This level was most commonly found near 700 hPa. Also, the temperature in these layers were ranged from -8 to -15°C at the bottom and -12 to -25°C at the top indicating that each layer had temperature zones between -14 and -17°C, a temperature range where the growth of ice crystals is maximized (Rogers 1979). The use of cross sections of EPV, M_g, and Θ_{es} illustrated the presence of CSI in four of the five cases and CI in the

orographic case. With CSI as the driving force of cyclonic and frontal events, indeed a banded structure to the events is expected in the radar imagery.

To further understand the environment of these events, mean sea level pressure and 1000 – 500 hPa thickness maps illustrated the positions of the surface cyclone south of the event location in each cyclonic event, west of the event in each frontal event, and not a factor in the orographic event. Also illustrated was the capability of the atmosphere to support snowfall by the 1000 – 500 hPa thickness plots and the temperature traces. In the 8 March 1999 frontal case, a strong low-level jet was evident at 850 hPa which helped to strengthen the event. Again no evidence of a low-level jet was present during the orographic event. At 700 hPa, absolute vorticity plots revealed that vorticity advection does not seem to play a major role in the development of these events. Lastly, plots at 250 hPa indicated regions of possible uplift as the cyclonic and frontal events generally occurred under the right entrance or left exit of a jet streak. Again, no indication of other forcings was present in the orographic event further illustrated that orographic events are locally driven.

3.5 Conclusions

This climatology has described when, where, and how the 706 electrified convective snowfall events from 1960-2005 identified in the surface station data across the continental United States occurred. All events were then examined spatially to determine the most frequent locations of occurrence, temporally to determine the months of the year and the hours of the day most likely to occur. Lastly, the events were classified synoptically according to environment responsible for the production of these

events. Five case studies were also included to describe environment of the most frequent synoptic types (2 cyclonic, 2 frontal, 1 orographic).

The spatial analysis revealed that a "corridor" of electrified convective snowfall exists across the United States. This area of most frequent electrified convective snowfall development stretches from Nevada in the west, through Kansas and Nebraska, into New England. The distribution discovered in this thesis differs from previous studies (e.g. Market et al. (2002)) which found more clustered events over Utah, northeastern Kansas, and the Great Lakes, over a shorter period record (1961-1990) rather than the continuous area of event locations over a larger period of record found by this study.

With this understanding of where electrified convective snowfall events occurred, the focus then shifted to when they occurred throughout the period of record. The diurnal analysis revealed a previously undiscovered pattern of a maximum of electrified convective snowfall occurrence in the late night and early morning hours. This may be attributed to the increase in the strength of the low-level jet during the hours and the ease of detecting lightning in the dark hours compared to during daylight hours. Secondly, the seasonal analysis demonstrated that electrified convective snowfall events occur most often in the late spring, typically in March and April. A smaller maximum of events was documented in November. These maxima can be attributed to the equatorward (poleward) movement of the polar front in the fall (winter) associated with many of these storms. This pattern is similar to the pattern found by Market et al. (2002).

The final focus of this climatology was on the environment producing the electrified convective snowfall events. This analysis resulted in seven possible classifications for the events including cyclone, coastal, orographic, lake effect/enhanced,

frontal, upslope, and unclassifiable. The cyclone associated events comprised 41% of all electrified convective snowfall events with frontal (30%), orographic (9%), coastal (9%), lake effect (6%), upslope (4%) and unclassifiable (1%) comprising the rest of electrified convective snowfall events.

From four of the five case studies, the environment conducive to electrified convective snowfall production was clearly associated with CSI. This instability is the driving force behind the elevated convection associated with each of these events. In the cyclonic and frontal cases, other forces such as the presence of the low-level jet, a low level deformation zone, and the position of jet streaks enhanced the strength of the convection and the event. However, CSI and these external forces were not present during the orographic event as CI was dominant. This lack of external forces indicates that the event was driven by the lift caused by the mountains and the low layer of CI only further indicating that orographic events are more local than the other event types.

With the construction of this climatology the next part of this thesis is to further investigate the most recent cases with both lightning data and radar imagery. This analysis will investigate the question of whether radar imagery possesses a banded structure when electrified convective snowfall events are occurring and will be the focus of the remainder of this thesis.

CHAPTER 4
LIGHTNING CHARACTERISTICS AND RADAR SIGNATURES

Identifying electrified convective snowfall events in radar imagery allows forecasters to inform the public as these events occur and identifies areas hardest hit by the events for immediate response. Only Schultz et al. (2004) has published findings of patterns in radar imagery associated with electrified convective snowfall events. Therefore, with a climatology of electrified convective snowfall events from 1960-2005 created to examine how, why and when these events occur, this chapter focuses on the lightning strike data and the associated radar imagery to identify and locate events in a nowcasting capacity. Three events were selected for further analysis using both the lightning strike data and radar imagery. The first event occurred from 26-27 January 1996 from Iowa through Michigan. The second event was on 8 March 1999 and electrified convective snowfall was reported from South Dakota to Nebraska. Finally, the third event took place on 24 November 2004 and stretched from Illinois to Michigan. These events were selected because of their long lifespan and large area of impact. The lifespan of these three electrified convective snowfall events was important, as the longer lifespan provided a relatively large amount of data for analysis compared to single station and report events.

4.1 Lightning Characteristics of Selected Electrified Convective Snowfall Events

The first step in the analysis of the three electrified convective snowfall events was to examine the lightning polarity and strength. The positive lightning flashes ranged from 30% in the 1996 event to 13% in the 2004 event (Fig. 4.1.1). These percentages are higher than the average percentage of positive flashes, which have been found to comprise 5% of all warm season flashes and 16% of cool season flashes (Orville and Huffins 2001). Although the sample size is not large enough to make a conclusive statement, late cold season electrified convective snowfall events may possess more positive lightning flashes than events earlier in the season. The tendency toward more positive flashes may be due to an increase in strength of the storms producing lightning. This increase in strength may result in a tripole electrical structure (Fig. 4.1.2) rather than a dipole structure (Fig. 4.1.3). Another explanation for the increase of positive flashes may be that intra-cloud flashes were misdiagnosed as cloud to ground (Fig. 4.1.4).

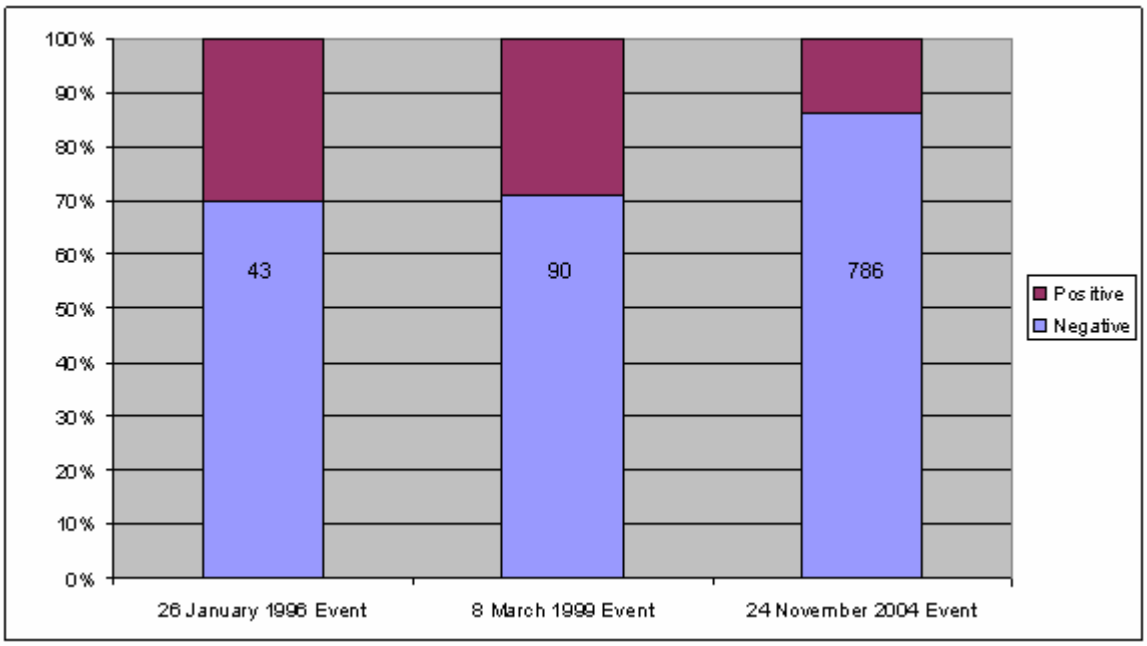

Fig. 4.1.1: The percentage of positive and negative polarity lightning strikes for each of the selected electrified convective snowfall events. Total number of flashes is indicated.

The tripole separation of charge schematic (Fig. 4.1.2) is one of two possible explanations for the increase of positive flashes in these electrified convective snowfall events compared with warm season convection. A tripole separation of charge has been shown to occur in areas of strong updrafts or in stratiform convective areas (Williams 2001). Also, due to the low temperatures at the surface and aloft, more frozen hydrometeors exist in the cool season convection than is typical in warm season convection. This increased presence of frozen hydrometeors in the cool season can lead to an increase in the positive charge area of the cloud as they have been shown to produce large positively charged areas in clouds (Williams 2001). The extra positive area creates the tripole separation of charge, and therefore, a result of this electrical structure is an increase in the number of positively charged flashes.

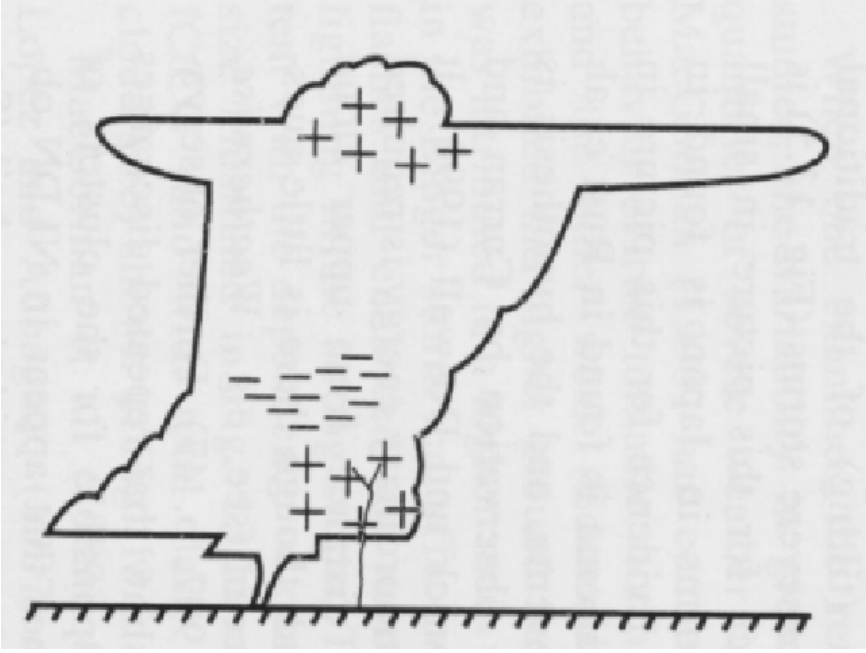

Fig 4.1.2: A tripole separation of charge schematic for positive polarity flashes from Williams (2001).

The tripole separation of charge was theorized by Williams (2001) to produce the positively charged flashes. While an increased percentage of positive lightning flashes exists in these electrified convective snowfall events compared to warm season lightning observations, the majority (typically from 70-80%) of the lightning flashes observed with these electrified convective snowfall events apparently originate from a dipole structure as shown in Fig. 4.1.3. In this dipole structure, the lower positively charged area is not present and thus the lightning flashes illustrated in this schematic are negatively charged. The dipole electrical structure is due to the collisions of hydrometeors resulting in the larger hydrometeors retaining a negative charge. The larger hydrometeors are pulled to the bottom of the cloud, creating a negatively charged area at the base and a relatively positively charged area higher in the cloud.

The possibility of false positive lightning strikes was also considered when examining the larger percentage of positive lightning flashes exhibited by these

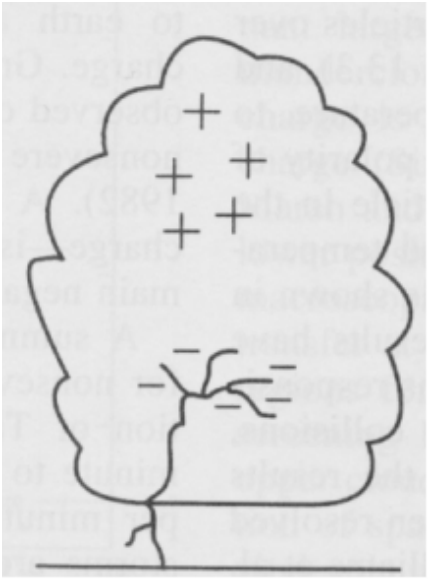

Fig 4.1.3: A dipole separation of charge schematic for negative polarity flashes from Williams (2001).

electrified convective snowfall events. In electrified convective snowfalls, there is a possibility that intra-cloud or cloud-to-cloud lightning may be recorded as a low amperage (less than 10 kA) positive strike. However, this is not a probable explanation for a larger than average percentage of positively recorded lightning flashes. Of the 200 low amperage positive flashes, 199 occurred in the 24 November 2004 event which had the lowest percentage of positively charged flashes of the three events. The tripole separation of charges theory is the most likely explanation for the increase in percentage of positively charged lightning flashes observed in the three electrified convective snowfall events compared to the average warm or cool season convection.

The remainder of this chapter focuses on these lightning data overlaid on coincident radar imagery to illustrate the banding within each event. Positive and negative flashes are recorded using a (+) and (-) respectively.

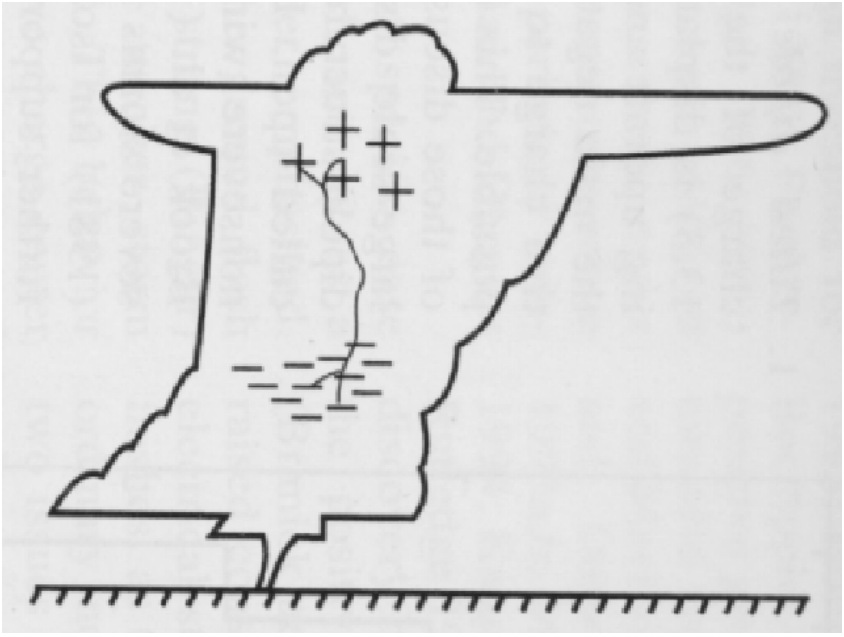

Fig 4.1.4: An intra-cloud separation of charge schematic for falsely recorded positive polarity flashes from Williams (2001).

4.2 26-27 January 1996

The first event in the radar analysis occurred 26-27 January 1996. This event was classified as a cyclonic type, and the lightning occurred in the western half of the storm in the "wrap around" region over and around Des Moines, Iowa (DSM) (Fig. 4.2.1 – Fig. 4.2.11). The first radar/lightning composite at 1820 UTC shows the snow shield to be relative smooth and kidney shaped (Fig. 4.2.1). However, on the eastern edge of the composite, four lightning flashes (3 positive and 1 negative) are seen in a ragged edge of the shield. These edges appear to have "finger-like" shapes and could possibly lead to a banded structure as the storm develops through time. Also, in this image, to the west of the lightning strikes appear to be an area or band of higher reflectivity.

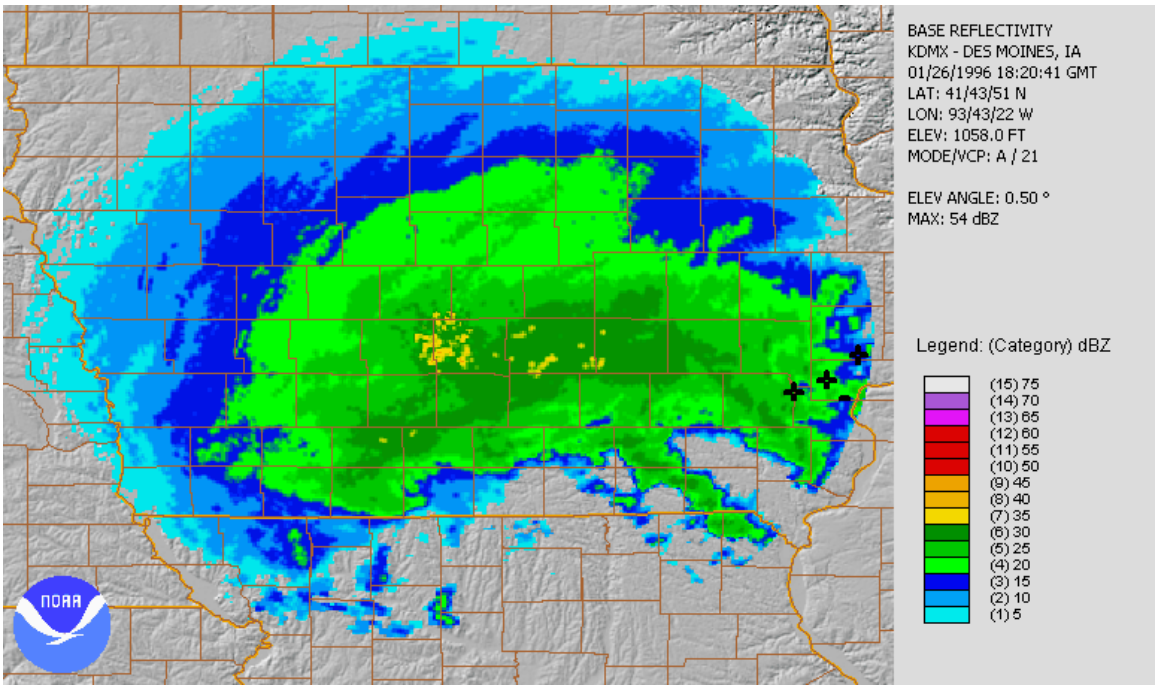

Fig 4.2.1: A base reflectivity image from Des Moines, IA, and lightning flashes at 1820 UTC 26 January 1996.

The next composite (Fig. 4.2.2) is from 1844 UTC, 24 minutes after the previous composite. In this composite, only one lightning flash is evident (negative); however, the flash was located in the band of heavier snowfall discussed in the previous image. More importantly, it appears that this heavier band of snowfall began to bifurcate at this time. This illustrates how lightning flashes may concentrate on the edge of a snow bands, even in a single banded storm in a single banded structure. These snow bands contained the heaviest snowfalls, and even though no lightning strikes have occurred in the bands, it is important to consider them.

The next several images at 1849 UTC (Fig. 4.2.3), 1912 UTC (Fig. 4.2.4), 1917 UTC (Fig. 4.2.5), 1923 UTC (Fig. 4.2.6), 1929 UTC (Fig. 4.2.7), 1941 UTC (Fig 4.2.8), and 1952 UTC (Fig. 4.2.9) all show a concentration of lightning flashes in or near the

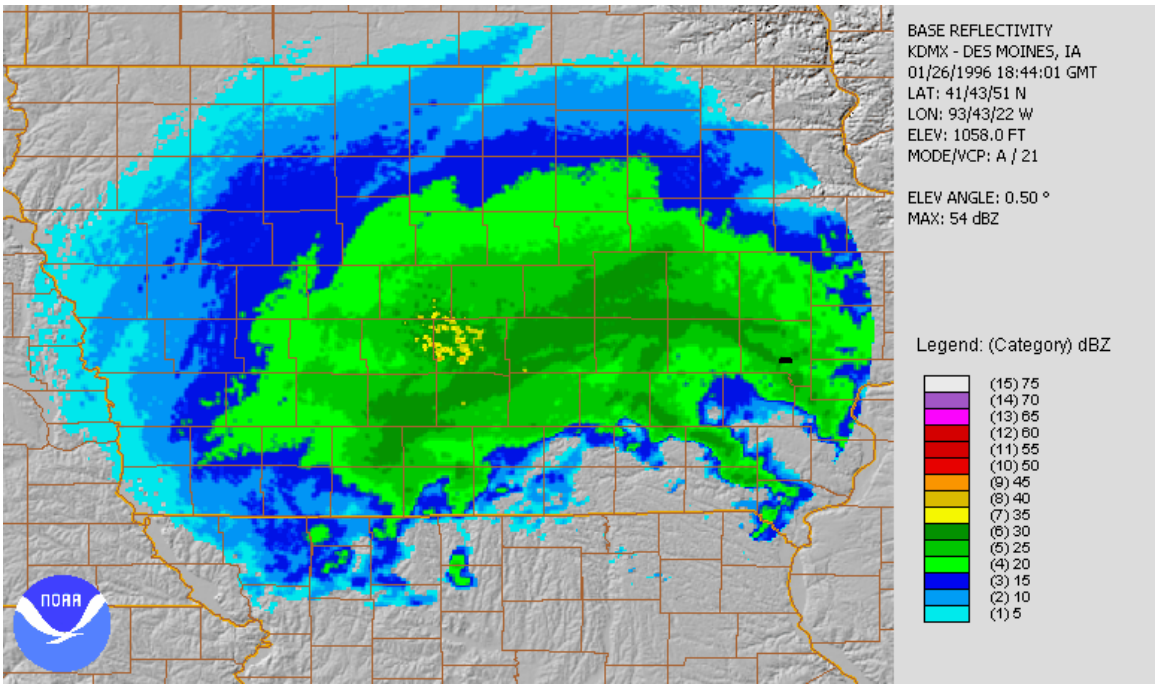

Fig 4.2.2: A base reflectivity image from Des Moines, IA, and lightning flashes at 1844 UTC 26 January 1996.

deformation zone as diagnosed in Chapter 3. Also evident in Fig. 4.2.7 and Fig. 4.2.10 are strikes at the edges of the heaviest precipitation band. A band of higher reflectivity forms briefly at 1941 UTC and was the only time in this series where positively charged flashes were observed along the band. Throughout the event, this band had the highest reflectivity and a special METAR from DSM was generated at 1939 UTC for heavy snowfall and thunder occurrences. This higher reflectivity suggests a stronger event and coupled with a high percentage of positive flashes further supports the tripole hypothesis of charge separation as discussed previously. Toward the end of the event from 2016 UTC to 2045 UTC (Figs. 4.2.10 and 4.2.11), the base reflectivity images suggest that splitting of the main snow band into three smaller bands took place. This division of bands could be the result of a decrease in the strength of the storm.

A definite banding pattern is present in the 26-27 January 1996 event and is likely due to the presence of CSI as identified in Chapter 3. It appears that lightning strikes occurred in and near the edges of the bands of the highest reflectivity. This may be a result of a stronger separation of charge existing in areas of heavier precipitation as suggested by the higher reflectivity values.

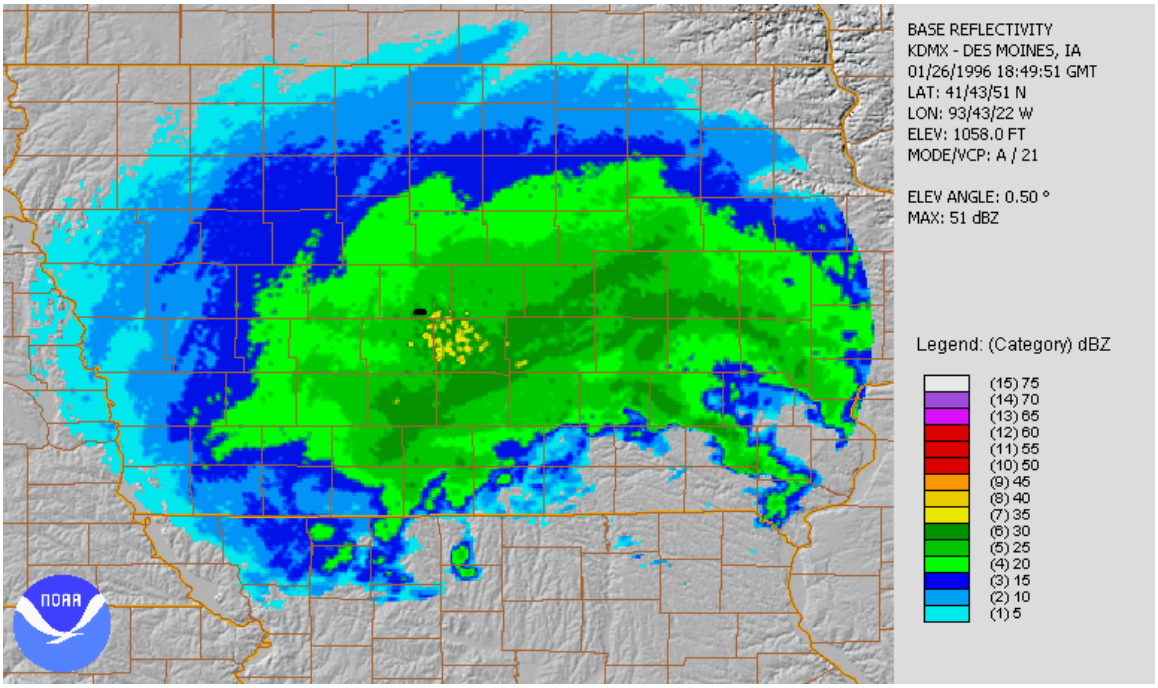

Fig 4.2.3: A base reflectivity image from Des Moines, IA, and lightning flashes at 1849 UTC 26 January 1996.

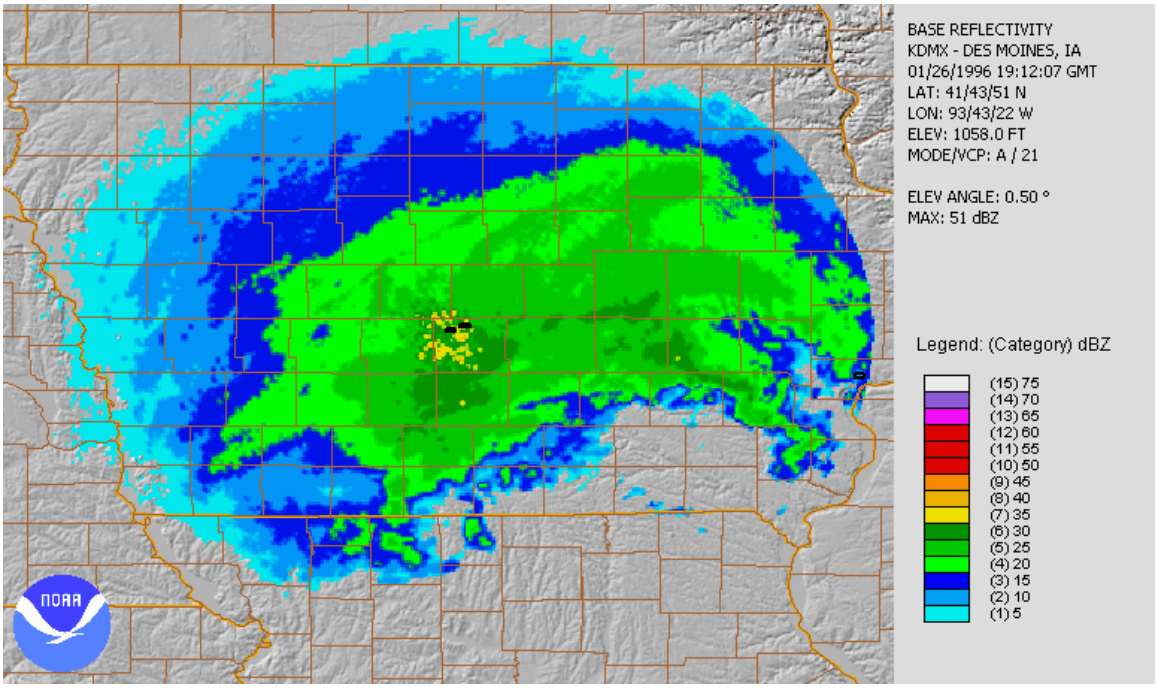

Fig 4.2.4: A base reflectivity image from Des Moines, IA, and lightning flashes at 1912 UTC 26 January 1996.

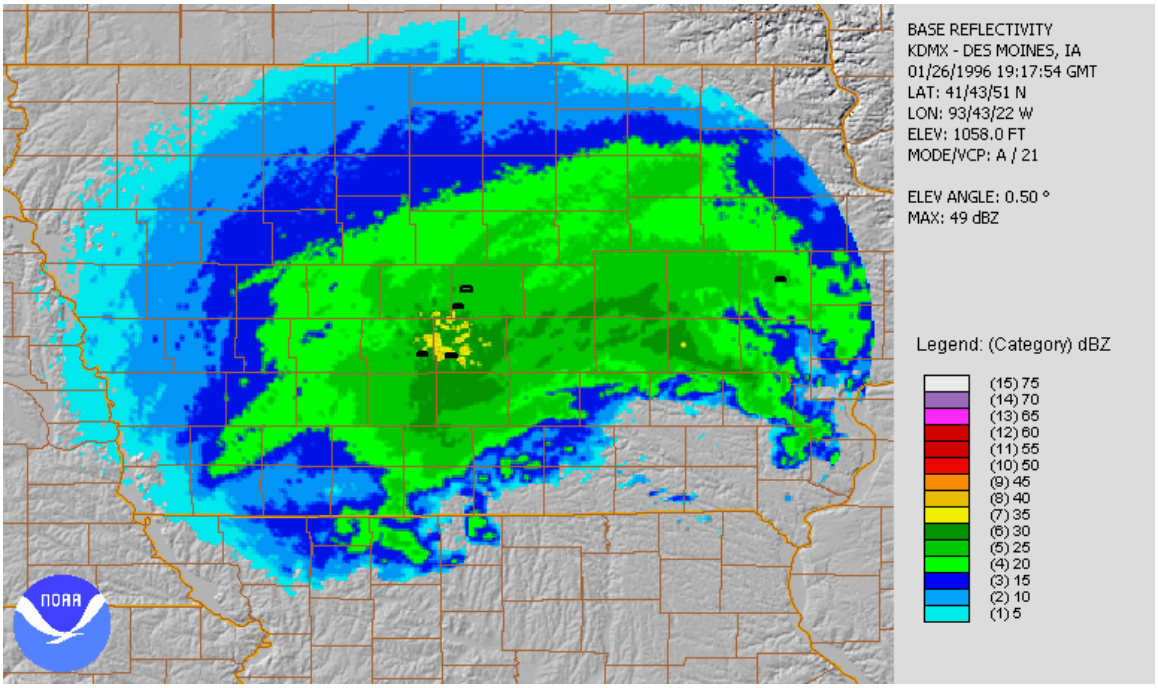

Fig 4.2.5: A base reflectivity image from Des Moines, IA, and lightning flashes at 1917 UTC 26 January 1996.

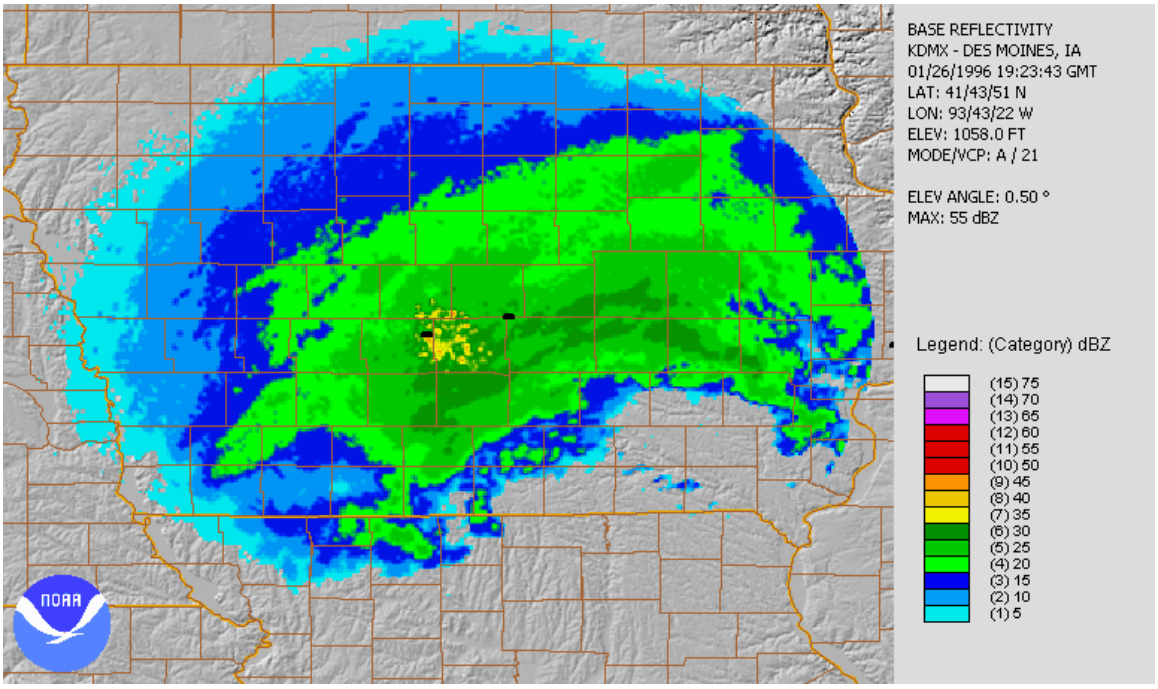

Fig 4.2.6: A base reflectivity image from Des Moines, IA, and lightning flashes at 1923 UTC 26 January 1996.

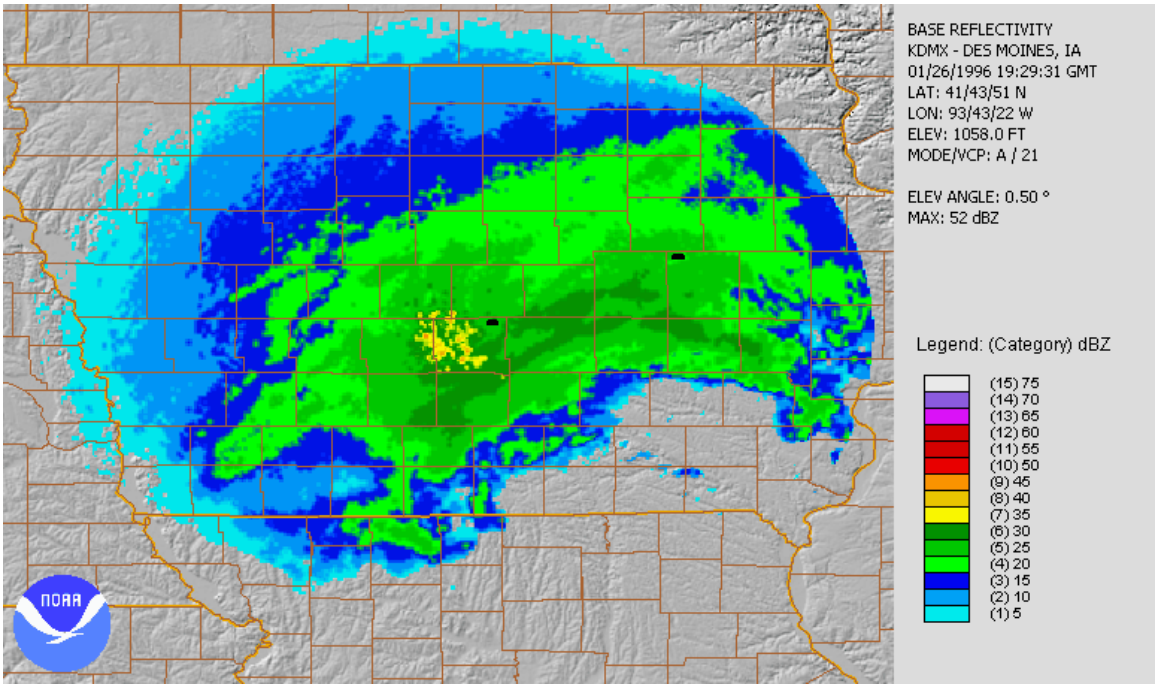

Fig 4.2.7: A base reflectivity image from Des Moines, IA, and lightning flashes at 1929 UTC 26 January 1996.

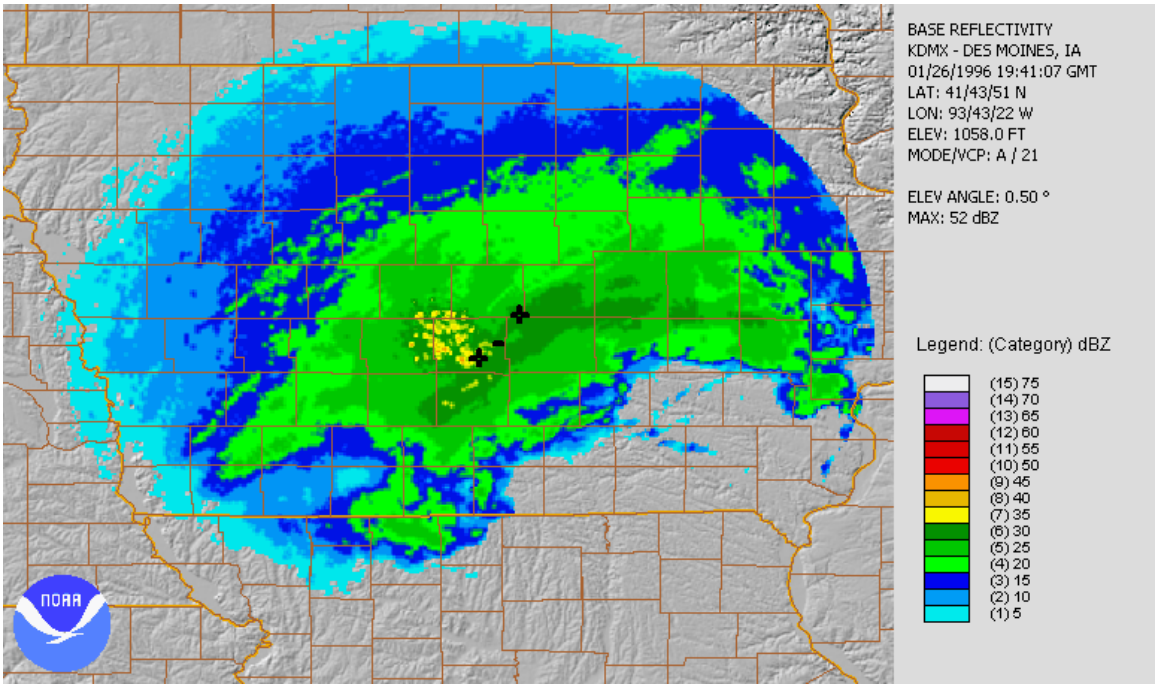

Fig 4.2.8: A base reflectivity image from Des Moines, IA, and lightning flashes at 1941 UTC 26 January 1996.

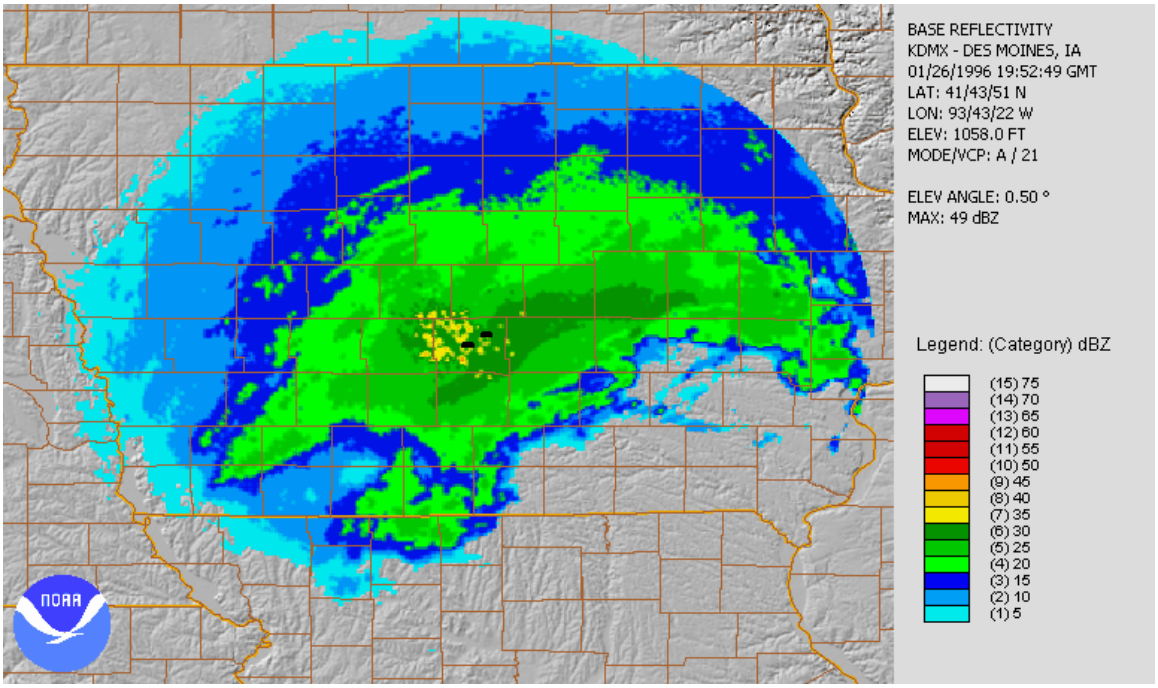

Fig 4.2.9: A base reflectivity image from Des Moines, IA, and lightning flashes at 1952 UTC 26 January 1996.

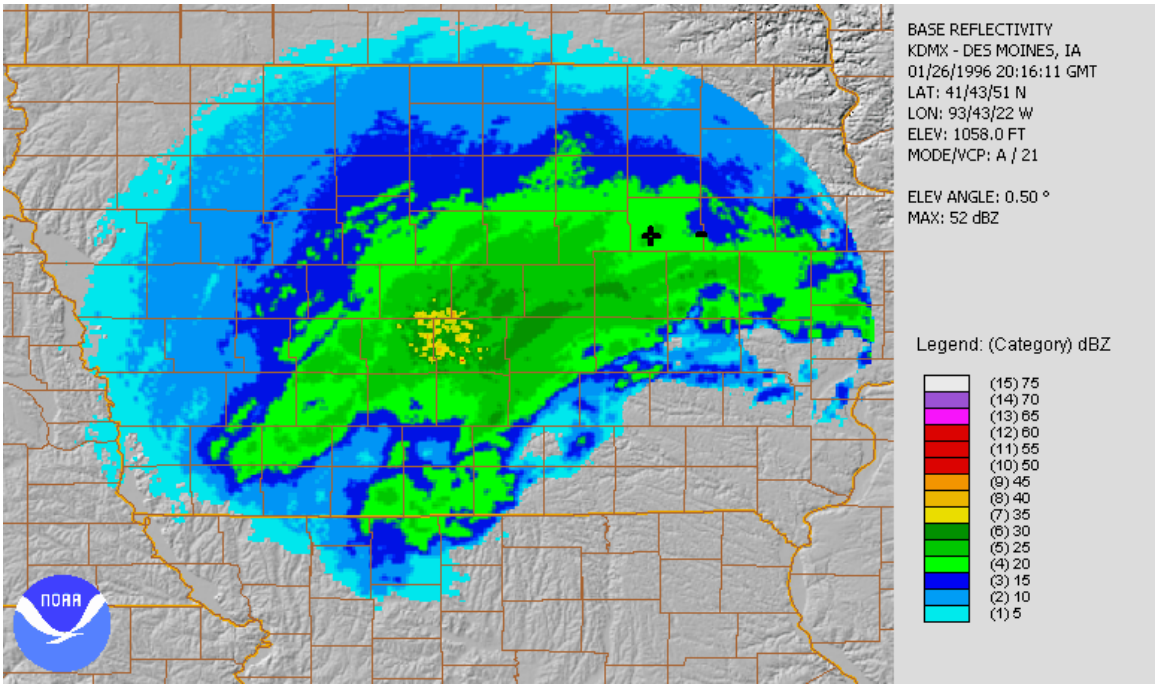

Fig 4.2.10: A base reflectivity image from Des Moines, IA, and lightning flashes at 2016 UTC 26 January 1996.

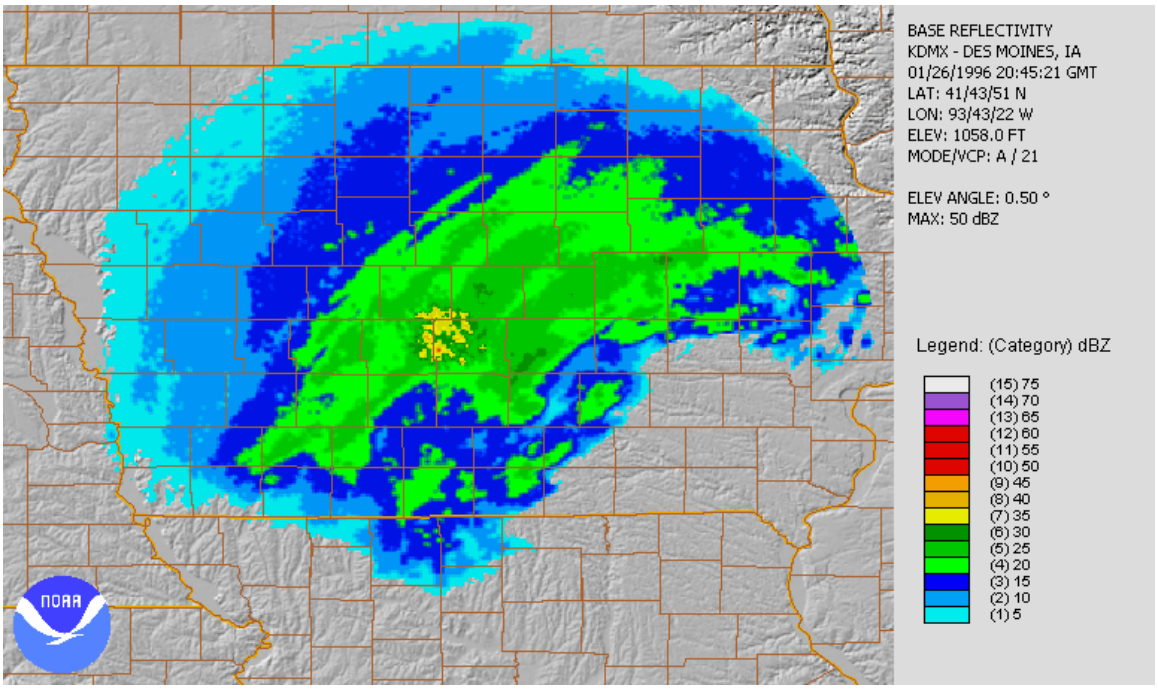

Fig 4.2.11: A base reflectivity image from Des Moines, IA, and lightning flashes at 2045 UTC 26 January 1996.

4.3 8 March 1999

The second event analyzed was classified as a frontal event. The event occurred near Sioux Falls, SD, (FSD) on 8 March 1999. No cyclonic circulation was evident in the radar imagery as it was too far removed from the electrified convective snowfall event. However, there was a constant southwest to northeast movement of the radar echoes as they traveled along the warm frontal boundary. The first composite at 0512 UTC (Fig. 4.3.1) of radar and lightning flash data shows that this event was more banded in structure than the previous event. It is clear that this area consisted of numerous small bands. This banded structure is further evidence that electrified convective snowfall events are created by elevated convection as this convection has been shown to result in precipitation bands (Xu 1989).

As evident from 0512 until 0645 UTC, all of the lightning flashes were located in the southern part of the scan where new electrified convective snowfall bands were developing (Fig. 4.3.1 – Fig. 4.3.7). The lightning flashes almost always occurred in the areas with the greatest base reflectivity. Conversely, from 0625 to 0836 UTC, the lightning flashes appeared farther north and within the more structured banded region (Fig. 4.3.8 – Fig. 4.3.12). This change in lightning flash location was likely due to the lack of development of new convective snow bands across the area and is illustrated in the base reflectivity by the expansion of the existing bands, the weakening of the banded structure, and the lack of new bands moving in from the south.

Therefore, the radar imagery and lightning flash composites show an organized and banded structure along the warm frontal zone. The majority of the lightning flashes occur in the area of convective snow band formation, which was likely the most unstable area within the event. When new snow band formation ceased, it appears that the snow bands still possessed a separation of electrical charge capable of producing flashes. Also, the lightning flash locations in electrified convective snowfall events should not be considered the only areas where heavy snowfall may occur, and these locations are not a continuous phenomenon throughout the area that the electrified convective snowfall occurs.

This frontal event clearly demonstrates a banded appearance in the radar imagery. The presence of CSI identified in Chapter 3 is related to banded precipitation as discussed in Chapter 1. Lightning strike locations vary from the development of bands at the onset of the event to the residual bands at the conclusion of the event. This may indicate that the event weakened time progressed.

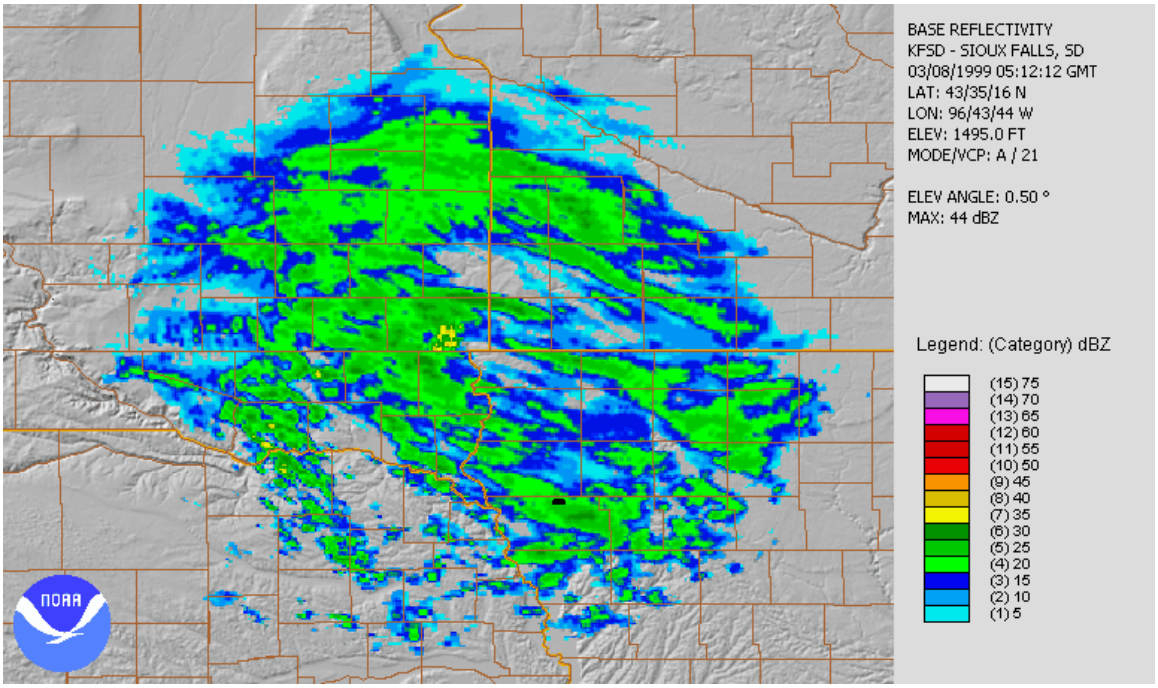

Fig 4.3.1: A base reflectivity image from Sioux Falls, SD, and lightning flashes at 0512 UTC 8 March 1999.

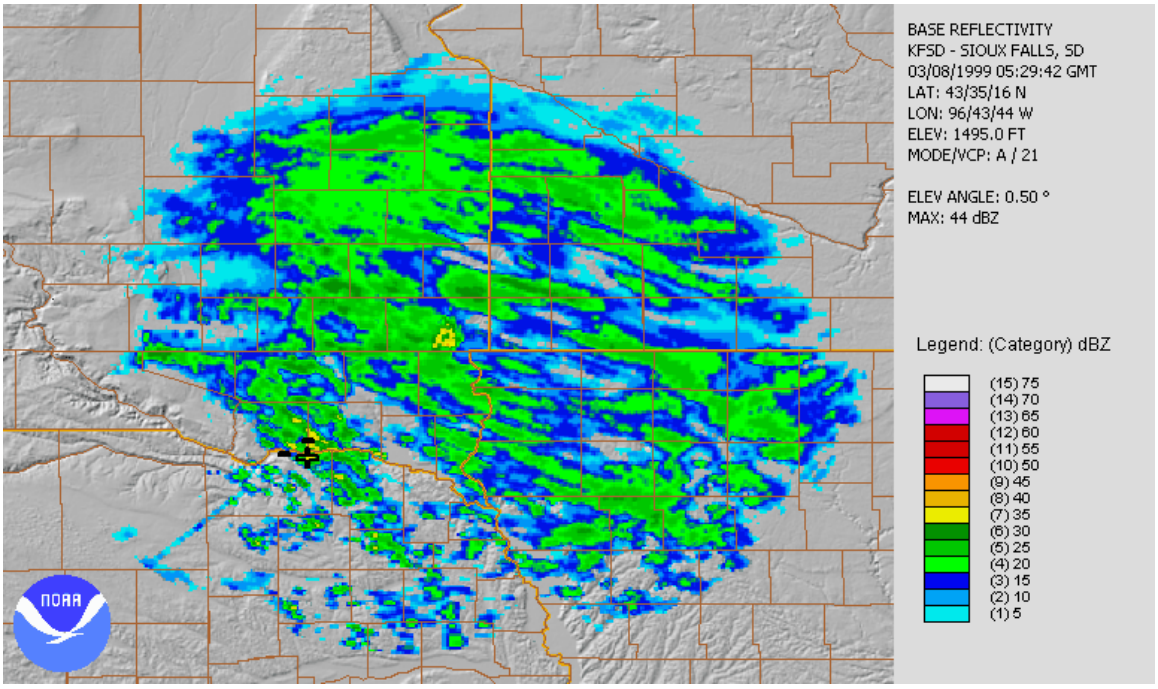

Fig 4.3.2: A base reflectivity image from Sioux Falls, SD, and lightning flashes at 0529 UTC 8 March 1999.

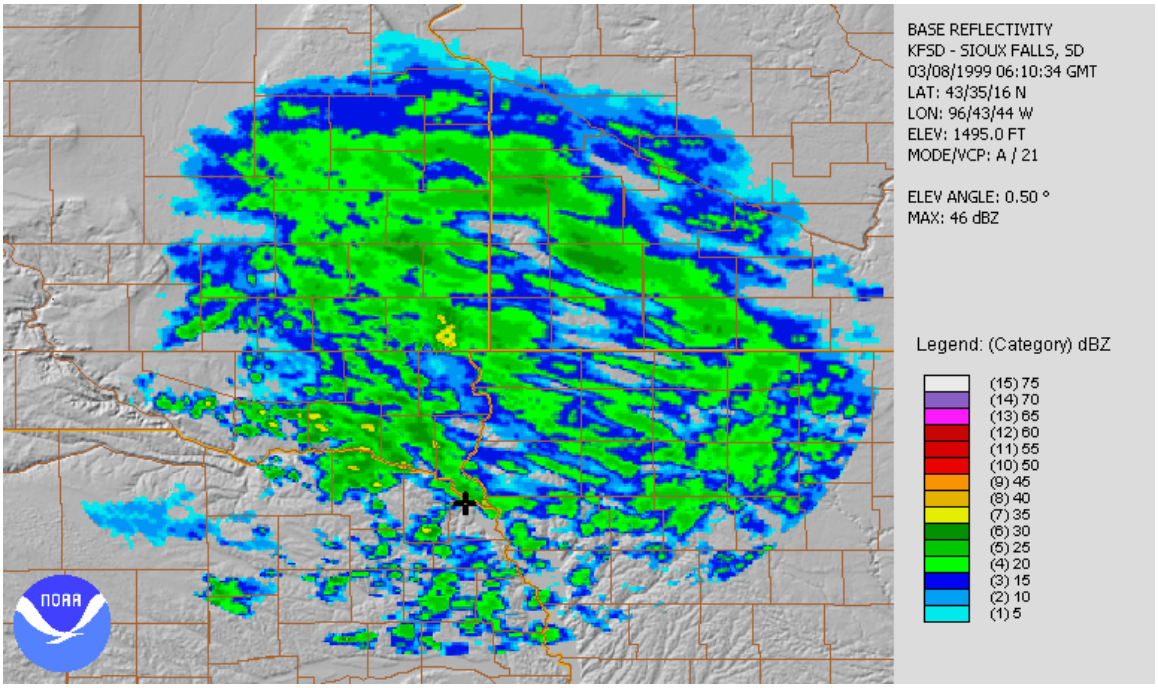

Fig 4.3.3: A base reflectivity image from Sioux Falls, SD, and lightning flashes at 0610 UTC 8 March 1999.

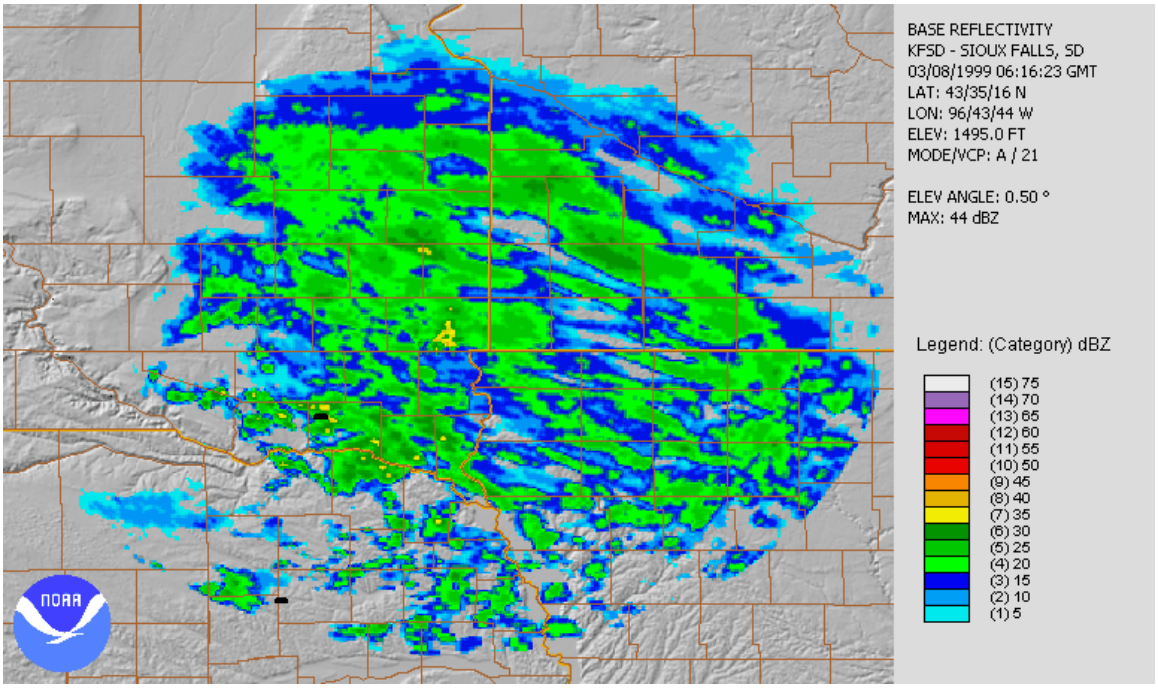

Fig 4.3.4: A base reflectivity image from Sioux Falls, SD, and lightning flashes at 0616 UTC 8 March 1999.

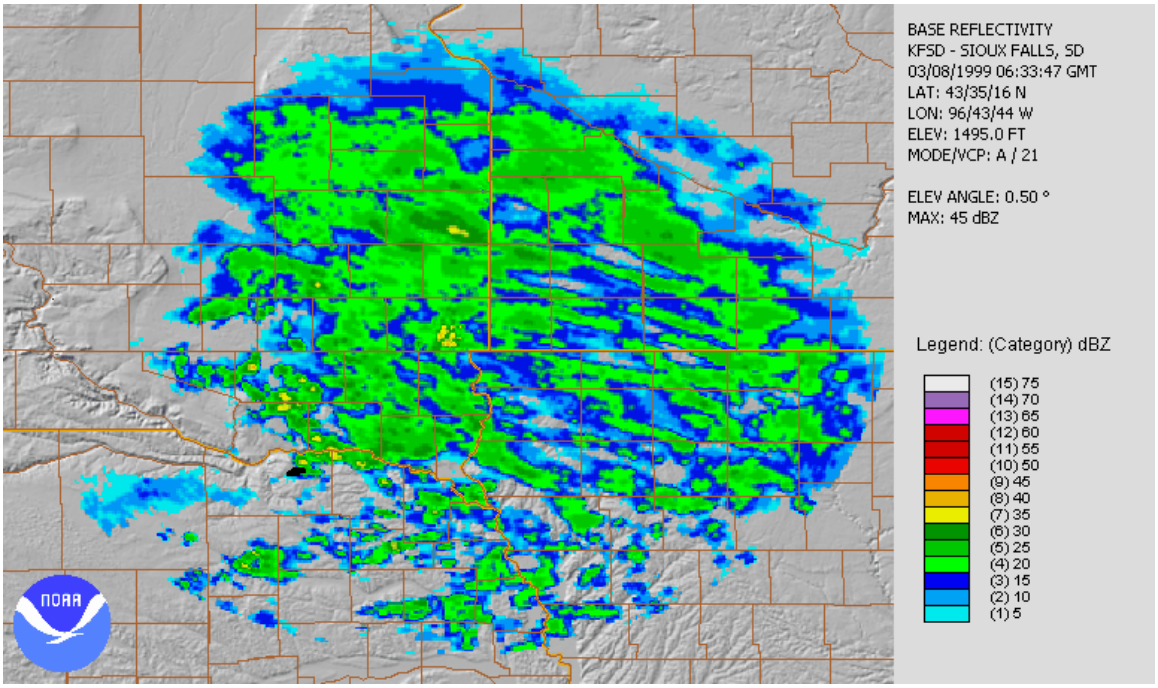

Fig 4.3.5: A base reflectivity image from Sioux Falls, SD, and lightning flashes at 0633 UTC 8 March 1999.

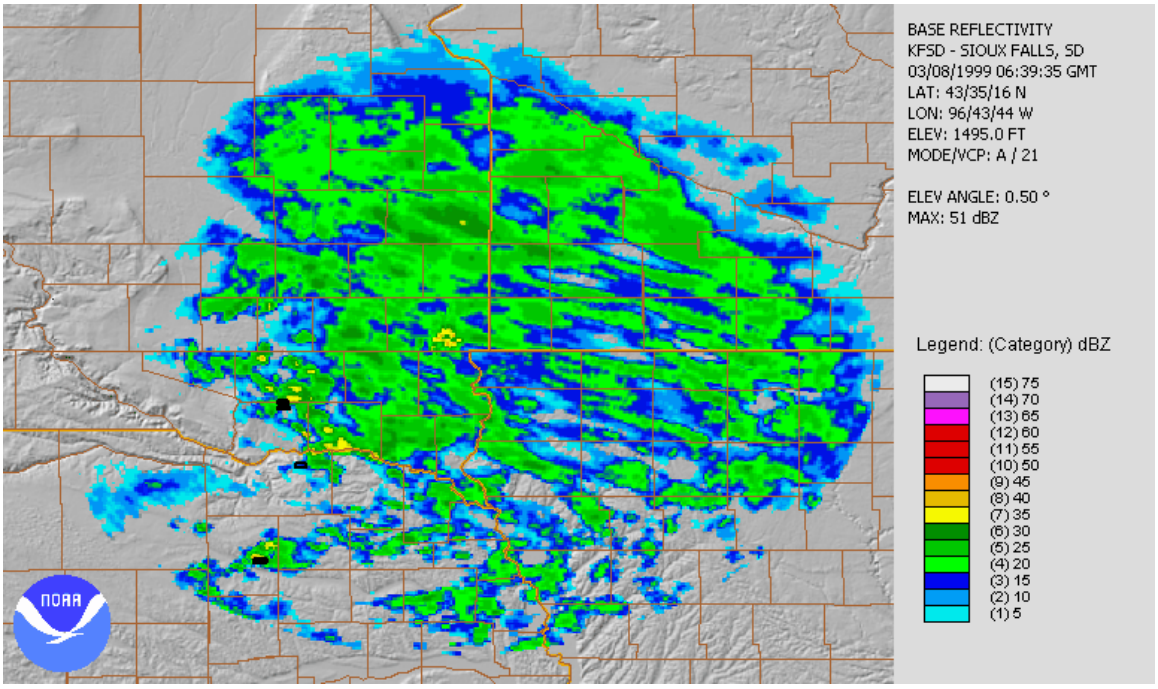

Fig 4.3.6: A base reflectivity image from Sioux Falls, SD and lightning flashes at 0639 UTC.

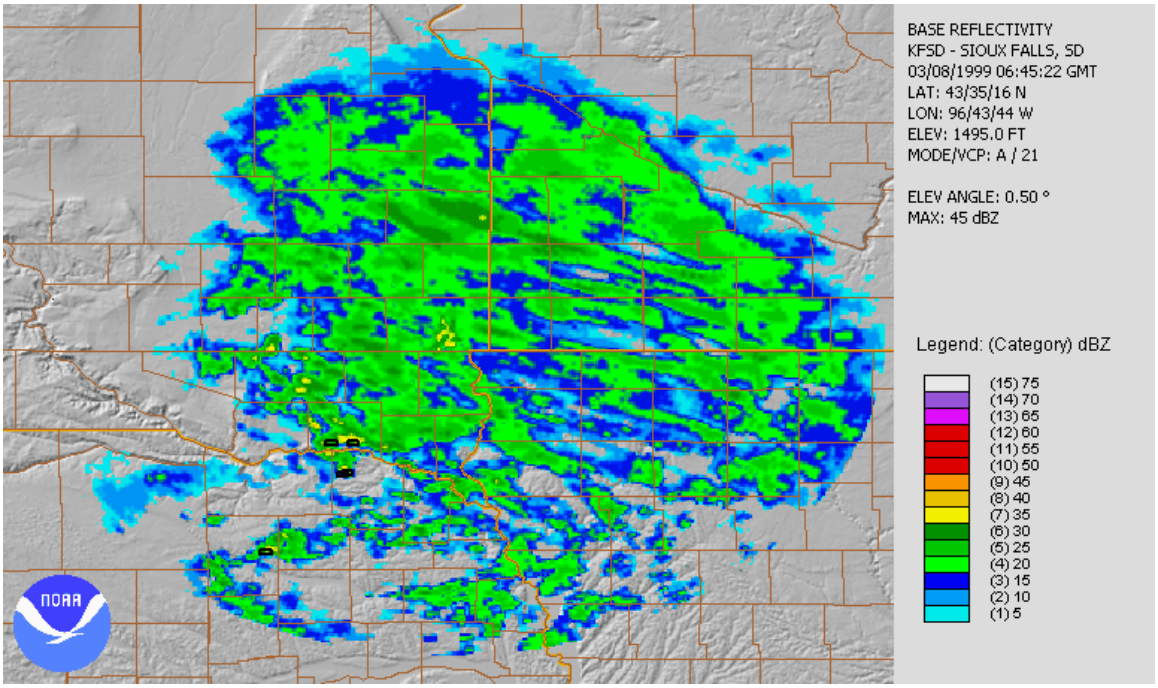

Fig 4.3.7: A base reflectivity image from Sioux Falls, SD, and lightning flashes at 0645 UTC 8 March 1999.

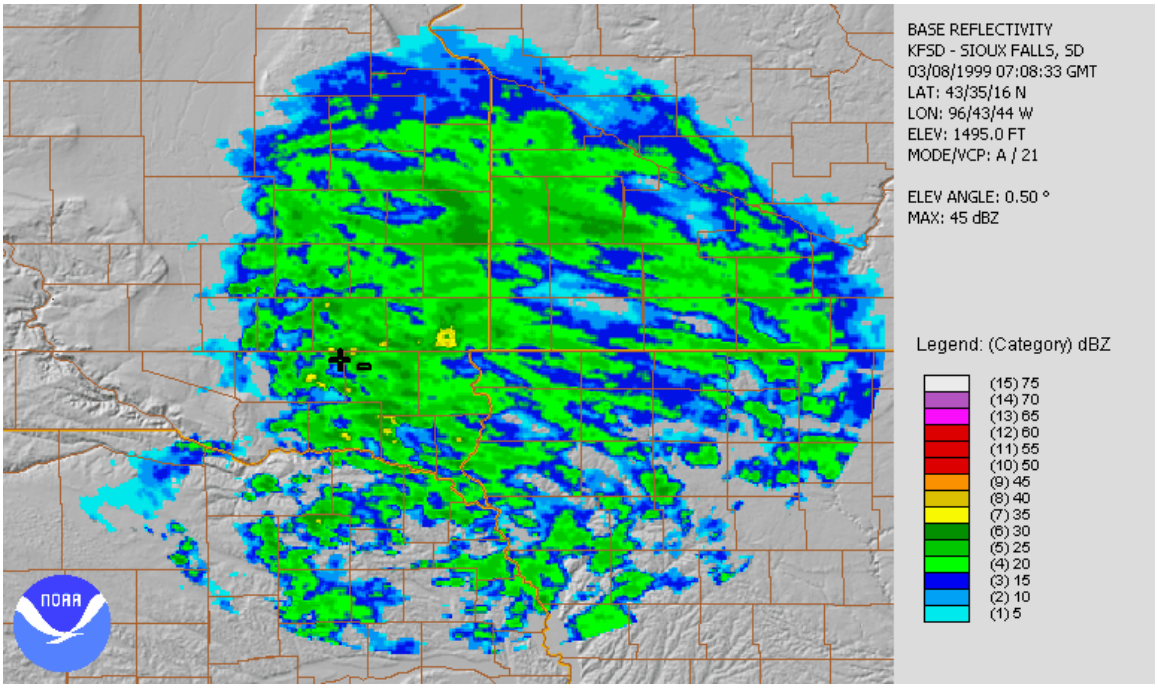

Fig 4.3.8: A base reflectivity image from Sioux Falls, SD, and lightning flashes at 0708 UTC 8 March 1999.

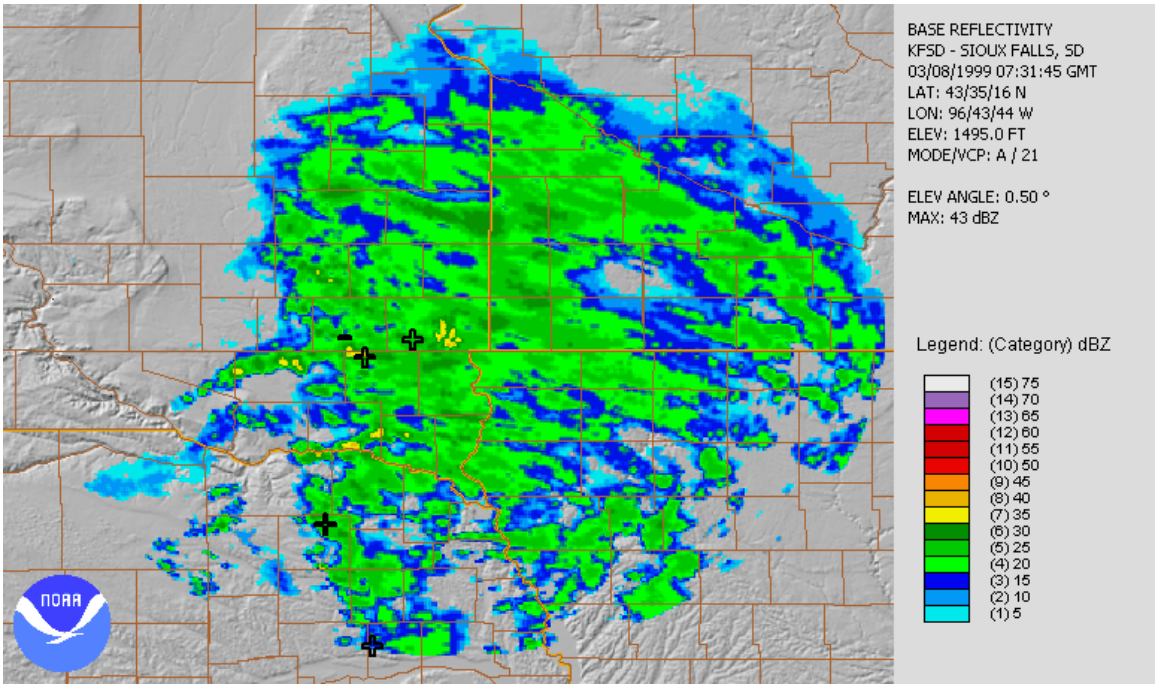

Fig 4.3.9: A base reflectivity image from Sioux Falls, SD, and lightning flashes at 0731 UTC 8 March 1999.

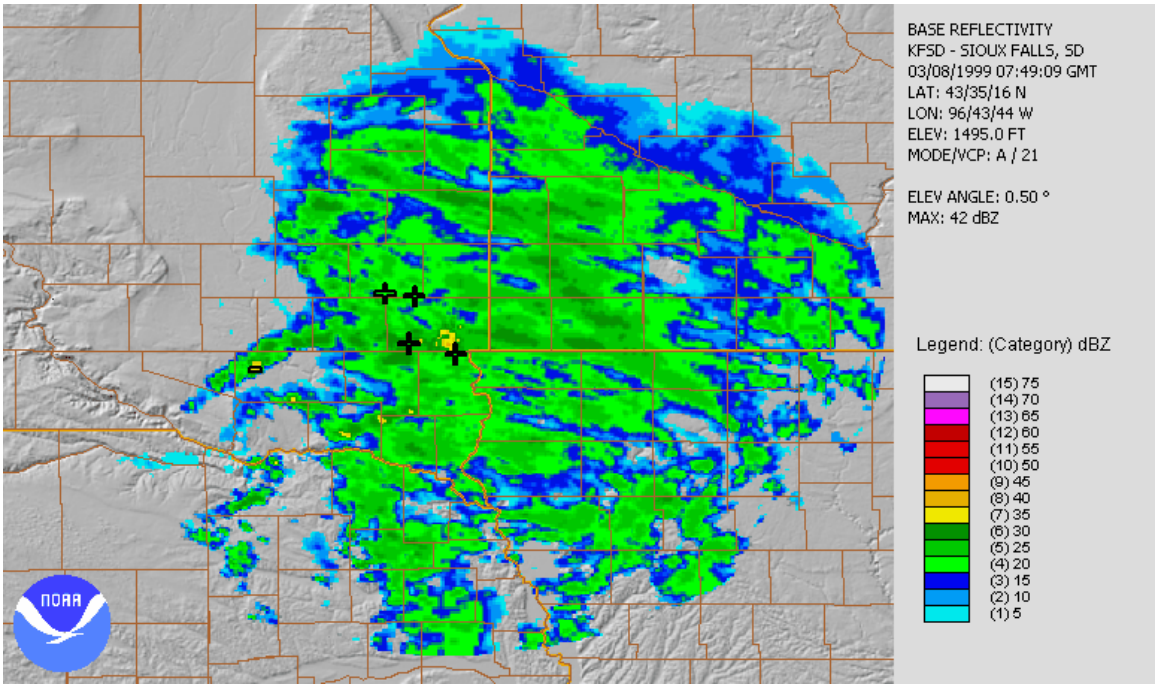

Fig 4.3.10: A base reflectivity image from Sioux Falls, SD, and lightning flashes at 0749 UTC 8 March 1999.

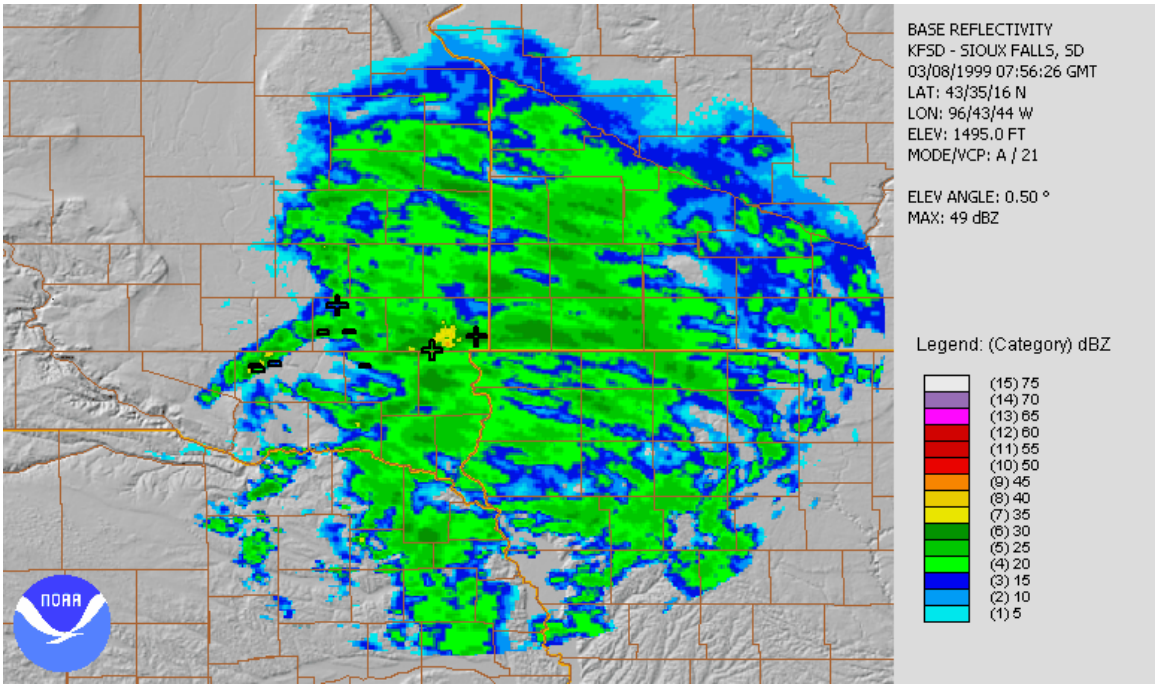

Fig 4.3.11: A base reflectivity image from Sioux Falls, SD, and lightning flashes at 0756 UTC 8 March 1999.

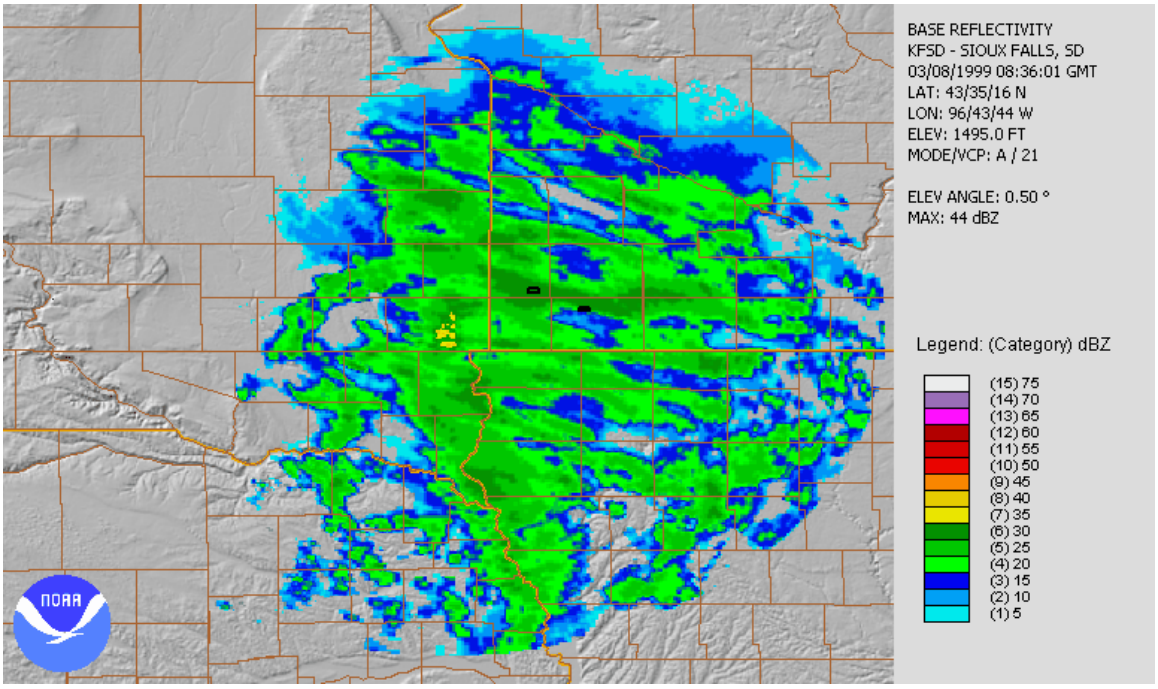

Fig 4.3.12: A base reflectivity image from Sioux Falls, SD, and lightning flashes at 0836 UTC 8 March 1999.

4.4 24 November 2004

The third case study using radar and lightning composites was a cyclonic event during 24 November 2004 across north-central Illinois. As with the first event in 1996, this event was also located in the western half of the cyclone in the "wrap around" region. The electrified convective snowfall occurred in the snow shield on the western side of the radar scan rather than the east. As with the 1996 event, the first composite at 1901 UTC (Fig. 4.4.1) reveals 3 lightning flashes (2 positive and 1 negative) near the deformation zone identified in Fig 3.4.12. Within the radar echoes, a stronger band of snowfall is seen in the middle of the snow shield. Also present in this composite were "finger-like" edges similar to the 1996 event as well (Fig. 4.2.1).

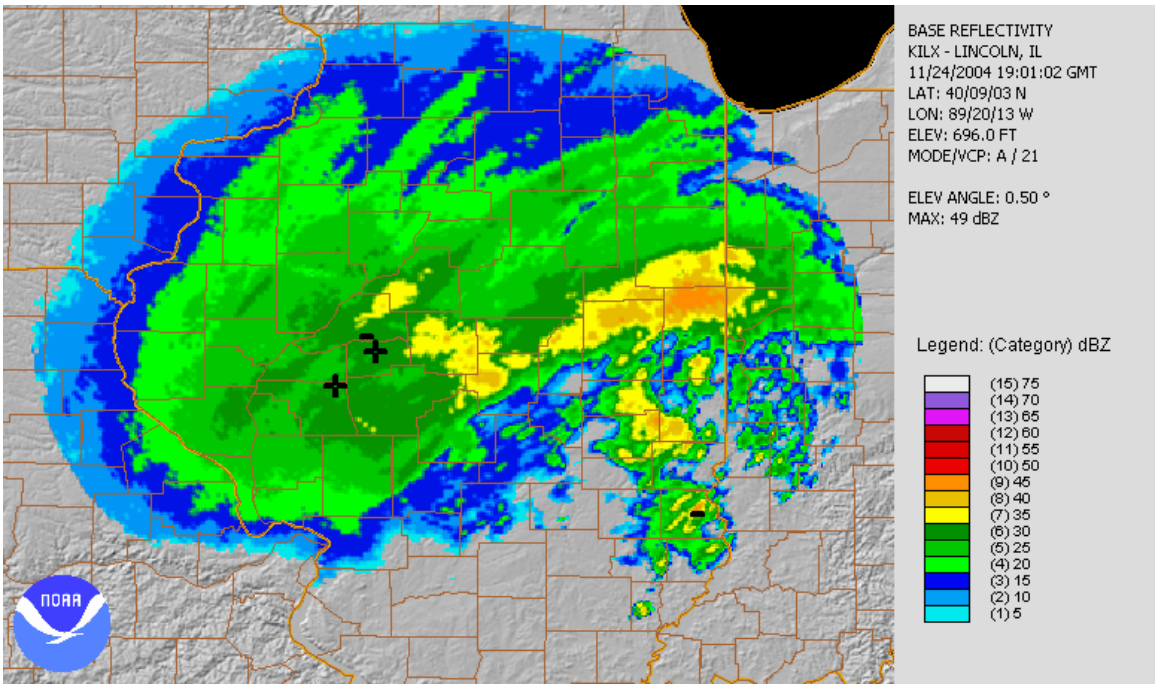

Fig. 4.4.1: A base reflectivity image from Lincoln, IL, and lightning flashes at 1901 UTC 24 November 2004.

The electrified snowfall bands developed during 1906 to 1918 UTC (Fig. 4.4.2 – Fig. 4.4.5). The composites reveal that the lightning flashes moved to the bands from the deformation area identified in Fig. 3.4.12. After this period of convective development, there was a lull in the lightning flashes until 1953 UTC (Fig. 4.4.5). Fig. 4.4.5 illustrates the development of banding north of the deformation zone with two negatively charged lightning flashes. Six minutes later, at 1959 UTC (Fig. 4.4.6) the rapid convective development was associated with a number of both positive and negatively charged lightning flashes. The bands north of the deformation were locations of the highest reflectivity values.

At the end of this event (Fig. 4.4.7 – Fig. 4.4.10), the bands running the length of the precipitation shield began to degenerate and the snow shield began to take a more ragged appearance. Again, this is likely due to the weakening of the organized elevated convection discussed in the Chapter 3. While the banding in this event was not extremely smooth, the radar imagery shows areas of heavier snowfall associated with the elevated convection. The degeneration of the organized elevated convection seemed to widen the existing snow bands as their intensities decreased until the banded structure was no longer apparent in the imagery.

Again, the banding illustrated in the radar imagery is clearly related the presence of CSI as identified in Chapter 3. The majority of the lightning strikes occur within the area of deformation as identified in Fig. 3.4.12. This is the only event where more than ten lightning strikes occurred in a five minute time period, and this may indicate rapid development within the event.

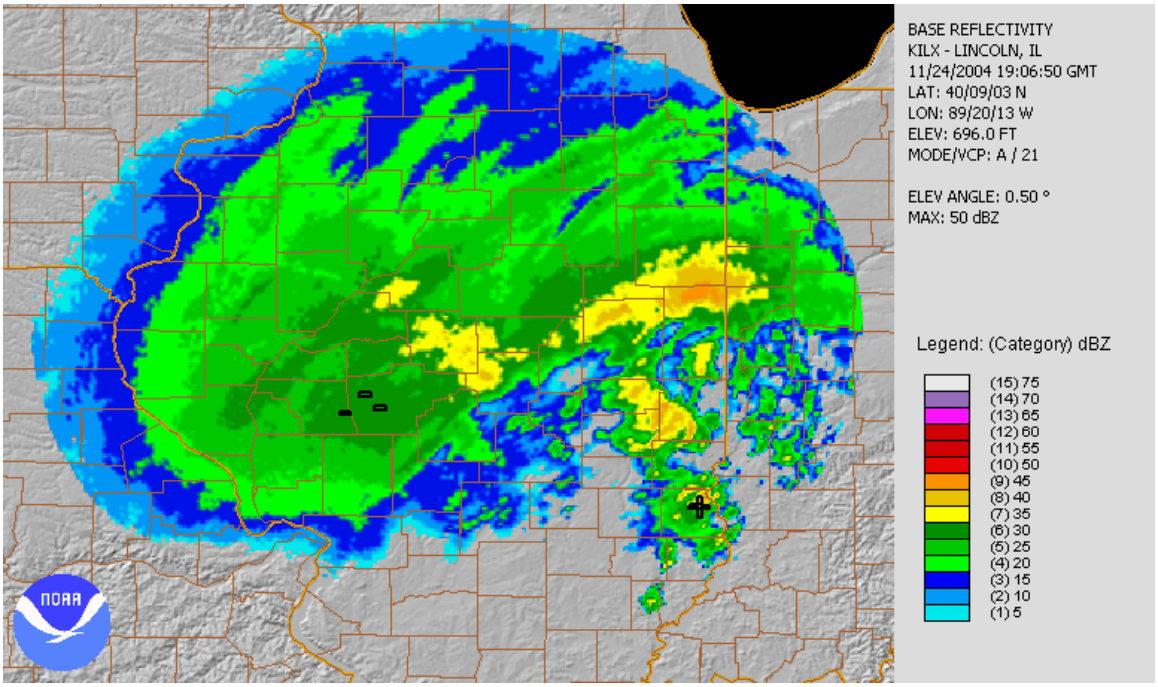

Fig 4.4.2: A base reflectivity image from Lincoln, IL, and lightning flashes at 1906 UTC 24 November 2004.

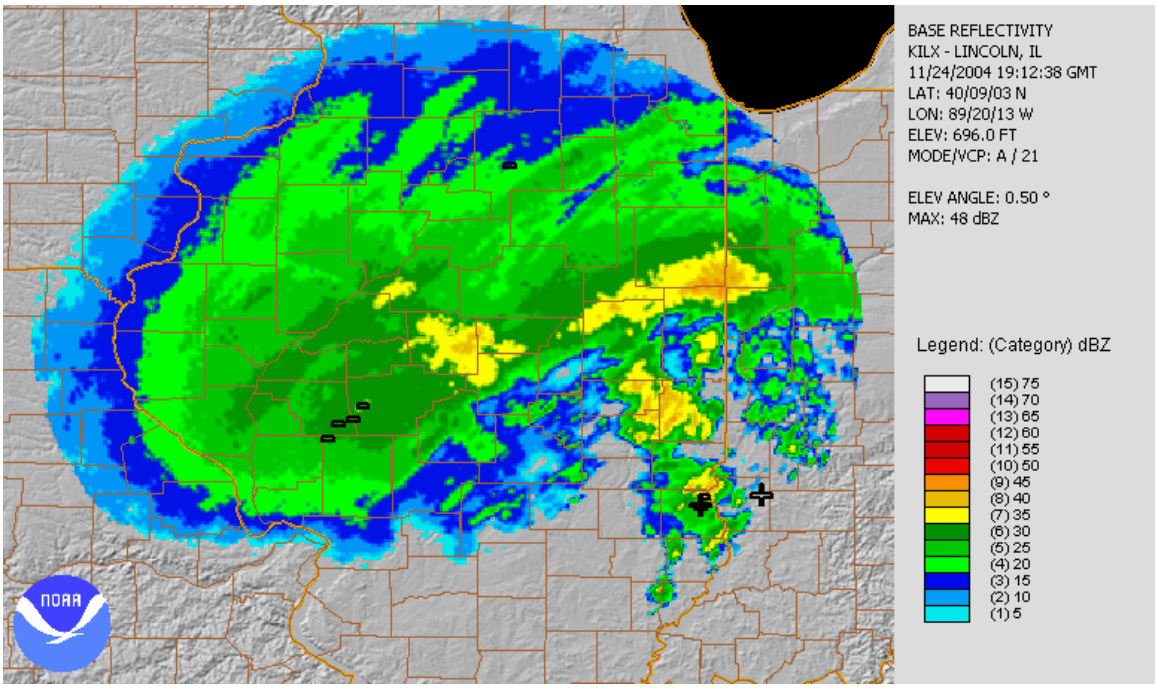

Fig 4.4.3: A base reflectivity image from Lincoln, IL, and lightning flashes at 1912 UTC 24 November 2004.

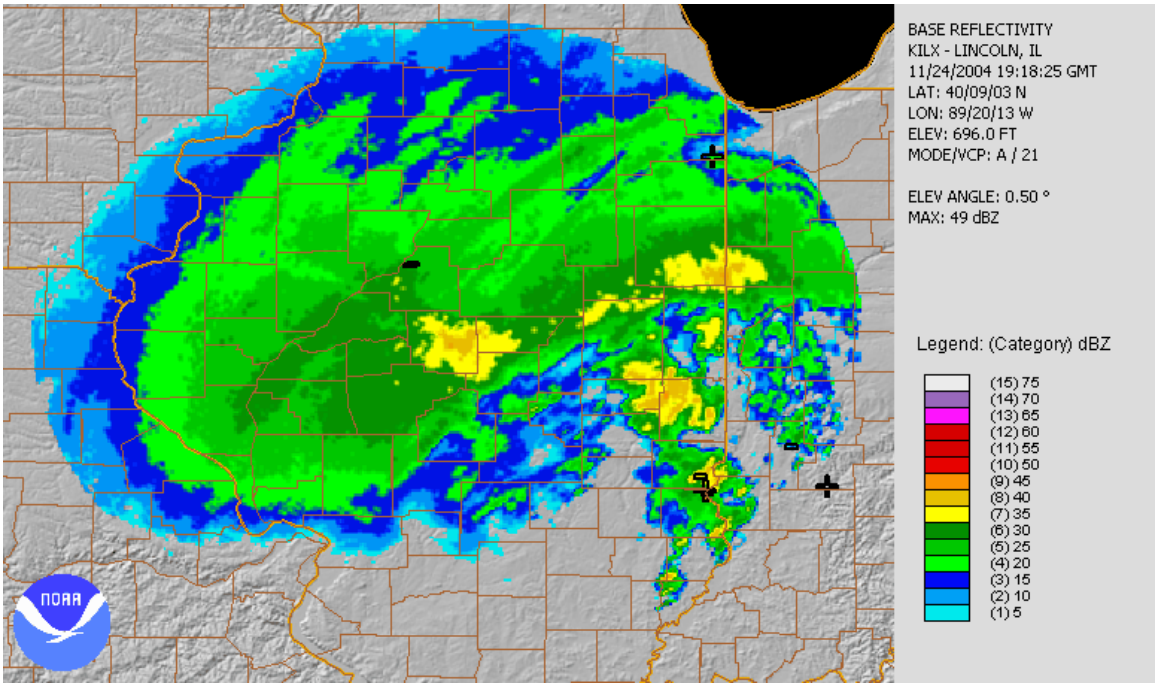

Fig 4.4.4: A base reflectivity image from Lincoln, IL, and lightning flashes at 1918 UTC 24 November 2004.

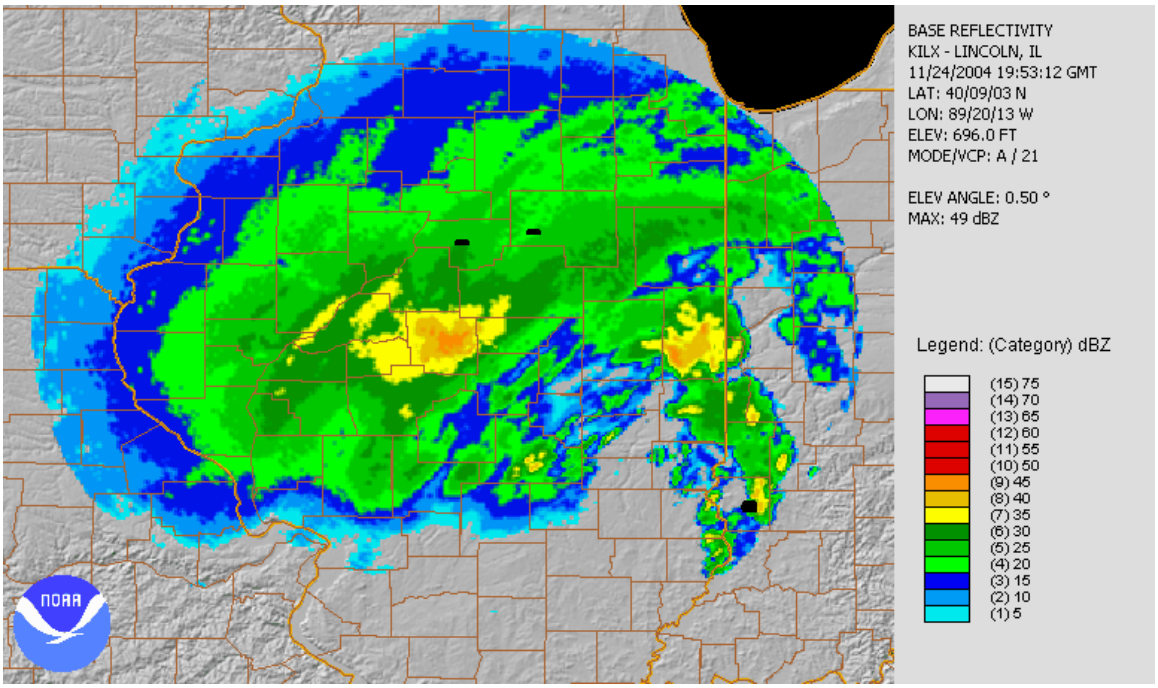

Fig 4.4.5: A base reflectivity image from Lincoln, IL, and lightning flashes at 1953 UTC 24 November 2004.

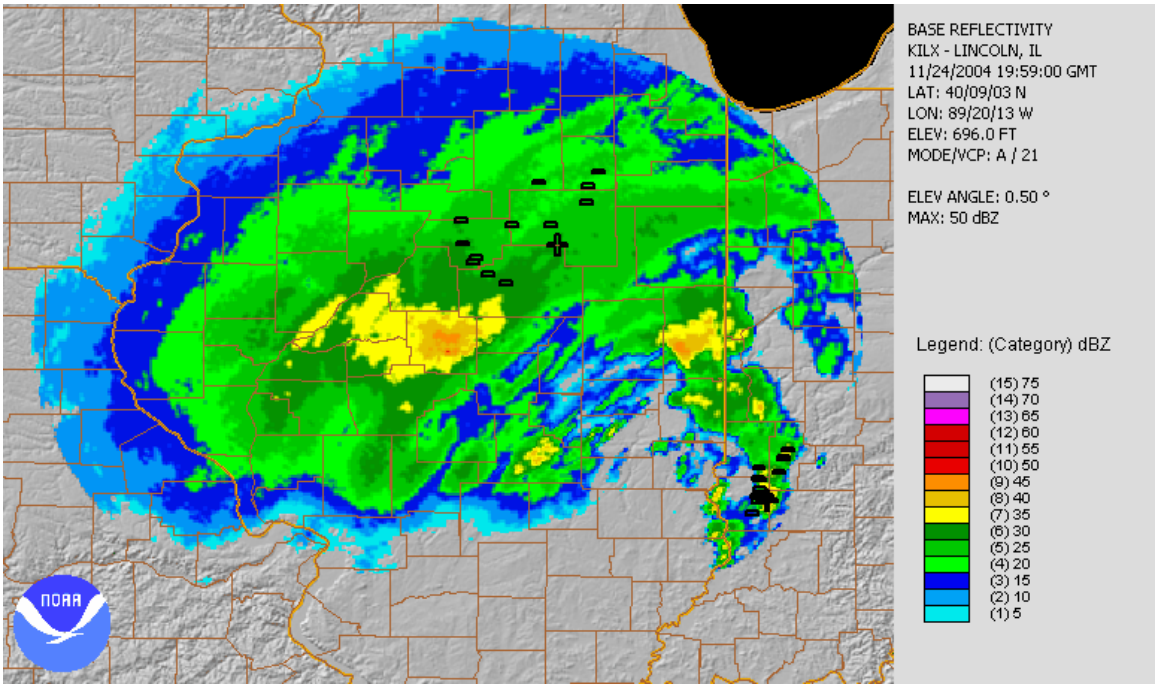

Fig 4.4.6: A base reflectivity image from Lincoln, IL, and lightning flashes at 1959 UTC 24 November 2004.

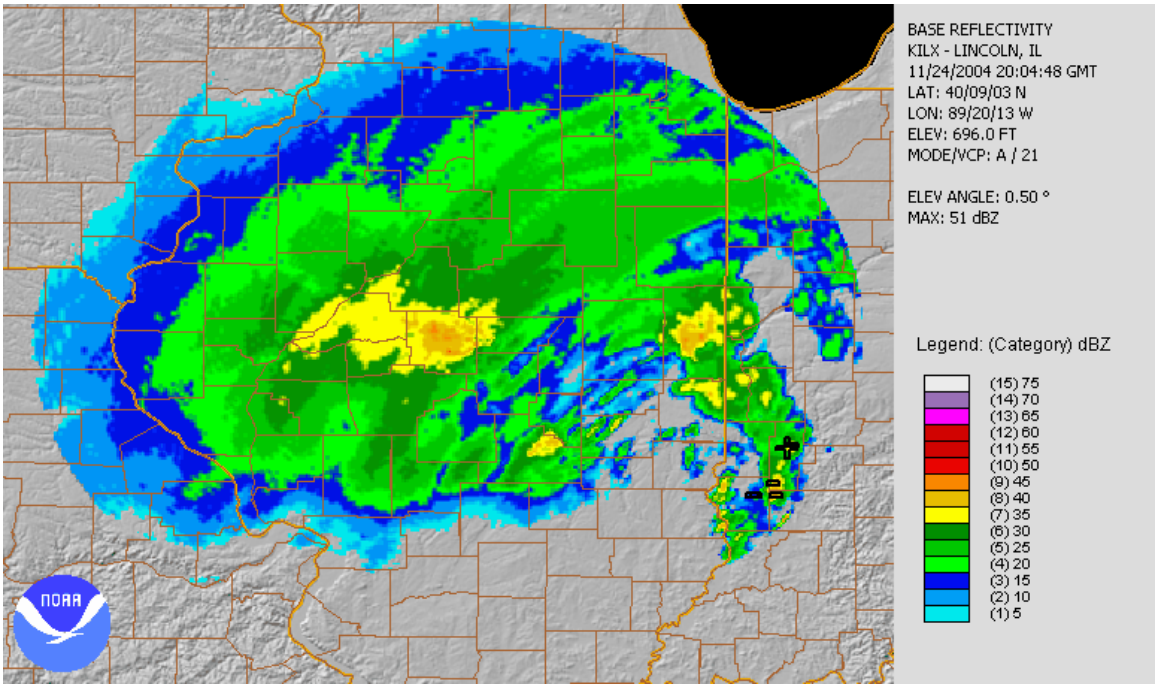

Fig 4.4.7: A base reflectivity image from Lincoln, IL, and lightning flashes at 2004 UTC 24 November 2004.

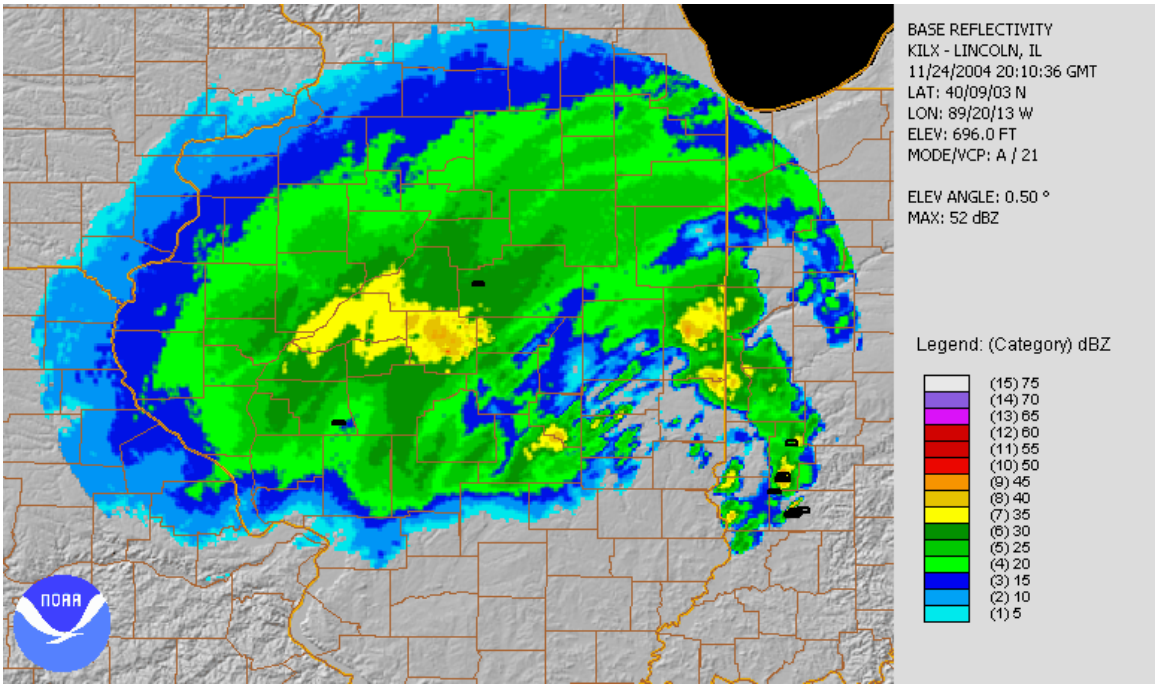

Fig 4.4.8: A base reflectivity image from Lincoln, IL, and lightning flashes at 2010 UTC 24 November 2004.

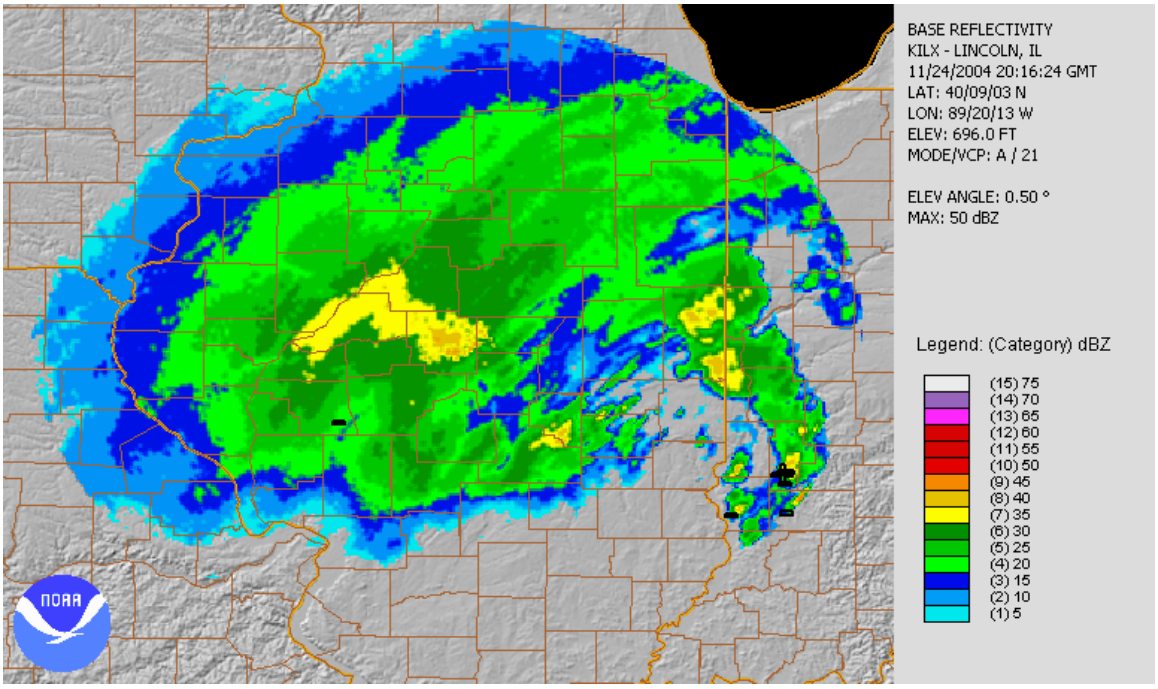

Fig 4.4.9: A base reflectivity image from Lincoln, IL, and lightning flashes at 2016 UTC 24 November 2004.

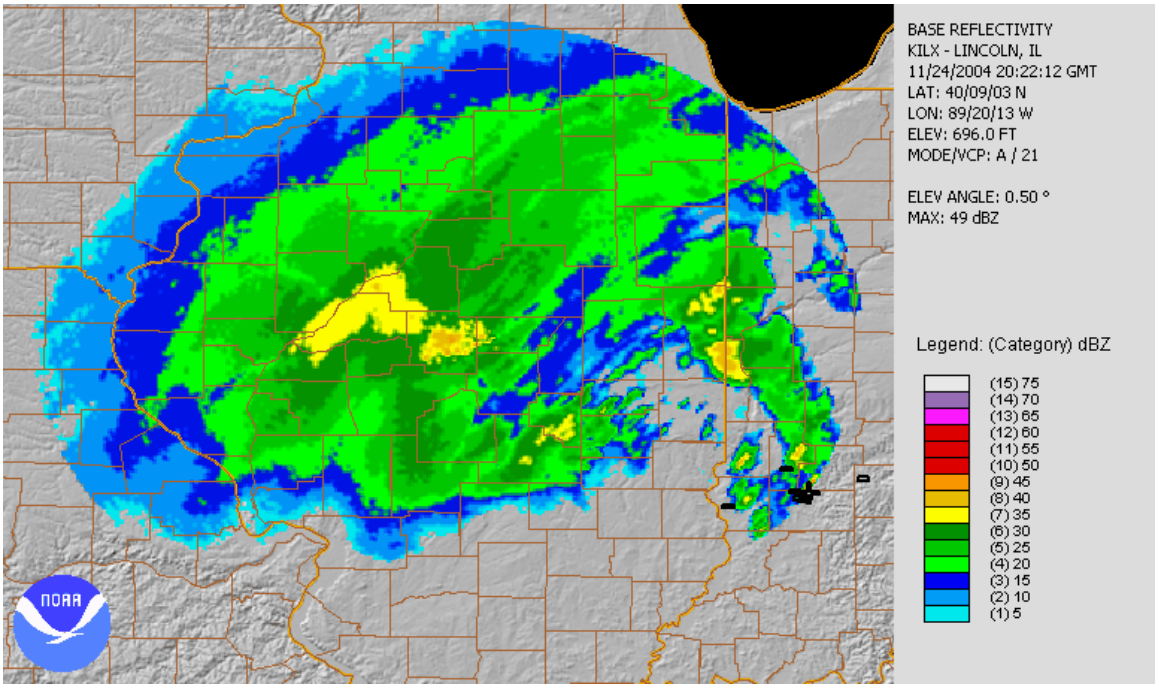

Fig 4.4.10: A base reflectivity image from Lincoln, IL, and lightning flashes at 2022 UTC 24 November 2004.

4.5 Conclusions

From the climatology created and described in the previous chapter, three electrified convective snowfall events were selected and analyzed using both radar imagery and lightning flash data. Other than Schultz et al. (2004), this is the only study that has identified electrified convective snowfall events using radar imagery. Two of these events were classified as cyclone induced events (the 26-27 January 1996 and 24 November 2004 events). The other event (8 March 1999) occurred along a warm frontal zone. These three events were selected for the analysis as they occurred over large areas with multiple lightning flashes.

The January and March electrified convective snowfall events had a higher percentage of positive lightning flashes recorded than the November event. However, all three events had a higher percentage of positive lightning flashes than most convection.

Two possible explanations exist for this characteristic. First and most likely, a tripole separation of charges (see Fig. 6.1.2) in the cloud could be initiated within the strongest stratiform or development areas. The second possibility was the mis-identification of intra-cloud or cloud-to-cloud lightning as a positive flash and was dismissed as there was too few low amperage strikes within the events. The tripole separation of charges is more likely since 199 of 200 low amperage flashes (ones which may have been miss identified) occurred in the 24 November 2004 event, the event with the lowest percentage of positive flashes.

In each of the three events, at least one band of higher reflectivity was present. The two cyclonic events seemed to favor a single band of heavier snowfall with most of the lightning flashes near the deformation zone during the strengthening of the event. The lightning flashes were most prevalent within the band as the bands slowly began to decrease in intensity. The cyclone events also had the presence of "finger-like" features at the edge of the precipitation shield. These features did contain multiple lightning flashes at the onset of each cyclone-associated electrified convective snowfall event.

A more banded structure was present in the event associated with the warm frontal zone. Banding has been associated with CSI by Schultz et al. (2004), Sherwood (2000), Schultz et al. (2000), Moore and Lambert (1993), Sanders (1986), Wolfsberg et al. (1986), and Sanders and Bosart (1985). The CSI associated with this event was identified in Chapter 3. The majority of the lightning flashes appeared in the area of development of new snow bands while the event was still developing. As each event began to lose its intensity, a noticeable shift occurred with the lightning flash locations as they moved farther north and into the established bands. This shift was likely due to the

degeneration of the elevated convection. Therefore, the established snow bands possessed a separation of charge and were able to produce more lightning flashes.

CHAPTER 5
CONCLUSIONS AND FUTURE RESEARCH

Due to the high snowfall rates and totals often associated with electrified convective snowfall events, many disruptions to business, transportation, and schools can occur with these events. People have been killed from roof collapses, tree collapses, or even heart attacks from removing the large accumulations of snow occurring during these events. The focus of this thesis has been to identify when, where, and how electrified convective snowfall events occur and to identify the appearance of these events in radar imagery. The investigation of these questions began with the creation of a climatology of electrified convective snowfall events for the period of record of 1960-2005. With this climatology and synoptic case studies of the most frequent synoptic types, three recent events were then selected for further analysis with both lightning flash data and base reflectivity radar imagery. The overarching objectives of this thesis were to identify the spatial and temporal characteristics of electrified convective snowfall, the environment conducive to their development, and to investigate radar signatures associated with these events.

5.1 Climatological Characteristics of Electrified Convective Snowfall Events

Three questions were answered by the climatology of electrified convective snowfall events including: (1) Where do these events occur? (2) When do these events occur? (3) What is the environment required for the development of these events? By

answering these questions a better understanding of electrified convective snowfall events has been obtained. This process revealed 706 events within the period of record of this study, considerably more than the 191 events identified by Market et al. (2002). This increase is expected as this study examined events using hourly surface observations rather than three-hourly observations over a 16 year longer period. A larger number of events affects the remainder of the climatological investigation. A "corridor" of electrified convective snowfall events is apparent from Nevada and to New England in the east. Events decreased in number both north and south of this corridor. A diurnal analysis revealed that electrified convective snowfall events occur most frequently between 2100 and 0200 local time. Two explanations for this include the increase in the strength of the low-level jet during this time period and the ease of identifying lightning during the night. The seasonal analysis demonstrated that electrified convective snowfall events are most likely to occur in March and April, but there was also a smaller secondary maximum in November. These two maxima can be explained by the migration of the polar front crossing the corridor identified in the spatial analysis. The spring maximum is likely larger due to the strength of storm systems moving through the area during this time coupled with the existence of cold air capable of supporting snowfall.

A synoptic analysis of the electrified convective snowfall categorized into seven groups including: coastal, cyclone, frontal, lake effect/enhanced, orographic, upslope, and unclassifiable. Cyclonic events were the most common, comprising 40% of all electrified convective snowfall events during the period. The remainder of events included frontal (30%), orographic (9%), coastal (9%), lake effect/enhanced (6%), upslope (4%) and

unclassifiable events (1%). Five events (2 cyclonic, 2 frontal, 1 orographic) were then selected as case studies to determine the environment conducive to producing these events. From these case studies, the synoptic environment was largely dominated by the presence of CSI or CI, warm air advection, a lower level zone of deformation, the low-level jet, and upper level divergence for the cyclonic and frontal events. The orographic event was the only one driven by the presence of CI. However, the other ingredients were not present as the lifting necessary for this event was provided by the mountains alone.

5.2 Lightning and Radar Characteristics of Electrified Convective Snowfall

The lightning data and radar imagery were used to determine the lightning characteristics and radar patterns associated with electrified convective snowfall events. The three most recent events from the case studies including 26-27 January 1996, 8 March 1999, and 24 November 2004 were investigated. The selection of more events was limited by the period of record of both the radar imagery and lightning data. The analysis of the lightning data revealed a higher fraction of positive polarity lightning flashes (as high as 30%) when compared to warm season convection (on average 5%). A higher percentage of positive polarity lightning flashes may be explained by a tripole separation of charges within the stronger areas of the stratiform clouds. This tripole separation of charges is the result of a stronger and more stratified storm structure which is associated with electrified convective snowfall events. The result of this tripole is a concentration of positively charged particles at the base of the cloud, therefore producing positive polarity lightning flashes.

Lightning flashes were typically in the areas of new snow band development as shown on base reflectivity radar imagery. When the band development ceased, due to the weakening or loss of convection, the lightning flashes were located within the bands identified in the radar imagery. This may be due to the ability of the cloud to retain a separation of charge while moving away from the area of initial development. Bands of highest reflectivity appeared in the radar imagery of each event. This banding pattern was key to the identification of the occurrence of electrified convective snowfall and is consistent with Schultz et al. (2004). This thesis, along with Schultz et al. (2004) are the only studies which have examined the characteristics of convective snowfall using radar imagery. With this information, it may be possible to identify and issue warnings for high snowfall rates from a nowcasting perspective.

5.3 Future Work

This study has shown the spatial and temporal characteristics of electrified convective snowfall events while it described the environment capable of producing the events and the radar imagery associated with the events. Because this study examined events from the cyclonic and frontal categories, it would be useful to look at events induced by coastal storms, lake effect/enhanced, orographic effects, and upslope effects to determine if the banding pattern identified in this thesis is present in other environments that produce the events as well. These events could be identified from the climatology presented by this study and investigated further in a similar manner to the second part of the study.

Numerical modeling may be another way to investigate some of the past events identified in this thesis. By using a model, it would be possible to investigate all synoptic categories discussed previously, and therefore, it would highlight the environmental differences between each synoptic type. Specifically, the role of the low-level jet may be identified. Modeling may also be able to determine the biases present in various models regarding electrified convective snowfall events. Also, the ability to forecast these events may be determined through this type of study.

Finally, additional work needs to be done with the lightning polarity. More events should be examined to confirm this increase in the percentage of positively charged lightning flashes in electrified convective snowfall events. New polarimetric radars being deployed to image the polarity of hydrometeors should be used to verify the separation of charges present in the cloud base. By examining the clouds with the radar, an understanding of exactly how the positive flashes occur in these events can be made. Also, polarimetric radar imaging may determine how the shift of lightning flashes from developmental bands to existing bands occurs. A better understanding of electrified convective snowfall events and how they develop at the microphysical level may lead to more accurate forecasting of these events and therefore save lives and prepare people in advance of these storms.

REFERENCES

Bennetts, D.A., and B.J. Hoskins, 1979: Conditional symmetric instability-A possible explanation for frontal rainbands. *Quart. J. Roy. Meteor. Soc.*, **105**, 945-962.

Colman, B.R., 1990a: Thunderstorms above frontal surfaces in environments without positive CAPE. Part I: A climatology. *Mon. Wea. Rev.*, **118**, 1103-1121.

Colman, B.R, 1990b: Thunderstorms above frontal surfaces in environments without positive CAPE. Part II: Organization and instability mechanisms. *Mon. Wea. Rev.*, **118**, 1123-1144.

Cummins, K. L., M. J. Murphy, E. A. Bardo, W. L. Hiscox, R. B. Pyle, and A. E. Pifer, 1998: A combined TOA/MDF technology upgrade of the U.S. National Lightning Detection Network, *J. Geophys. Res.*, **103** *(*D8), 9035-9044.

Curran, J.T., and A.D. Pearson, 1971: Proximity soundings for thunderstorms with snow. *Preprints, 7th Conf. on Severe Local Storms, Kansas City, MO*, Amer. Meteor. Soc., 118-119.

desJardins, M. L., and R. A. Petersen, 1985: GEMPAK: A meteorological system for research and education. Preprints, *First International Conference on Interactive Information and Processing Systems for Meteorology, Oceanography, and Hydrology*, Los Angeles, Amer. Meteor. Soc., 313-319.

Djurić, D., and D. S. Ladwig, 1983: Southerly low-level jet in the winter cyclones of the southwestern Great Plains. *Mon. Wea. Rev.* **111**, 2275-2281.

Emanuel, K.A., 1979: Inertial instability and mesoscale convective event: A review and comparison of techniques for assessing vertical motion fields. *Natl. Wea. Dig.,* **18,** 31–54.

Emanuel, K.A., 1983: The lagrangian parcel dynamics of moist symmetric instability. *J. Atmos. Sci.* **40**, 2368-2376.

Emanuel, K.A., 1985: Frontal circulations in the presence of small moist symmetric stability. *J. Atmos. Sci.*, **42**, 1062-1071.

Emanuel, K. A., 1986: Overview and definition of mesoscale meteorology. *Mesoscale Meteorology and Forecasting,* P. S. Ray, ed., Amer. Meteor. Soc., 1–17.

Greenstein, M.D., 2006: Mesoscale Structure of Precipitation Regions in Northeast Winter Storms. M. S. Thesis, University at Albany, State University of New York, 116 pp.

Holle, R.L., and J.V. Cortinas, 1998: Thunderstorms observed at surface temperatures below freezing across North America. *Preprints, 18th Conf. on Severe Local Storms, Minneapolis, MN*, Amer. Meteor. Soc., 705-708.

Holle, R.L., J.V. Cortinas, and C.C. Robbins, 1998: Winter thunderstorms in the United States. *Preprints, 16th Conf. on Weather Analysis and Forecasting, Phoenix, AZ*, Amer. Meteor. Soc., 298-300.

Hunter, S.M., S.J. Underwood, R.L. Holle, and T.L. Mote, 2001: Winter lightning and heavy frozen precipitation in the southeast United States. *Wea. Forecasting*, **16**, 478-490.

Lott, N.: The Big One! A Review of the March 12-14, 1993: "Storm of the Century". NOAA Technical Reports. [Available online at: http://www1.ncdc.noaa.gov/pub/data/techrpts/tr9301/tr9301.pdf].

Market, P.S., C. E. Halcomb, and R. L. Ebert, 2002: A climatology of thundersnow events over the contiguous United States. *Wea. Forecasting*, **17**, 1290-1295.

McCann, D.W., 1995: Three-Dimensional Computations of Equivalent Potential Vorticity. *Wea. Forecasting*, **10**, 798-802.

Mesinger, F., G. DiMego, E. Kalnay, K. Mitchell, P.C. Shafran, W. Ebisuzaki, D. Jović, J. Woollen, E. Rogers, E. Berbery, M.B. Ek, Y. Fan, R. Grumbine, W. Higgins, H. Li, Y. Lin, G. Manikin, D. Parrish, and W. Shi, 2006: North American Regional Reanalysis. *Bull. of the Amer. Meteor. Soc.* **87,** 343-360.

Moore, J.T., and P. D. Blakeley, 1988: The role of frontogenetical forcing and conditional symmetric instability in the midwest snowstorm of 30–31 January 1982. *Mon. Wea. Rev.,* **116,** 2155–2171.

Moore, J.T.; Czarnetzki, A.C.; Market, P.S., 1998: Heavy precipitation associated with elevated thunderstorms formed in a convectively unstable layer aloft. *Meteor. Appl.,* **5**, 373-384.

Moore, J.T., and T.E. Lambert, 1993: The use of equivalent potential vorticity to diagnose regions of conditional symmetric instability. *Wea. Forecasting*, **8**, 301-308.

.

National Oceanic and Atmospheric Administration (NOAA), 1960-2005: *Daily Weather Map Series.* U.S. Department of Commerce, NOAA Central Library Data Imaging Project, National Climatic Data Center, Silver Spring, MD. [Available online at: http://docs.lib.noaa.gov/rescue/dwm/data_rescue_daily_weather_maps.html]

Nicosia, D.J., and R.H. Grumm, 1999: Mesoscale band formation in three major northeastern United States snowstorms. *Wea. Forecasting*, **14**, 346-368.

Novak, D. R., L. F. Bosart, D. Keyser, and J. S. Waldstreicher, 2004: An observational study of cold season-banded precipitation in northeast U.S. cyclones. *Wea. Forecasting*, **19,** 993–1010.

Novak, D. R., J. S. Waldstreicher, L. F. Bosart, D. Keyser, 2006: A forecast strategy for anticipating cold season mesoscale band formation within eastern U.S. cyclones. *Wea. Forecasting*, **21,** 3–23.

Orlanski, I., 1975: A rational subdivision of scales for atmospheric processes. *Bull. Amer. Meteor. Soc.,* **56,** 527–530.

Orville, R.E. and Huffins, G.R., 2001: Cloud to ground lightning in the United States: NLDN results in the first decade, 1989-98. *Mon. Wea. Rev.,* **129**, 1179-1193.

Rogers, R.R., 1979: *A Short Course in Cloud Physics*. 2nd ed. Pergamon Press, New York, 235 pp.

Rooney, J.F., 1967: The urban snow hazard in the United States: An appraisal of disruption. *Geogr. Rev.,* **57**, 538-559.

Sanders, F., and L.F. Bosart, 1985: Mesoscale structure in the megalopolitan snowstorm of 11-12 February 1983. Part I: Frontogenetical forcing and symmetric instability. *J. Atmos. Sci.*, **42**, 1050-1061.

Sanders, F., 1986: Frotogenesis and symmetric stability in a major New England snowstorm. *Mon. Wea. Rev*., **18**, 1847-62.

Schultz, D.M., 1999: Lake-effect snowstorms in northern Utah and western New York with and without lightning. *Wea. Forecasting*, **14**, 1023-1031.

Schultz, D.M., 2006: The Use and Misuse of Conditional Symmetric Instability. Cooperative Program for Operational Meteorology, Education, and Training (COMET) [Available online at: http://meted.ucar.edu/export/csi/csi_v51.htm].

Schultz, D.M., D.S. Arndt, D. J. Stensrud, and J. W. Hanna, 2004: Snowbands during the cold-air outbreak of 23 January 2003. *Mon. Wea. Rev.,* **132**, 827-842.

Schultz, D.M., P.N. Schumacher, and C.A. Doswell III, 2000: The intricacies of instabilities. *Mon. Wea. Rev.,* **128**, 4143-4148.

Sherwood, S.C., 2000: On moist instability. *Mon. Wea. Rev.,* **128**, 4139-4142.

Shields, M. T., R. M. Rauber, and M. K. Ramamurthy, 1991: Dynamical forcing and mesoscale organization of precipitation bands in a midwest winter cyclonic storm. *Mon. Wea. Rev.,* **119,** 936–964.

Trapp, R. J., D. M. Schultz, A. V. Ryzhkov, and R. L. Holle, 2001: Multiscale structure and evolution of an Oklahoma winter precipitation event. *Mon. Wea. Rev*., **129**, 486-501.

Whiteman, C.D., X. Bian, and S. Zhong, 1997: Low-Level Jet Climatology from Enhanced Rawinsonde Observations at a Site in the Southern Great Plains. *J. App. Met.,* **36***,* 1363–1376*.*

Williams, E.R., 2001: The electrification of severe storms. *Meteor. Monog.,* **7**, Amer. Meteor. Soc., 527-561.

Wolfsberg, D. G., K. A. Emanuel, and R. E. Passarelli, 1986: Band formation in a New England snowstorm. *Mon. Wea. Rev.,* **114,** 1552–1569.

Xu, Q., 1989: Extended Sawyer–Eliassen equation for frontal circulations in the presence of small viscous moist symmetric stability. *J. Atmos. Sci.,* **46,** 2671–2683.